ADDIS ABABA UNIVERSITY

OFFICE OF RESEARCH AND GRADUATE PROGRAMS

COLLEGE OF NATURAL AND COMPUTATIONAL SCIENCES

DEPARTMENT OF CHEMISTRY

SYNTHESES OF PYRROLOBENZOTRIAZOLEDIONE- AND PYRROLOBENZOTHIADIAZOLEDIONE-BASED CONJUGATED COPOLYMERS AND A PDI-BASED SMALL MOLECULE ACCEPTOR

By

Bisrat Kiros

Advisor: Prof. Wendimagegn Mammo

A Thesis Submitted to the Department of Chemistry, Office of Research and Graduate Programs of Addis Ababa University, in Partial Fulfillment of the Requirements for the Degree of Master of Science in Chemistry.

September 2018

Declaration

I, the undersigned, declare that this MSc thesis is my original work and has not been presented for any degree in any other university and that all sources of materials used for this project have been duly acknowledged.

Name: **Bisrat Kiros**

Signature:_____

This MSc. thesis has been submitted for examination with my approval as a university advisor.

Name: **Prof. Wendimagegn Mammo**

Signature: _____

Date and place of submission: Department of Chemistry

Addis Ababa University

September 2018

ADDIS ABABA UNIVERSITY

COLLEGE OF NATURAL AND COMPUTATIONAL SCIENCES

DEPARTMENT OF CHEMISTRY

Syntheses of Pyrrolobenzotriazoledione- and Pyrrolobenzothiadiazoledione-based Conjugated Copolymers and a PDI-Based Small Molecule Acceptor

By Bisrat Kiros

Approved by the Examining Board:	Signature	Date
1. Prof. Wendimagegn Mammo Advisor	_____	_____
2. Dr. Estifanos Ele Examiner	_____	_____
3. Dr. Mekonnen Abebayehu Examiner	_____	_____
4. Dr. Ahmed Mustefa Chairman, Department of Chemistry	_____	_____

ACKNOWLEDGMENTS

I thank my God and my Savior Jesus Christ for making my education possible and for being a present help every day to cheer and guide me.

I also thank my family members for being active participants in my education emotionally and financially especially my brother Gebru who persuaded me to pursue my education by offering to cover my expenses.

I am privileged and blessed to have Prof. Wendimagegn Mammo as my advisor who is excellent in knowledge and superb in character. I appreciate him very much for addressing my needs and surpassing all my expectations while making the journey a memorable one with his kindness.

I have shared lab room 216 with Birhan A. Abdulahi who invested much of his time in showing me how to execute my research work, who performed my NMR, UV and CV analyses, edited my thesis draft and answered my endless questions. I thank him for his friendship, great patience and wonderful sense of humor.

I am grateful for Melaku Assefa, Yohannis Meaza and Dr. Mesfin Getachew for running some of my NMR analyses and assisting me in many other ways.

I appreciate the Female Scholarship sponsor for covering my tuition, so that I could pursue my MSc in this prestigious university.

Last but not least, my gratitude goes out to the staff of the Department of Chemistry for facilitating my research work.

Table of Contents

LIST OF FIGURES

LIST OF SCHEMES

LIST OF TABLES

LIST OF APPENDICES

LIST OF ABBREVIATIONS

A	Acceptor
AcOH	Acetic acid
BDT	Benzodithiophene
BHJ	Bulk heterojunction
^{13}C NMR	Carbon-13 nuclear magnetic resonance
$CDCl_3$	Chloroform
D	Donor
d	Doublet
DCM	Dichloromethane
dd	Doublet of doublet
DEPT	Distortionless Enhancement by Polarization Transfer
DMF	*N*,*N*-Dimethylformamide
DMSO	Dimethylsulfoxide
E_g	Energy gap
E_g^{opt}	Optical bandgap
EtOH	Ethanol
FF	Fill factor
h	Hour
HOMO	Highest occupied molecular orbital
Hz	Hertz
ICT	Intramolecular charge transfer
J	coupling constant
J_{sc}	Short circuit current density
LBG	Low bandgap
LUMO	Lowest unoccupied molecular orbital
m	Multiplet

NBS	*N*-bromosuccinimide
o-DCB	*ortho*-dichlorobenzene
OPV	Organic photovoltaic
OSC	Organic solar cell
P(*o*-tolyl)$_3$	Tri(*o*-tolyl)phosphine
PCE	Power conversion efficiency
$Pd_2(dba)_3$	Tris(dibenzylideneacetone)dipalladium(0)
%	Percent
PDI	Perylene diimide
ppm	parts per million
^{1}H NMR	Proton nuclear magnetic resonance
rt	Room temperature
s	Singlet
t	Triplet
THF	Tetrahydrofuran
TMSCl	Trimethylsilylchloride
UV-Vis	Ultraviolet-visible
V_{oc}	Open circuit voltage
δ	Delta (chemical shift unit)

Syntheses of Pyrrolobenzotriazoledione- and Pyrrolobenzothiadiazoledione-based Conjugated Copolymers and a PDI-based Small Molecule Acceptor

By

Bisrat Kiros

Advisor: Prof. Wendimagegn Mammo

ABSTRACT

Three donor-acceptor (D-A) alternating copolymers were synthesized using 4,8-bis(5-bromothiophen-2-yl)-6-octyl-5H-[1,2,5]thiadiazolo[3,4-f]isoindole-5,7(6H)-dione; 4,8-bis(5-bromothiophen-2-yl)-2-(2-ethylhexyl)-6-octyl-[1,2,3]triazolo[4,5-f]isoindole-5,7(2H,6H)-dione and 4,8-bis(5-bromothiophen-2-yl)-2,6-dioctyl-[1,2,3]triazolo[4,5-f]isoindole-5,7(2H,6H)-dione as acceptor monomers and 4,8-bis(5-(2-ethylhexyl)thieno[3,2-b]thiophen-2-yl)benzo[1,2-b:4,5-b']dithiophene-2,6-diyl)bis(trimethylstannane) as a donor monomer by Stille coupling polymerization reactions. The resulting copolymers possessed good solubility in common organic solvents such as chloroform and o-dichlorobenzene. These copolymers were characterized using UV-Vis spectrometry and cyclic voltammetry. In addition, a PDI-based acceptor 11,11'-(9,9'-spirobi[fluorene]-2,7-diyl)bis(2,8-bis(2-ethylhexyl)-1H-pyrido[3',4',5':4,5]naphtho[2,1,8-cde]-pyrido[3',4',5':4,5]naphtho[8,1,2-ghi]isoindole-1,3,7,9(2H,5H,8H)-tetraone) was synthesized via modified Suzuki coupling reaction.

1. INTRODUCTION

Necessity is the mother of invention. Thus, nonrenewable and polluting energy sources with social, economic, environmental and geopolitical consequences have called for the development of sustainable and clean energy. While renewable energy has been harvested from flowing streams, wind, and hot springs, the "only fully renewable source that has the capability to meet the world's large and growing energy demand is solar energy."[1, 2] Hence, solar cells based on silicon and other inorganic materials, with high power conversion efficiencies (PCEs) of 15-22%, have dominated the market of solar cells. However, not only are they heavy and rigid,[3] but also pose high cost of manufacturing and incorporate hazardous components. Consequently, they have not been widely commercialized.[4] Alternatively, organic photovoltaics (OPVs), which use semiconducting polymers or small molecules to create electrical current from sunlight, hold the potential for a "highly scalable and inexpensive solar energy production" and "offer the attractive prospect of low-temperature, solution-processed fabrication such as roll-to-roll and inkjet printing, that have the potential to dramatically lower the cost of solar energy production. Furthermore, the potential for large-area, lightweight and mechanically flexible modules, with options for semi-transparent and colored films, opens up new opportunities for building-integrated photovoltaics among other applications."[5, 6, 7]

Though organic materials are generally insulators, they can conduct electricity when they are highly conjugated with planar structures. As the numbers of continuously alternating single and double bonds in a compound greatly increase, the increased number of overlapping atomic orbitals lead to a decreased energy gap between the highest occupied molecular orbital (HOMO) and the lowest unoccupied molecular orbital (LUMO). When this energy gap is within the UV and visible radiation energy, irradiation with sunlight can excite an electron into its LUMO.

(Figure 1) The photo-excitation of organic semiconductors produces bound electron-hole pairs, known as excitons, which have large binding energy between 0.2–1.0 eV that drives the electron and hole to recombine after photo-excitation. In solar cells, this undesirable recombination process is overcome by combining two organic semiconductors with slightly offset HOMO and LUMO energies, such that the photo-excited electron in the donor is transferred to the LUMO of the acceptor allowing for the charges to be separated at the junction between these two semiconductors.[5, 8] Then through the built-in potential, the electrons in the acceptor move into the cathode and the holes in the donor flow into the anode which creates current.[5, 9]

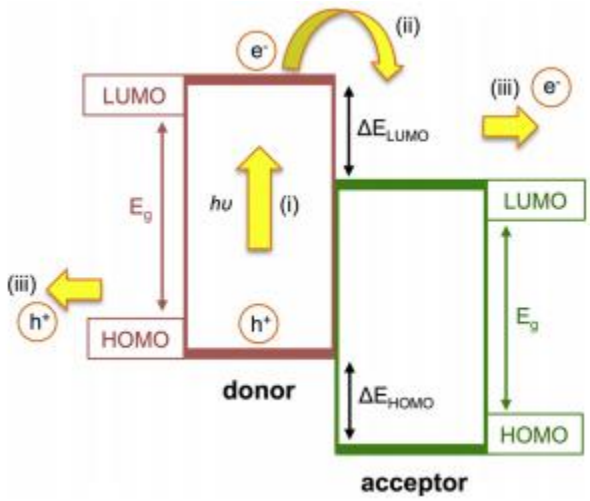

Figure 1: Mechanism of organic solar cell converting sunlight into electricity: (i) donor absorption of solar radiation leading to the excitation of an electron from the HOMO to the LUMO; (ii) migration of the electron to the LUMO of the acceptor; (iii) pull of the electron and hole towards the attracting electrodes

Organic solar cells (OSCs) of regular cell structure (see Figure 2)[10] are composed of an organic active layer made up of p-type semiconducting donor (*D*) and n-type semiconducting acceptor (*A*) materials sandwiched between a transparent indium tin oxide, ITO, anode and metal cathode such as Al or Ag. However, since direct contact of the electrodes with the active layer leads to undesirable effects such as high charge recombination, buffer layers are incorporated for

both of the electrodes.[9] A thin layer of transparent poly(3,4-ethylenedioxythiophene): poly(styrene sulfonate) (PEDOT: PSS) is used as hole transporting layer to the anode and a Ca or LiF as electron transporting layer to the cathode. Finally, the ITO is covered with a transparent and flexible substrate whose side faces the sun.[11] However, due to air instability of the acidic hole transporting layer PEDOT:PSS and the easily oxidized Al metal cathode of a regular cell structure, an inverted cell structure has been developed. In this type of cell (Figure 2), not only are the positions of the electrodes reversed with respect to the side of the cell that faces the sun, but also the types of the electrodes and buffers are mostly different. Here, the ITO becomes the cathode and is buffered with a transition metal oxide such as ZnO or TiO_x, while Ag or Au is used as the anode with PEDOT:PSS or a transition metal oxide such as MoO_3 or V_2O_5 as hole transporting layer.[12] Despite its many advantages, however, the inverted cell architecture also has its own drawbacks such as low conductivity and high-work function of TiO_x needing radiation treatments that lead to cell instability.[13]

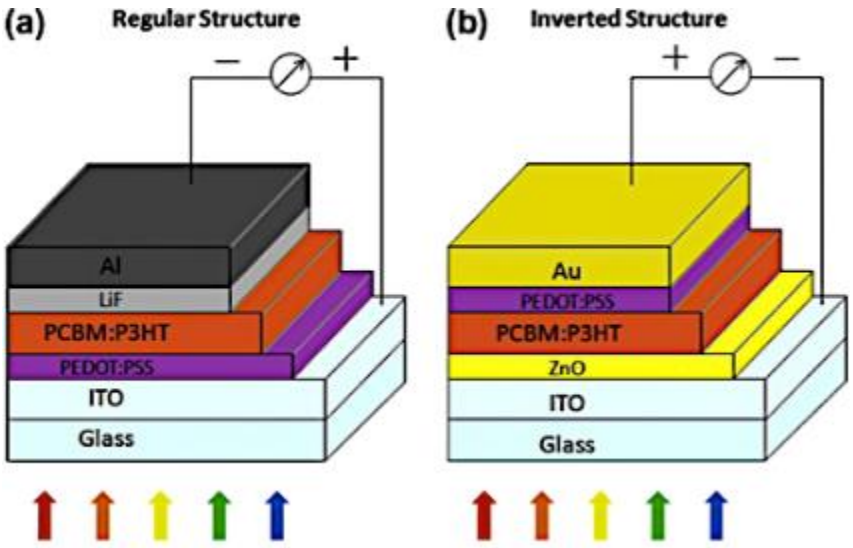

Figure 2: Components of (a) regular and (b) inverted organic solar cell structures

The architecture of the active layer of organic solar cells has grown in number over the decades. The first kind was a single-layer made up of a thin layer of a polymer or small molecule which delivered very low PCE due to high recombination of excitons. Then a bilayer consisting of individual layers of the donor and acceptor semiconductors was constructed which improved the PCE. Later on, an innovative active layer with a blend of the donor and acceptor known as bulk heterojunction (BHJ) was developed to further reduce exciton recombination leading to better PCE and has become the prominent one.[7]

2. LITERATURE REVIEW

As high as 120,000 TW of solar power reaches the Earth's surface every year which exceedingly surpasses the world's energy need of 15 TW/year.[14] This translates to an energy density of about 1000 W/m^2 with a photon flux of $4.31 \times 10^{21}\ s^{-1}\ m^{-2}$ in a wavelength range from 280 to 4000 nm. However, 70% of the solar energy is concentrated in the visible and near-infrared (NIR) region between 380-900 nm. Thus, to efficiently harvest solar energy, PSCs should have absorptions that correspond with the solar spectrum in this range.[11, 15]

The research goals on organic semiconductors for high performance solar cells are to increase the PCE, stability, safety and reduce costs.[16] To achieve this, several parameters must be considered. Since PCE is a product of the open-circuit voltage (V_{oc}), short-circuit current density (J_{sc}) and fill factor (FF), optimization of each variable leads to improved PCE. The V_{oc} is the electrical potential difference between the two terminals of an organic solar cell when no current is flowing through the cell.[17] It is positively correlated with the energy difference of the HOMO of the donor and LUMO of the acceptor. So, increasing this energy difference would lead to improved PCE. However, since $J_{sc,}$ which is the short-circuit current density when the voltage across the cell is zero[18], increases with decreasing bandgap, optimizing it would lead to

the diminishing of the value of the V_{oc}. So their interrelationship leads to a trade-off that must be minimized.[19] In addition, when attempting to lower the bandgap of the donor, while still lowering its HOMO energy level, it must be in such a way that there is still a minimum energy difference of 0.3 eV between the LUMOs of the donor and the fullerene-based acceptor. This energy difference or interface band gap is critical in driving exciton splitting and charge dissociation at the interface of the donor and acceptor if it is less than the exciton binding energy.[9] Since $PC_{61}BM$, the more affordable fullerene-based acceptor, has a LUMO energy level of -4.2 eV, the lowest possible LUMO energy level of the donor would have to be -3.9 eV. Additionally, the bandgap of the donor that matches closely with the range of intense solar radiation is around 1.5 eV making the ideal HOMO energy level of the donor be -5.4 eV. The last variable of PCE is fill factor (FF) which is the ratio of maximum power from the solar cell to the theoretical power of the product of V_{oc} and short-circuit current (I_{sc}). FF is greatly affected by the morphology of the active layer which must be optimized to promote charge separation and mobility thereby not only improving FF but also J_{sc}. Unlike crystalline inorganic solar cells which have greater than 80% fill factor, organic solar cells generally yield lower values mainly because of non-ideal nanomorphology and differences between electron and hole mobility.[17]

2.1. Design Rules of Conjugated Polymers

To design high-performance organic semiconductors, three components of the conjugated polymer are considered. These components are arbitrarily categorized as the backbone repeating unit, substituents and side chains. The conjugated backbone is the one that mainly determines the optical, electrochemical and photovoltaic properties of the polymer. Therefore, its construction is of high importance in the continued development of PSCs. Without side chains, conjugated polymers would be insoluble. In making conjugated polymers soluble, alkyl side chains allow for

the molecular weight to increase which results in polymers with low bandgap thereby improving the J_{sc}. Substituents such as F and CN have been employed to modify some properties of polymers. The modifications could include lowering the HOMO energy level or improving intramolecular and intermolecular interactions.

2.2. Backbone Repeating Unit

After years of research to fine-tune the energy levels and lower the band gaps of homopolymers of fused aromatic systems, a breakthrough was achieved through the donor-acceptor (*D-A*) strategy where the conjugated copolymer incorporates electron-rich donor and electron-deficient-acceptor moieties.[11] This method works well because the charge transfer between the donor and acceptor moieties (as shown in Figure 3) leads to hybridization of molecular orbitals with lower HOMO and LUMO energy levels for a low bandgap and planar structure.[20] Additionally, *D-A* copolymer donors exhibit a special feature with HOMO energy levels more close to that of the donor moiety while their LUMO energy levels are similar to the acceptor moiety. This allows for modifying the HOMO or LUMO without greatly affecting the other.

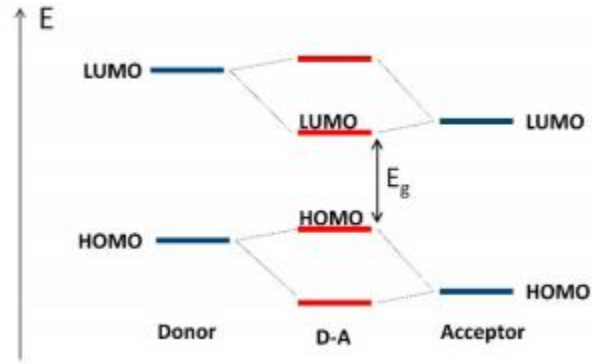

Figure 3: Molecular orbital theory explanation for band gap reduction in D-A copolymer

To further modify the physical properties, π-spacers have been incorporated between the donor and acceptor moieties of *D-A* copolymer donors. This reduces the steric hindrance between donor and acceptor moieties resulting in a planar structure. Not only does this improve the optical property of the polymer, but it also leads to improved π-π stacking resulting in improved intermolecular interaction for higher PCE. Aromatic rings varying from thiophene, selenophene, and furan have been introduced as π-spacers into *D–A* type polymers. Depending on the π-spacer moiety, variation of the optical, electrochemical, and photovoltaic properties has been observed. For instance the replacement of thiophene with selenophene as a π-spacer has been noted as one of the best approaches for synthesizing π-conjugated polymers with a narrow low band gap (LBG) in order to harvest more solar flux.[21]

2.3. Substituents

To fine tune the physical properties of conjugated donor and acceptor polymers, substituents such as F and CN are used.[22] Fluorine, the most electronegative element, is frequently used as a substituent and has diverse effects on physical and morphological properties.[23] It is used to down-shift the energy levels for greater V_{oc} without greatly affecting other parameters.[24] Additionally, it leads to increased intramolecular and intermolecular interactions via hydrogen and dipole-dipole bonding for greater planarity with enhanced J_{sc}, reduced charge recombination, and improved morphology, resulting in greater FF for an overall higher PCE.[25] Furthermore, the substitution of hydrogen with fluorine makes the polymer resistant to oxidation and heat for better stability without affecting solubility.[2]

2.4. Side Chains

Side chains incorporated on the backbone repeating unit of conjugated polymers, judiciously placed to prevent steric hindrance, enable for the solubility of conjugated polymers

even at greater molecular weight.[9, 26, 27] The large molecular weight results in greater numbers of conjugated bonds which lower the bandgap for improved PCEs. The most commonly used side chains are alkyl derivatives of straight or branched forms. Since they are weak electron-donating groups, their effect on the energy levels of the polymer are minimal. Studies on the size and topography of side chains have indicated that variations lead to drastic changes. It is commonly observed that moderately bulky side chains give good results.[26, 28, 29]

Alkyl side chains are not always fully aliphatic; rather, variations have been developed that not only address solubility but also introduce other changes. For instance, alkoxy side chains are used for the added benefit of reducing steric hindrance for better crystallinity even though the electron-donating oxygen raises the HOMO energy level.[14,30] So, in some cases, alkylthienlys are preferred over alkoxy groups because sulfur lowers the HOMO energy level for greater V_{oc} and red-shifts the absorption for lower bandgap compared to the alkyl equivalents.[24, 31, 32] Another modified side chain is an alkylsilyl group which differs in that silicon has the capacity to accommodate up to three equivalents of alkyl side chains and gives better results with short and straight alkyl groups.[24, 31, 33, 34, 35]

2.5. Morphology

High performance OSCs can be achieved when donor and acceptor semiconductors give optimal morphology.[36] The morphology of the active layer has to obtain a specific distribution of donor and acceptor phase in the blend for optimum exciton splitting and percolating pathways for charge mobility.[17] The domain size of the donor and acceptor phase should be about 20 nm which is twice the diffusion length of the exciton in order for the exciton to dissociate at the interface and eventually move into the corresponding electrodes of the cell.[9] Several methods have been developed to obtain optimum morphology. They include solvent or thermal

annealing.[36] In addition, additives such as 1,8-diiodooctane (DIO) are incorporated with the active components to dissolve them and improve the interpenetration of the donor and acceptor parts. The PTB7:PC71BM blend, a model system for morphological studies of solvent additives, was investigated by Lou *et al*. and showed that DIO specifically dissolved the acceptor large domains while it aided the crystallization of the donor for better phase separation. This led to obtaining remarkable PCE of 9.5% from 6.4% which was obtained without the use of additives.[12, 37]

2.6. Donors

Some of the commonly reported p-type donors which incorporate many of the design rules of high-performance conjugated polymers are *D-A* copolymers of benzodithiophene-based donor moieties[31, 38, 39, 40, 41] with either benzothiadiazole- or benzotriazole-based acceptor moieties. [42, 38, 43, 44, 45, 46] The donor moiety, which is a planar three-fused ring system, is an electron donor with several sites for substituents and side chains. On the other hand, the core acceptor moiety (benzothiadiazole) is an electron acceptor with sites for π-spacers and substituents. Due to the lack of a site for side chains on the thiadiazole ring, its polymers suffer from poor solubility.[43] However, benzotriazole circumvents the solubility issue with the central nitrogen of the triazole ring being able to be alkylated. Even though benzotriazole is not a strong-electron acceptor as benzothiadiazole, the sites available on the benzene ring offer for optoelectronic modification with F or fused diimide functionality which has added site for alkylation for greater solubility.[22, 28, 47, 48, 49]

In 2016, Liuyuan *et al.*[39] synthesized the *D-A* p-type conjugated copolymer **P1** (Figure 4) based on 4,8-di(thien-2-yl)-6-octyl-2-octyl-5*H*-pyrrolo[3,4-*f*]benzotriazole-5,7(6*H*)-dione as the acceptor unit and 4,8-bis(5-(2-ethylhexyl)thiophen-2-yl)benzo[1,2-*b*:4,5-*b'*]dithiophene as the

donor unit. **P1** exhibited a wide bandgap of 1.81 eV along with relatively deep HOMO energy level of −5.34 eV. The single-junction polymer solar cell based on **P1**:$PC_{71}BM$ blend film afforded a PCE of 8.63% with an V_{oc} of 0.87 V, a J_{sc} of 13.50 mA cm^{-2}, and a FF of 73.95%, which was among the highest values reported for wide-bandgap polymer-based single-junction organic solar cells at the time.

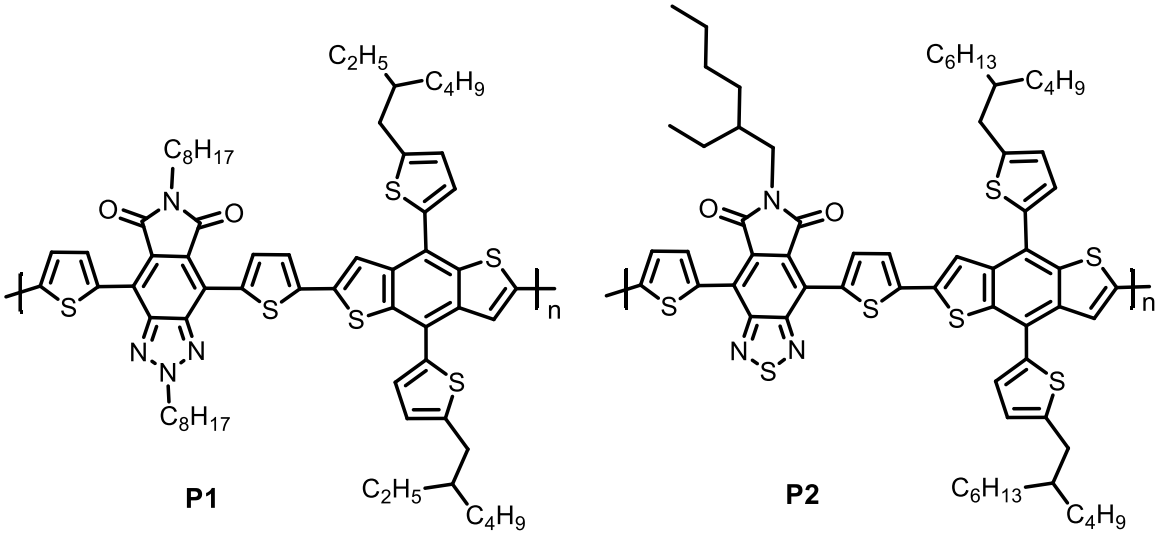

Figure 4: Copolymers **P1** and **P2**

In 2013, Wang *et al*.[50] reported the design, synthesis and characterization of **P2** (Figure 4) a copolymer incorporating *N*-alkyl-4,7-di(thien-2-yl)-2,1,3-benzothiadiazole-5,6-dicarboxylic imide (DI) and benzo[1,2-*b*:4,5-*b′*]dithiophene (BDT) units. By incorporating the DI unit, the polymer showed a red-shifted absorption with a deep-lying HOMO energy level. **P2** exhibited an intense absorption in the longer wavelength region, a deep-lying HOMO energy level, and a high carrier mobility. PSCs based on **P2:** $PC_{71}BM$ afforded a high PCE of 5.19% and an V_{oc} of 0.91 V.

2.7. Nonfullerene Acceptors

Fullerene-based soluble [6,6]-phenyl-C_{60}-butyric acid methyl ester ($PC_{61}BM$) or [6,6]-phenyl-C_{70}-butyric acid methyl ester ($PC_{71}BM$) derivatives have become the ubiquitous acceptors in PSCs.[51] Their dominance in the OPV research arises from their highly valued characteristics of strong electron acceptance and transportation, high electron mobility, and compatibility with vast numbers of donors. However, they have limitations such as weak absorption in the intense solar radiation region, structural inflexibility, high cost of preparations, and morphological instability.[51] Consequently, non-fullerene acceptors (NFAs) have been sought for that possess the advantageous properties of the fullerene-based acceptors while overcoming their shortcomings.[52, 53]

In the search for non-fullerene n-type acceptors, perylene diimide (PDI)-based acceptors have dominated the research scene due to their large and rigid planar π-conjugated structure, leading to excellent structural stability, high electron mobility and high electron affinity which compares to fullerene acceptors. The perylene-3,4,9,10-tetracarboxylic dianhydride structure (Figure 5) has several sites for introducing side chains for solubility and aryl substituents at the *ortho* and bay positions to modify physical properties.[54] PDI-based acceptors possess strong π−π stacking, which is desirable for charge mobility, but not for charge separation due to the large domain formed, resulting in non-ideal donor-acceptor phase which leads to weakening of the performance.[55, 56]

To optimize the π-π stacking of PDI molecules, several methods have been used. For monomeric PDI derivatives, aryl substituents at the *ortho* and *bay* positions (see Figure 6) introduce steric hindrance that diminish the large domain formation. For PDI dimers, conjugated bridges such as single or fused rings of benzene, thiophene or selenophene are placed between

two PDI units that result in twisted structures breaking the planarity of the molecule. Additional means of lowering the self-aggregation is to synthesized three dimensional structures.[54]

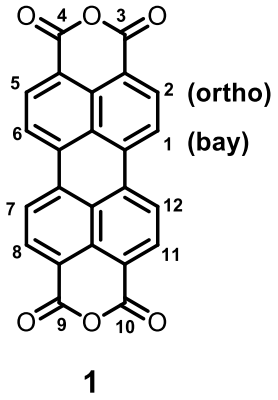

Figure 5: Perylene-3,4,9,10-tetracarboxylic dianhydride (**1**) position numbering and naming

In 2016, Hendsbee *et al*.[57] synthesized and characterized bay-linked *N*-annulated two dimensional PDI derivative acceptors (Figure 6). Solar cells in which a BHJ blend of compound **2** and donor **P3** was the active layer delivered a PCE of 7.55% with V_{oc} of 1.13 eV, J_{sc} of 11.04 mA/cm^2 and FF of 0.61.

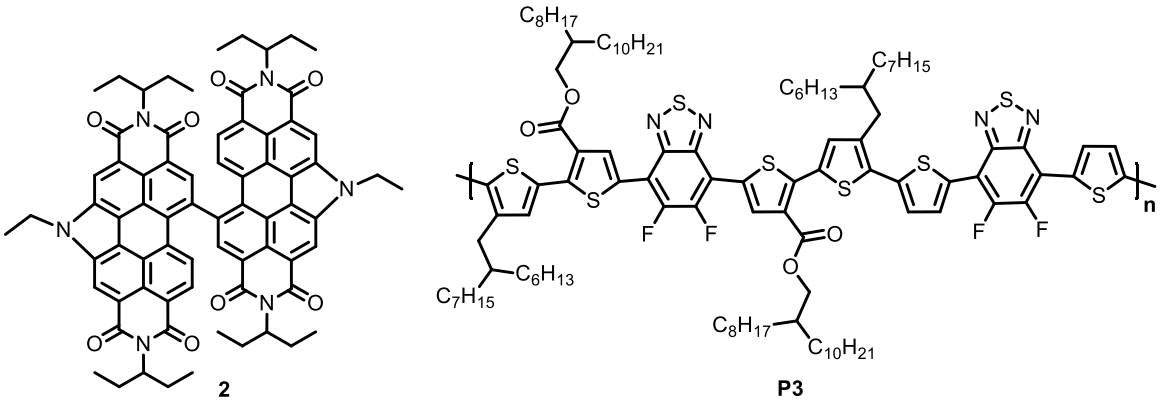

Figure 6: Bay-linked *N*-annulated PDI-based acceptor (**2**) and donor **P3**.[58]

In 2017, *Zhou et al.*[58] published the photovoltaic performances of blends of PDI-based two dimensional isomerized small molecules **3** and **4** (Figure 7) with the polymer donor **P4**. The differences in the substitution positions of the spirobifluorene molecules led to different degrees of twisting and electronic distributions between the two acceptors affecting PCEs. Compound **3** had HOMO and LUMO levels of -5.94 and -3.42 eV, respectively, and solar cells fabricated from a blend of compound **3** and **P4** had a PCE of 4.19%, V_{oc} of 0.90 eV, J_{sc} of 9.83 mA/cm^2 and a FF of 47.30%. On the other hand, the HOMO and LUMO energy levels of compound **4** were -5.79 and -3.42 eV respectively, and it had improved overall parameters of PCE of 4.56%, an V_{oc} of 0.94 eV, a J_{sc} of 10.36 mA/cm^2 and a FF of 46.81%.

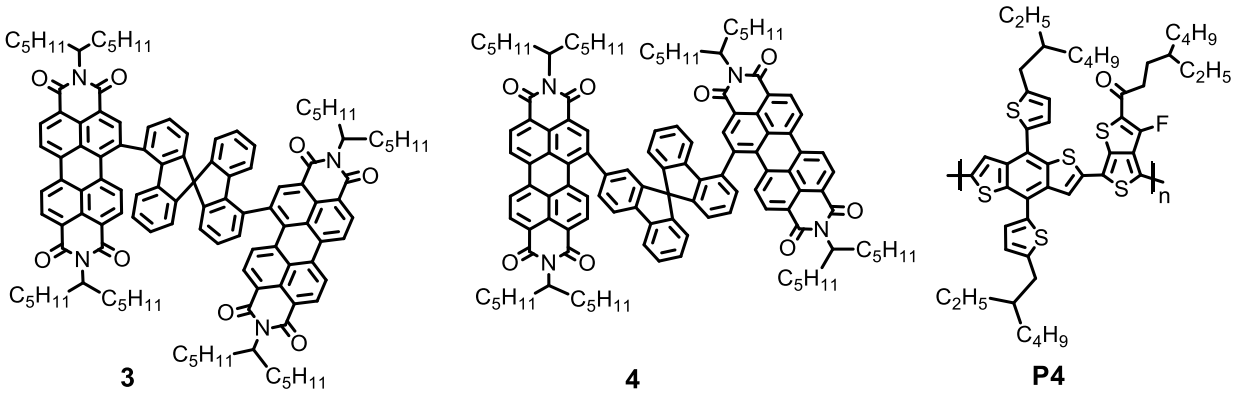

Figure 7: PDI-based two dimensional isomerized small molecule acceptors **3**, **4** and donor **P4**[5]

"With the continuous improvement of lab cell efficiency, the interest of commercialization of OPV technology has been growing larger. To move this technology from research laboratory to volume industrial production, many aspects have to be optimized and overcome."[9] The current expensive synthetic methods and materials, hazardous reagents and solvents, and low stability of OSCs have to be fully addressed for low-cost, stable and safe OSCs.[5] While it is hopeful that some reports are addressing these issues[59, 60, 61], it is clear that much work is ahead, considering the low PCEs obtained when implementing the low-cost and

safe methods.[60] Nevertheless, the fast progress that has been made in the last three decades is indicative of the strong will of researches to making organic solar cell that are not only efficient but also affordable and environmentally friendly.

3. THE OBJECTIVE OF THE RESEARCH

The objective of this research is to synthesize and characterize some alternating donor copolymers using the donor-acceptor strategy. It is also aimed to prepare a PDI-based small molecule acceptor. Acceptor moieties such as 4,8-bis(5-bromothiophen-2-yl)-6-octyl-5*H*-[1,2,5]thiadiazolo[3,4-*f*]isoindole-5,7(6*H*)-dione (**15**), 4,8-bis(5-bromothiophen-2-yl)-2-(2-ethylhexyl)-6-octyl-[1,2,3]triazolo[4,5-*f*]isoindole-5,7(2*H*,6*H*)-dione (**19**) and 4,8-bis(5-bromothiophen-2-yl)-2,6-dioctyl-[1,2,3]triazolo[4,5-*f*]isoindole-5,7(2*H*,6*H*)-dione (**21**) as well as the n-type semiconducting small molecule acceptor 11,11'-(9,9'-spirobi[fluorene]-2,7-diyl)bis(2,8-bis(2-ethylhexyl)-1*H*-pyrido[3',4',5':4,5]naphtho[2,1,8-*cde*]pyrido[3',4',5':4,5]naphtho[8,1,2-*ghi*]isoindole-1,3,7,9(2*H*,5*H*,8*H*)-tetraone) (**30**) will be synthesized starting from small molecules. NMR spectroscopy will be used to characterize intermediates, monomers and the small molecule while their optical properties and energy levels will be determined using UV-Vis spectrometry and cyclic voltammetry, respectively.

4. RESULTS AND DISCUSSION

In the course of this work, three monomers, specifically 4,8-bis(5-bromothiophen-2-yl)-6-octyl-5*H*-[1,2,5]thiadiazolo[3,4-*f*]isoindole-5,7(6*H*)-dione, 4,8-bis(5-bromothiophen-2-yl)-2-(2-ethylhexyl)-6-octyl-[1,2,3]triazolo[4,5-*f*]isoindole-5,7(2*H*,6*H*)-dione and 4,8-bis(5-bromothiophen-2-yl)-2,6-dioctyl-[1,2,3]triazolo[4,5-*f*]isoindole-5,7(2*H*,6*H*)-dione and a PDI-based acceptor 11,11'-(9,9'-spirobi[fluorene]-2,7-diyl)bis(2,8-bis(2-ethylhexyl)-1*H*-

pyrido[3',4',5':4,5]naphtho[2,1,8-*cde*]pyrido[3',4',5':4,5]naphtho[8,1,2-*ghi*]isoindole-1,3,7,9(2*H*,5*H*,8*H*)-tetraone) were synthesized and characterized by their ^{1}H- and ^{13}C-NMR spectra. The monomers were subsequently polymerized using Stille polycondensation polymerization reaction. The syntheses of the monomers, polymers and small molecule acceptor are described below.

4.1. Synthesis of 4,8-bis(5-bromothiophen-2-yl)-6-octyl-5*H*-[1,2,5]thiadiazolo[3,4-*f*]isoindole-5,7(6*H*)-dione (15)

The synthesis of compound **15** was started from 2,5-dibromothiophene (**5**) following the reported procedures.[62,63,64] Thus, nitration of compound **5** with concentrated H_2SO_4, fuming H_2SO_4 and fuming HNO_3 at room temperature gave 2,5-dibromo-3,4-dinitrothiophene (**6**) as shown in Scheme 1. The compound was obtained as a pale yellow powder in 56.4% yield. The structure of compound **6** was confirmed with its ^{13}C-NMR spectrum.

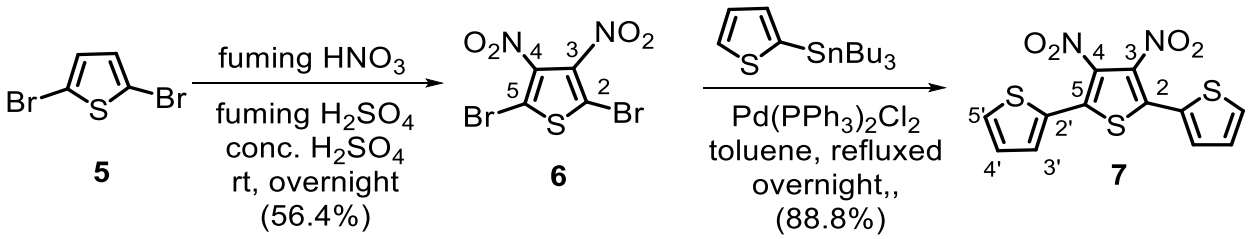

Scheme 1: Synthesis of compounds **6** and **7**

Compound **6** does not show any proton signal in its ^{1}H-NMR spectrum indicating that the 3,4-positions of the starting material were nitrated under the reaction conditions. The ^{13}C-NMR spectrum of compound **6** showed two carbon signals. The signal at δ 140.7 can be assigned to C-3 and C-4 while the one at δ 113.4 can be attributed to C-2 and C-5 which are chemically equivalent due to the symmetry of the compound. Compared to C-3 and C-4, C-2 and C-5 are

expected to be more shielded due to the heavy atom effect of bromine atoms[65] attached to them. On the other hand, the inductive effect of the electron withdrawing nitro groups attached to C-3 and C-4 makes them more deshielded.

Compound **6** underwent Stille coupling reaction with 2-tributylstannylthiophene in dry toluene using $Pd(PPh_3)_2Cl_2$ as catalyst to furnish 3',4'-dinitro-2,2':5',2''-terthiophene (**7**) as depicted in Scheme 1. Compound **7** was obtained in 88.8% yield as brown crystals, and its structure was confirmed with its ^{1}H- and ^{13}C-NMR spectra.

The ^{1}H-NMR spectrum of compound **7** (Table 1) displayed three doublet of doublets in the aromatic region at δ 7.64, 7.57 and 7.20 corresponding to H-5', H-3' and H-4', respectively. The ^{13}C-NMR spectrum of compound **7** (Table 2) revealed six carbon resonances in the aromatic region three of which are due to quaternary carbons and the remaining three are due to methine carbons of the thiophene rings as evidenced by the DEPT-135 spectrum. The quaternary carbon signals at δ 136.0, 133.9 and 128.1 are attributed to C-2 and C-5, C-3 and C-4, and C-2', respectively, and the signals at δ 131.3, 131.2 and 128.4 are due to the methine carbons C-5', C-4' and C-3', respectively. The reason for the deshielding of C-2 and C-5 relative to C-4 might be predominantly due to the mesomeric electron withdrawing effect of the nitro groups. A similar effect of the nitro groups might be responsible for the chemical shift differences observed between the methine carbon signals.

Table 1: The ^{1}H NMR (400.13 MHz, $CDCl_3$) data (δ_{ppm}) of compounds **7**, **8** and **9**

7	**8**	**9**
7.64	7.30	7.58
(*dd*, *J* = 1.2, 5.2 Hz, 2H, H-5')	(*dd*, *J* = 1.2, 4.8 Hz, 2H, H-5')	(*dd*, 1.2, 3.6 Hz, 2H, H-3')
7.57	7.14-7.10	7.35
(*dd*, *J* = 1.2, 4.0 Hz, 2H, H-3')	(unresolved *m*, 4H, H-3', 4')	(*dd*, 1.2, 5.2 Hz, 2H, H-5')
7.20	3.76	7.12
(*dd*, *J* = 4.0, 5.2 Hz, 2H, H-4')	(*s*, 4H, H-1")	(*dd*, *J* = 3.6, 5.0 Hz, 2H, H-4')

The reduction of compound **7** to 2,5-bis(2-thienyl)-3,4-diaminothiophene (**8**) was accomplished using a solution of anhydrous $SnCl_2$ in an anhydrous ethanol and concentrated aqueous HCl as shown in Scheme 2. Compound **8** was obtained as brown cake and used without purification in the next reaction.

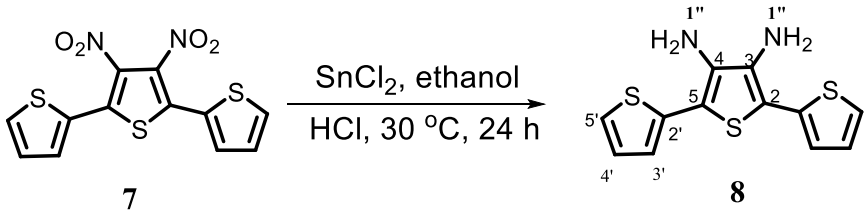

7 **8**

Scheme 2: Synthesis of 2,5-bis(2-thienyl)-3,4-diaminothiophene (**8**)

The ^{1}H-NMR spectrum of compound **8** (Table 1) showed three signals two of which are in the aromatic region while the remaining signal is found in the aliphatic region. The two-proton doublet of doublets at δ 7.30 is due to H-5' and the unresolved four-proton multiplet from δ 7.14-7.10 is due to H-3' and H-4'. The remaining singlet at δ 3.76 is due the NH_2 groups' H-1".

The ^{13}C-NMR spectrum of compound **8** (Table 2) revealed six carbon resonances in the aromatic region along with some impurity signals. The DEPT-135 spectrum revealed that the signals at δ 136.0, 133.7, and 125.4 can be accounted for the quaternary carbon atoms C-3 and

C-4, C-2 and C-5 and C-2', respectively. The other three carbon signals at δ 127.8, 124.0 and 123.9 are due to methine carbon atoms and can be attributed to C-3', C-4' and C-5', respectively.

Table 2: The ^{13}C-NMR (100.6 MHz, $CDCl_3$) data (δ_{ppm}) of compounds **7** and **8**.

Carbon	**7**	Carbon	**8**	Carbon	**9**
2, 5	136.0	3, 4	136.0	7, 8	156.3
3, 4	133.9	2, 5	133.7	4, 6	135.0
5'	131.3	2'	127.8	5'	128.3
4'	131.2	3'	125.4	4'	125.5
3'	128.4	4'	124.0	3'	124.3
2'	128.1	5'	123.9	2'	112.4

The synthesis of 4,6-di(thiophen-2-yl)-1,3-dihydrothieno[3,4-*c*][1,2,5]thiadiazole (**9**) was achieved by using *N*-thionly aniline as a cyclizing agent as shown in Scheme 3. Thus, *N*-thionyl aniline and trimethylsilyl chloride were added into a solution of **8** and dry pyridine. Then the mixture was stirred for 24 h at room temperature to yield the desired product (**9**) in 97% yield. The identity of the product was confirmed by its ^{1}H- and ^{13}C-NMR spectra.

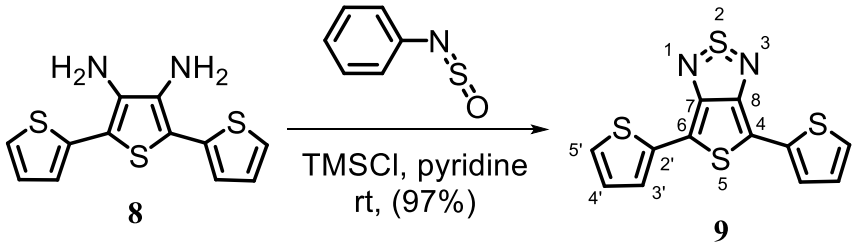

Scheme 3: Synthesis of 4,6-di(thiophen-2-yl)-1,3-dihydrothieno[3,4-*c*][1,2,5]thiadiazole (**9**)

The ^{1}H-NMR spectrum (Table 1) of compound **9** showed three doublet of doublets at δ 7.58, 7.35, and 7.12 due to H-3', H-5', and H-4', respectively. Compared to the proton signals of the starting material, the signals for compound **9** are more deshielded because of the introduction of the highly electronegative thiadiazole unit. The ^{13}C-NMR spectrum (Table 2) of compound **9**

showed six different carbon signals, three of which are due to quaternary carbon atoms and the other three are due to methine carbons. The quaternary carbon signals at δ 156.3, 135.0 and 112.4 correspond with carbons C-7 and 8, C-4 and 6, and C-2', respectively, and the methine carbon signals at δ 128.3, 125.5 and 124.3 are due to C-5', C-4' and C-3', respectively.

Compound **9** was transformed to 4,8-di(thiophen-2-yl)isobenzofuro[5,6-*c*][1,2,5]thiadiazole-5,7-dione (**13**) in three steps as depicted in Scheme 4. Thus, compound **9** was subjected to a Diels-Alder reaction with dimethyl acetylenedicarboxylate (**10**) in *o*-xylene under reflux for 24 h to afford dimethyl 4,7-di(thiophen-2-yl)benzo[*c*][1,2,5]thiadiazole-5,6-dicarboxylate (**11**) in 74% yield. The ester functions of compound **11** were then hydrolyzed using sodium hydroxide in ethanol to obtain 4,7-di(thiophen-2-yl)benzo[*c*][1,2,5]thiadiazole-5,6-dicarboxylic acid (**12**) in 87 % yield. Treatment of compound **12** with acetic anhydride in *o*-xylene afforded compound **13** as red crystals which was purified by recrystallization from ethanol. The structures of compounds **11**, **12** and **13** were confirmed by their ^{1}H- and ^{13}C-NMR spectra as discussed below.

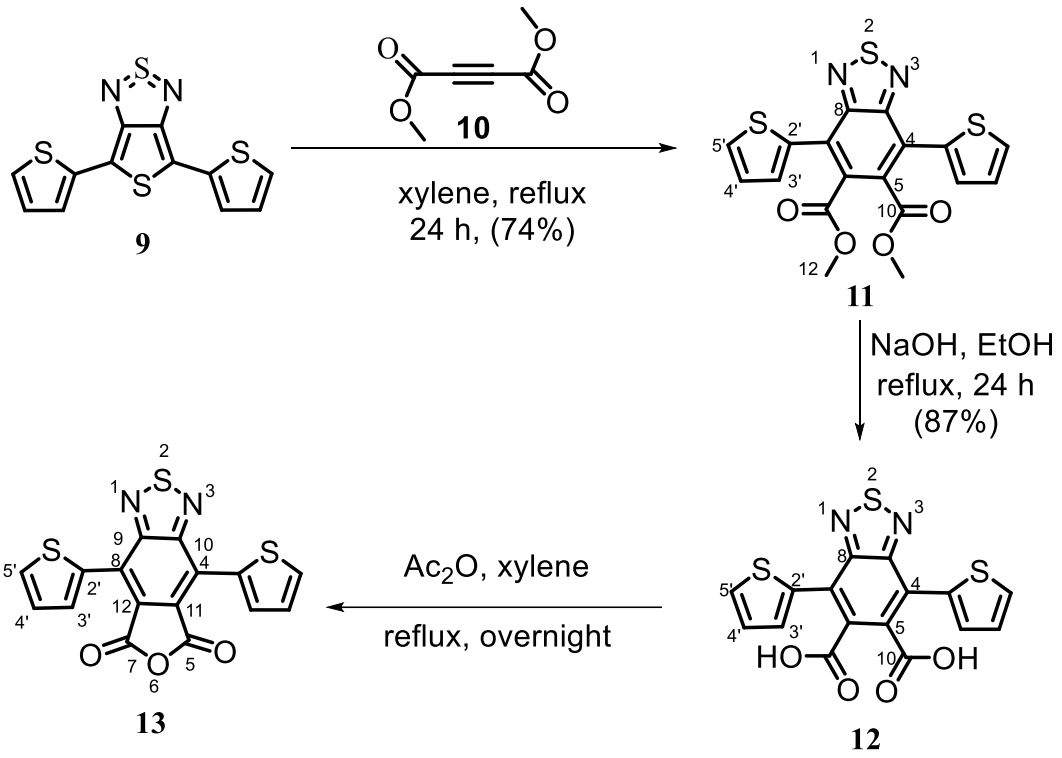

Scheme 4: Synthesis of compound **11, 12** and **13**

The ^{1}H NMR spectrum of compound **11** (Table 3) showed three doublets of doublets at δ 7.62, 7.45 and 7.22 in the aromatic region which can be attributed to H-5', H-3' and H-4', respectively. The six-proton singlet at δ 3.79 is due to the two chemically equivalent methyl ester groups.

The ^{13}C-NMR spectrum (Table 4) of compound **11** displayed the existence of nine carbon resonances eight of which are in the aromatic region and the remaining one is in the aliphatic region. The DEPT-135 spectrum revealed the presence of three methine carbon signals in the aromatic region and one methyl carbon resonance in the aliphatic region. The most deshielded carbon resonance at δ 168.0 can be attributed to the ester carbonyl carbons. The signals at δ 168.0, 153.6, 135.0, 132.0 and 126.2 are due to quaternary carbon atoms while the signals at δ 129.7, 128.9 and 127.2 are due to the methine carbons of the two thiophene rings as shown in

Table 4. The signal at δ 53.0 is due to the methyl carbons of the two methyl ester groups. The ^{1}H- and ^{13}C-NMR data are in good agreement with the structure of compound **11**.

Table 3: The ^{1}H-NMR (400.13 MHz, $CDCl_3$) data (δ_{ppm}) of compounds **11**, **12** and **13**

11	**12**	**13**
7.62 (*dd*, *J* = 1.2, 5.0 Hz, 2H, H-5')	7.87 (*dd*, *J* = 1.2, 3.6 Hz, 2H, H-3')	7.78 (*dd*, *J* = 1.2, 5.2 Hz, 2H, H-5')
7.45 (*dd*, *J* = 1.2, 3.6 Hz, 2H, H-3'	7.47 (*dd*, *J* = 1.2, 5.2 Hz, 2H, H-5')	7.46 (*dd*, *J* = 0.8, 3.2 Hz, 2H, H-3')
7.22 (*dd*, *J* = 3.6, 5.0 Hz, 2H, H-4'	7.25 (*dd*, *J* = 3.6, 5.2 Hz, 2H, H-4')	7.21 (*dd*, *J* = 3.6, 4.8 Hz, 2H, H-4')
3.79 (*s*, 6H, H-12)		

The ^{1}H-NMR spectrum of compound **12** (Table 3) showed the presence of three different proton environments in the aromatic region. The fact that compound **12** is symmetrical is evident from the ^{1}H-NMR spectrum. The absence of protons in the aliphatic region indicated the complete hydrolysis of the methyl ester groups. The three doublet of doublets at δ 7.87, 7.47 and 7.25 are assigned to H-3', H-5' and H-4'.

Table 4: The ^{13}C-NMR (100.6 MHz, $CDCl_3$) data (δ_{ppm}) of compounds **11**, **12** and **13**

Carbon	**11**	carbon	**12**	Carbon	**13**
10	168.0	10	168.0	5, 7	168.9
8	153.6	8	153.1	9, 10	153.1
2'	135.0	2'	135.3	11, 12	135.3
5	132.0	5	133.6	4, 8	133.7
5'	129.7	5'	130.2	5'	130.0
4'	128.9	4'	129.8	4'	129.5
3'	127.2	3'	127.7	3'	127.5
4	126.2	4	124.3	2'	124.3
12	53.0				

The ^{13}C-NMR spectrum of compound **12** (Table 4) displayed eight carbon resonances, five of which are quaternary carbons and the remaining three are attributed to methine carbons. The signal at δ 168.0 is due to the carboxyl groups while the quaternary carbon signals at δ 153.1, 135.3, 133.6 and 124.3 correspond to C-8, C-5, C-4 and C-2', respectively. The remaining three methine carbon signals at δ 130.2, 129.8, and 127.7 are due to C-5', C-4' and C-3' respectively.

The ^{1}H-NMR spectrum of compound **13** (Table 3) showed three aromatic proton signals along with signals of impurities in the aliphatic region. The signals due to the thiophene-ring protons appeared at δ 7.78, 7.46 and 7.21 as doublet of doublets and are attributed to H-5', H-3' and H-4', respectively.

The ^{13}C-NMR spectrum of compound **13** (Table 4) showed a total of eight carbon resonances. The signal at δ 168.9 is due to the carbonyl carbon atoms C-5 and 7. The remaining seven carbon resonances in the aromatic region can be attributed to the seven aromatic carbons, each signal representing two chemically equivalent carbons of the symmetrical molecule. Of the seven signals, four are due to quaternary carbons as expected and the remaining three represent the methine carbons of the thiophene moieties as shown in Table 4.

The next step in the synthetic plan was to convert **13** to the pyrrolobenzothiadiazole-dione-based monomer **15** as depicted in Scheme 5. Thus, the reaction of compound **13** with octylamine in glacial acetic acid was first carried out overnight at 110 ^{o}C and then with acetic anhydride to afford 6-octyl-4,8-di(thiophen-2-yl)-5*H*-[1,2,5]thiadiazolo[3,4-*f*]isoindole-5,7(6*H*)-dione (**14**) as orange powder in 95% yield. In the subsequent step, bromination of compound **14**, was carried out using *N*-bromosuccinimide in tetrahydrofuran to yield 4,8-bis(5-bromothiophen-

2-yl)-6-octyl-5*H*-[1,2,5]thiadiazolo[3,4-*f*]isoindole-5,7(6*H*)-dione (**15**) as red powder in 82% yield. Compounds **14** and **15** were characterized based on their ^{1}H- and ^{13}C-NMR data as described below.

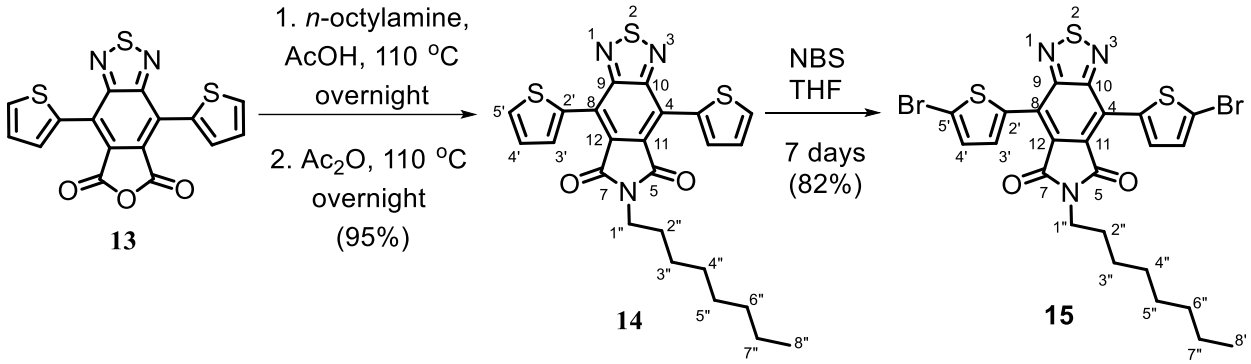

Scheme 5: Synthesis of compounds **14** and **15**

The ^{1}H-NMR spectrum of compound **14** (Table 5) showed three signals in the aromatic region and four signals in the aliphatic region. The three doublet of doublets in the aromatic region at δ 7.92, 7.73 and 7.29 are attributable to H-3', H-5' and H-4', respectively. The two-proton triplet at δ 3.74 in the aliphatic region of the ^{1}H-NMR spectrum is due to H-1". The two-proton quintet at δ 1.71 is assignable to H-2". The unresolved broad signal between δ 1.34 and 1.28 is due to methylene groups on the octyl side chain. The triplet at δ 0.89 is due to the terminal methyl group on the octyl side chain.

The ^{13}C-NMR spectrum of compound **14** (Table 6) displayed a total of 15-carbon resonances, eight of which appeared in the aromatic region and seven in the aliphatic region besides signals of the alkylating agent as impurity. The DEPT-135 spectrum revealed five quaternary and three methine carbon signals in the aromatic region. Out of the seven signals in the aliphatic region, six are due to methylene carbons and one is due to the terminal methyl group. The intense methylene carbon signal at δ 29.2 corresponds to two carbon atoms and can

be attributed to C-3" and C-4". Both the ^{1}H- and ^{13}C-NMR data agree very well with the structure of compound **14**.

Table 5: The ^{1}H-NMR (400.13 MHz, $CDCl_3$) data (δ_{ppm}) of compounds **14** and **15**.

14	**15**
7.92 (*dd*, *J* = 1.2, 3.6 Hz, 2H, H-3')	7.82 (*d*, *J* = 4.0 Hz, 2H, H-3')
7.73 (*dd*, *J* = 1.2, 5.2 Hz, 2H, H-5')	7.23 (*d*, *J* = 4.0 Hz, 2H, H-4')
7.29 (*dd*, *J* = 3.6, 5.0 Hz, 2H, H-4')	3.74 (*t*, *J* = 7.2 Hz, 2H, H-1")
3.74 (*t*, *J* = 7.2 Hz, 2H, H-1")	1.71 (*quin*, 2H, H-2")
1.71 (*quin*, 2H, H-2")	1.34-1.27 (unresolved, 10H, H-(3, 4, 5, 6, 7)"
1.34-1.28 (unresolved, 10H, H-(3, 4, 5, 6, 7)"	0.88 (*t*, *J* = 6.8 Hz, 3H, H-8")
0.89 (*t*, *J* = 7.2 Hz, 3H, H-8")	

The ^{1}H-NMR spectrum of compound **15** (Table 5) showed a total of six signals in the spectrum, two of which are in the aromatic region and the remaining four are in the aliphatic region. The two doublets at δ 7.82 and 7.23 are due to the methine protons of the thiophene units and can be attributed to H-3' and H-4', respectively. In the aliphatic region of the spectrum, the triplet at δ 3.74 is due to H-1". The quintet at δ 1.71 can be due to H-2" and the unresolved broad signal between δ 1.34 and 1.27 corresponds to five methylene protons (H-3"- H-7"). The triplet at δ 0.88 is due to the terminal methyl protons. The disappearance of the signal due to H-5' in the ^{1}H-NMR spectrum of **15** indicated the complete dibromination of the starting material.

The ^{13}C-NMR spectrum of compound **15** (Table 6) revealed fifteen carbon resonances of which eight are in the aromatic region and the remaining seven are in the aliphatic region. From

the aromatic carbon signals two are due to methine carbons and the remaining six resonances represent quaternary carbons. The most downfield signal in the aromatic region is due to the carbonyl carbons which appeared at δ 165.6. The most shielded quaternary carbon signal at δ 118.8 can be attributed to the brominated carbon atoms C-5'.

Table 6: The ^{13}C-NMR (100.6 MHz, $CDCl_3$) data (δ_{ppm}) of compounds **14** and **15**

Carbon	**14**	Carbon	**15**
5, 7	165.8	5, 7	165.6
9, 10	156.5	9, 10	155.9
5'	133.3	4'	134.1
2'	131.6	2'	133.1
4'	130.3	3'	129.8
11, 12	127.0	11, 12	126.3
3'	126.9	4	125.9
4	126.6	5'	118.7
1"	38.9	1"	39.0
2"	31.8	2"	31.8
3", 4"	29.2	3", 4"	29.2
5"	28.3	5"	28.3
6"	27.0	6"	27.0
7"	22.7	7"	22.6
8"	14.1	8"	14.1

4.2. Synthesis of 4,8-bis(5-bromothiophen-2-yl)-2-(2-ethylhexyl)-6-octyl-[1,2,3]triazolo[4,5-*f*]isoindole-5,7(2*H*,6*H*)-dione (19)

Compound **19** was prepared by using modified procedures reported in the literature.[3] Scheme 6 shows the four-step synthesis of **19** starting from **14** whose synthesis was described above. Thus, the reduction of **14** with iron powder in acetic acid afforded the intermediate compound **16** which was subsequently converted to 6-octyl-4,8-di(thiophen-2-yl)-[1,2,3]triazolo[4,5-*f*]isoindole-5,7(2*H*,6*H*)-dione (**17**) by treatment with $NaNO_2$ in acetic acid at room temperature.

The crude product containing tautomers **17** and **17A** was used without further purification in the subsequent reaction step. Alkylation of triazoles **17** and **17A** with 1-bromo-2-ethylhexane in the presence of potassium carbonate in DMF gave a mixture of products which was purified by silica gel column chromatography to afford the symmetrical 2-(2-ethylhexyl)-6-octyl-4,8-di(thiophen-2-yl)-[1,2,3]triazolo[4,5-*f*]isoindole-5,7(2*H*,6*H*)-dione (**18**) in 71% yield. Finally, compound **18** was brominated using *N*-bromosuccinimide in a mixture of chloroform/acetic acid to obtain 4,8-bis(5-bromothiophen-2-yl)-1-(2-ethylhexyl)-6-octyl-4,8-di(thiophen-2-yl)-[1,2,3]triazolo[4,5-*f*]isoindole-5,7(1*H*,6*H*)-dione (**19**) as yellow solid in 57% yield. The structure of monomer **19** was confirmed by its ^{1}H and ^{13}C NMR spectra as discussed below.

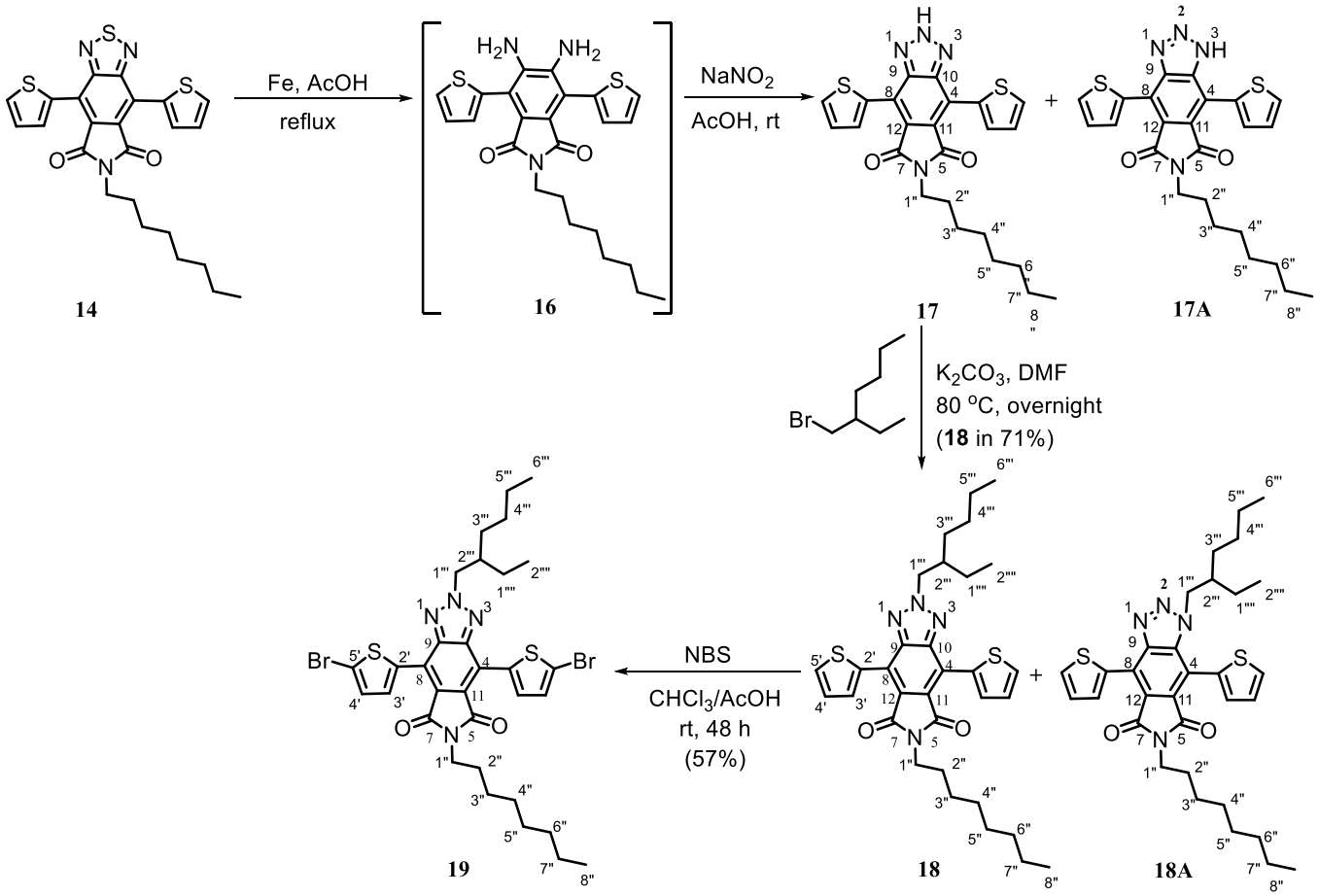

Scheme 6: Synthesis of compounds **17**, **18** and **19**

The ^{1}H NMR spectrum (Table 7) of compound **18** showed three signals in the aromatic region and seven signals in the aliphatic region. The three doublet of doublets at δ 8.14, 7.67 and 7.27 are ascribed to H-3', H-5'and H-4', respectively. The remaining seven signals appeared in the aliphatic region of which the doublet at δ 4.69 and the triplet at δ 3.73 can be due to methylene protons H-1"' and H-1", respectively. The one-proton multiplet at δ 2.25 and the two-proton quintet at δ 1.71 correspond to H-2"' and H-2", respectively. The unresolved signal between δ 1.38 and 1.28 for eighteen protons can be due to the remaining methylene protons on the octyl and ethylhexyl side chains. The signals due to the three terminal methyl protons appeared at δ 1.00 correlating to H-2" and between 0.95-0.87 corresponding to H-6" and 8".

The ^{13}C NMR spectrum (Table 8) of compound **18** displayed twenty-one carbon resonances of which eight are in the aromatic region and the remaining thirteen in the aliphatic region. It was evident from the spectrum that there was some signal overlapping since the total number of carbon resonances expected for compound **18** is twenty-four. The DEPT-135 spectrum revealed the presence of three methine carbon signals in the aromatic region, ten methylene, one methine and three methyl carbon signals in the aliphatic region. The remaining five signals correspond to aromatic quaternary carbon atoms in agreement with the structure of compound **18**.

Table 7: The ^{1}H-NMR (400.13 MHz, $CDCl_3$) data (δ_{ppm}) of compounds **18** and **19**

18	**19**
8.14 (*dd*, *J* = 1.2, 3.8 Hz, 2H, H-3')	8.04 (*d*, *J* = 4.0 Hz, 2H, H-3')
7.67 (*dd*, *J* = 0.8, 5.0 Hz, 2H, H-5')	7.21 (*d*, *J* = 4.0 Hz, 2H, H-4')
7.27 (*dd*, *J* = 4.0, 5.0 Hz, H-4')	4.70 (*d*, *J* = 6.8 Hz, 2H, H-1")
4.69 (*d*, *J* = 6.8 Hz, 2H, H-1"')	3.71 (*t*, *J* = 7.6 Hz, 2H, H-1")
3.73 (*t*, *J* = 7.6 Hz, 2H, H-1")	2.23 (*m*, 1H, H-2"')
2.25 (*m*, 1H, H-2"')	1.69 (*quin*, 2H, H-2")
1.71 (*quin*, 2H, H-2")	1.36-1.27 (unresolved, 18H, H-(3, 4, 5)","', 1"", 6", 7")
1.38-1.28 (unresolved, 18H, H-(3, 4, 5)", "", 1"", 6", 7")	1.00 (*t*, *J* = 7.2 Hz, 3H, H-2"")
1.00 (*t*, *J* = 7.2 Hz, 3H, H-2"")	0.93 (*t*, *J* = 7.2 Hz, 3H, H-6"')
0.95-0.87 (unresolved, 6H, H-6"', 8")	0.88 (*t*, *J* = 7.2 Hz, 3H, H-8")

Table 8: The ^{13}C-NMR (100.6 MHz, $CDCl_3$) data (δ_{ppm}) of compounds **18** and **19**

Carbon	**18**	Carbon	**19**
5	166.6	5	166.5
2’	145.7	9	145.2
5’	133.0	3’	134.0
4	132.2	11	133.8
4’	129.7	4‘	129.8
3’	126.8	4	123.9
11	125.0	2’	123.5
9	123.8	5’	118.0
1”’	60.3	1”’	60.4
2”’	40.4	2”’	40.5
1”	38.5	1”	38.6
2”	31.8	2”	31.8
3”’	30.6	3”’	30.6
3”	29.2	3”	29.2
1””	29.2	1””, 4”	28.4
4”, 4”’	28.4	4”’	27.0
5”	27.1	5”	24.0
5”’	24.0	5”’, 6”	23.0
6”	23.0	7”	22.6
7”	22.7	2””, 6”’	14.1
2””	14.1	8”	10.6
6”’	14.1		
8”	10.6		

The ^{1}H NMR spectrum (Table 7) of compound **19** clearly showed that it is a symmetrical compound and that dibromination took place at the 5’ position of the thiophene rings. Thus, two proton resonances were observed in the aromatic region and eight signals in the aliphatic region. The doublets at δ 8.04 and 7.21 (J = 4.0 Hz) are due to H-3’ and H-4’, respectively. The doublet at δ 4.70 and the triplet at δ 3.71 are due to H-1”’ and H-1””, respectively. The one-proton quintet at δ 2.23 is attributed to H-2”’ and the two-proton multiplet at δ 1.69 corresponds to H-2”. The remaining multiplets between δ 1.36 and 1.27 can be due to the eighteen-proton methylene protons of the two substituted alkyl side chains. The three terminal methyl proton

signals appeared as triplets at δ 1.00, 0.93 and 0.88 corresponding to H-2"", H-6"' and H-8", respectively.

The ^{13}C NMR spectrum (Table 8) of compound **19** showed a total of twenty-one carbon signals of which eight appeared in aromatic region and thirteen in aliphatic region. The signals at δ 134.0 and 129.8 are due to methine carbons as confirmed by the upward appearance of the signals in the DEPT-135 spectrum. The remaining signals in the aromatic region are due to quaternary carbon atoms. The most upfield quaternary carbon signal at δ 118.0 is attributed to C-5' to which the bromine atoms are attached. The aliphatic region of the DEPT-135 spectrum showed ten methylene, one methine and two methyl carbon signals. It was evident from the spectra that some of the carbon signals overlapped. In general, the ^{1}H and ^{13}C NMR data agree very well with the structure of compound **19**.

4.3. Synthesis of 4,8-bis(5-bromothiophen-2-yl)-2,6-dioctyl-[1,2,3]triazolo[4,5-*f*]isoindole-5,7(2*H*,6*H*)-dione (21)

Compound **21** was prepared following the procedures used for compound **19**. Scheme 7 shows the two-step synthesis of **21** starting from a mixture of tautomers **17** and **17A** whose synthesis was described above. Thus, alkylation of triazoles **17** and **17A** with 1-bromooctane in the presence of potassium carbonate in DMF gave a mixture of products which was purified by silica gel column chromatography to afford the symmetrical 2-(octyl)-6-octyl-4,8-di(thiophen-2-yl)[1,2,3]triazolo[4,5-*f*]isoindole-5,7-(2*H*,6*H*)-dione (**20**) in 66% yield. Finally, compound **20** was brominated using *N*-bromosuccinimide in a mixture of chloroform/acetic acid to obtain 4,8-bis(5-bromothiophen-2-yl)-2,6-dioctyl-4,8-di(thiophen-2-yl)-[1,2,3]triazolo[4,5-*f*]isoindole-5,7(1*H*,6*H*)-dione (**21**) as an orange solid in 57% yield. The structure of monomer **21** was confirmed by its ^{1}H and ^{13}C NMR spectra as discussed below.

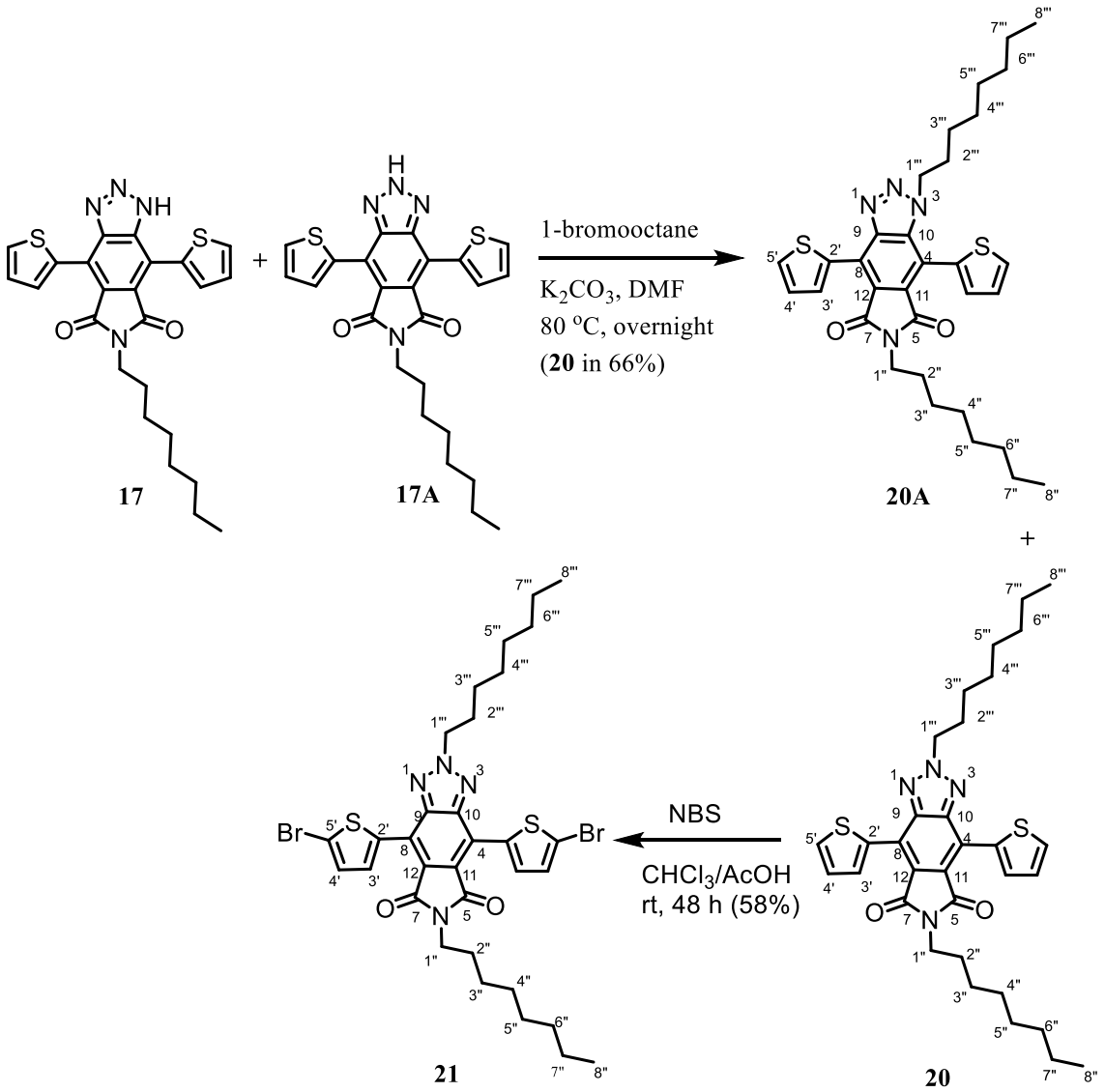

Scheme 7: Synthesis of compounds **20** and **21**

Table 9: The ^{1}H NMR (400.13 MHz, $CDCl_3$) data (δ_{ppm}) of compounds **20** and **21**

20	**21**
8.11	8.03
(*dd*, *J* = 0.8, 3.6 Hz, 2H, H-3')	(*d*, *J* = 4.0 Hz, 2H, H-3')
7.67	7.20
(*dd*, *J* = 1.2, 5.0 Hz, 2H, H-5')	(*d*, *J* = 4.0 Hz, 2H, H-4')
7.27	4.74
(*dd*, *J* = 4.0, 5.2 Hz, 2H, H-4')	(*t*, *J* =7.2 Hz, 2H, H-1"')
4.74	3.69
(*t*, *J* =7.2 Hz, 2H, H-1"')	(*t*, *J* =7.6 Hz, 2H, H-1")
3.72	2.15
(*t*, *J* =7.2 Hz, 2H, H-1")	(*quin*, 2H, H-2"')
2.15	1.68
(*quin*, 2H, H-2"')	(*quin*, 2H, H-2")
1.71	1.41-1.30
(*quin*, 2H, H-2")	(unresolved, 20H, H-(3, 4, 5, 6, 7)", "'
1.39-1.28	0.90-0.88
(unresolved, 20H, H-(3, 4, 5, 6, 7)", "')	(unresolved, 6H, H-8", 8"')
0.90-0.89	
(unresolved, 6H, 8", 8"')	

The ^{1}H NMR spectrum (Table 9) of compound **20** showed three signals in the aromatic region and six signals in the aliphatic region. The three doublet of doublets at δ 8.11, 7.67 and 7.27 are ascribed to H-3', H-5' and H-4', respectively. The remaining six signals appeared in the aliphatic region of which the doublet at δ 4.74 and the triplet at δ 3.72 are due to methylene protons H-1"' and H-1", respectively. The two-proton quintets at δ 2.15 and 1.71 correspond to H-2"' and H-2", respectively. The unresolved signal between δ 1.39 and 1.28 are due to the remaining methylene protons on the two octyl side chains. The signals due to the two terminal methyl protons appeared between δ 0.90 and 0.89.

The ^{13}C NMR spectrum (Table 10) of compound **20** displayed twenty-two carbon resonances eight of which are in the aromatic region and the remaining fourteen in the aliphatic region. It was evident from the spectrum that there was some signal overlapping since the total

number of carbon resonances expected for compound **20** is twenty-four. The DEPT-135 spectrum revealed the presence of three methine carbon signals in the aromatic region and thirteen methylene and one methyl carbon signals in the aliphatic region. The remaining five signals correspond to aromatic quaternary carbon atoms in agreement with the structure of **20**.

Table 10: The ^{13}C-NMR (100.6 MHz, $CDCl_3$) data (δ_{ppm}) of compound **20** and **21**

Carbon	**20**	Carbon	**21**
5, 7	166.5	5, 7	166.4
9, 10	145.8	9, 10	145.2
5’	132.9	4’	134.0
11, 12	132.0	4	133.7
4’	129.6	3’	129.8
3’	126.7	11, 12	123.8
2’	124.9	2’	123.4
4	123.8	5’	118.0
1”’	57.4	1”’	57.5
1”	38.5	1”	38.6
2”’	31.8	2”’	31.8
2”	31.7	2”	31.7
3”’	29.8	3”’	29.8
3”	29.2	3”, 4”’	29.2
4”’	29.1	4”	29.2
4”	29.0	5”’	28.9
5”’	28.9	5”	28.3
5”	28.4	6”’	27.0
6”’	27.0	6”	26.5
6”	26.5	7”, 7”’	22.7
7”, 7”’	22.6	8”, 8”’	14.1
8”, 8”’	14.0		

The ^{1}H NMR spectrum (Table 9) of compound **21** clearly showed that it is a symmetrical compound and that dibromination took place at the 5’ position of the thiophene rings. Thus, two proton resonances were observed in the aromatic region and six signals in the aliphatic region. The doublets at δ 8.03 and 7.20 (J = 4.0 Hz) are due to H-3’ and H-4’, respectively. The two-triplets at δ 4.74 and 3.69 are due to H-1”’ and H-1””, respectively. The one- and two-proton

quintets at δ 2.15 and 1.68 correspond to H-2”’ and H-2”, respectively. The remaining unresolved twenty-proton signals between δ 1.41 and 1.30 can be due to the methylene protons of the two alkyl side chains. The two terminal methyl proton signals appeared as overlapping triplets at δ 0.90 and 0.88.

The ^{13}C NMR spectrum (Table 10) of compound **21** showed a total of twenty-one carbon signals of which eight appeared in aromatic region and thirteen in aliphatic region. The signals at δ 134.0 and 129.8 are due to methine carbons as confirmed by the upward appearance of the signals in the DEPT-135 spectrum. The remaining signals in the aromatic region are due to quaternary carbon atoms. The most upfield quaternary carbon signal at δ 118.0 is attributed to C-5’ to which the bromine atoms are attached. The aliphatic region of the DEPT-135 spectrum showed twelve methylene, one methyl carbon signals. It was evident from the spectra that some of the carbon signals overlapped. In general, the ^{1}H and ^{13}C NMR data agree very well with the structure of compound **21**.

4.4. Synthesis and characterization of the copolymers

As described in section 2.1, in designing D-A type of conjugated polymers donor and acceptor monomers are required. In the course of this work, three different copolymers were synthesized from the synthesized acceptor monomers and commercially available donor monomer and were partially characterized. The synthesis and characterizations of these polymers are described below.

4.4.1. Synthesis of copolymers P5, P6 and P7

Scheme 11 depicts the syntheses of polymers **P5**, **P6** and **P7** by reacting commercially available donor monomer 4,8-bis(5-(2-ethylhexyl)thieno[3,2-*b*]thiophen-2-yl)benzo[1,2-*b*:4,5-

b]dithiophene-2,6-diyl)bis(trimethylstannane) (**30**) with synthesized monomers **15**, **19** and **21**, respectively, using the palladium-catalyzed Stille polycondensation polymerization reaction. The polymers were end-capped with 2-bromothiophene and 2-(tributylstannyl)thiophene.

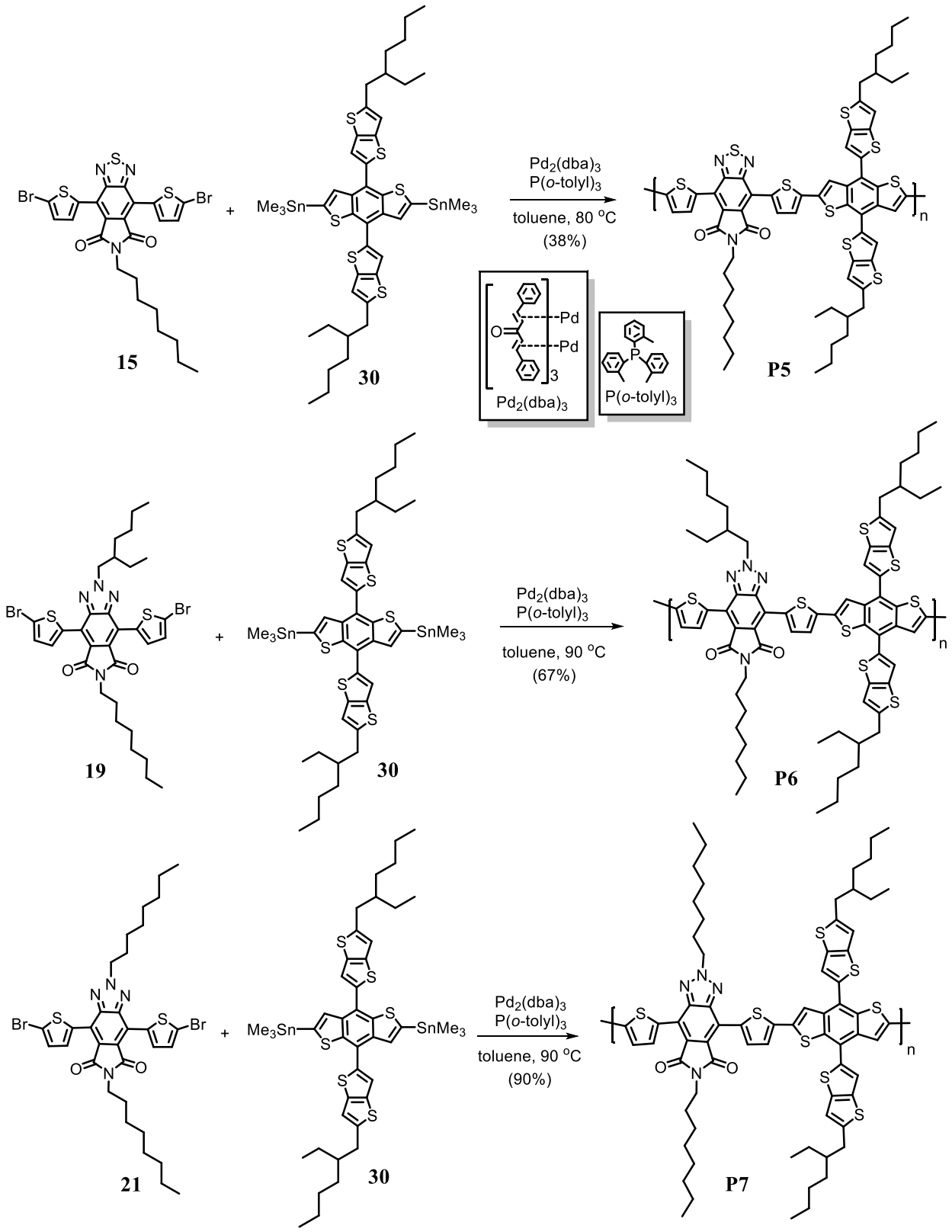

Scheme 11: Synthesis of copolymers **P5**, **P6** and **P7** via Stille polymerization technique

After the reactions were completed, the resulting polymers were precipitated in methanol and purified by Soxhlet extraction with methanol and diethyl ether to remove some residual catalysts and low molecular weight oligomers. Finally, the chloroform extract was collected and further purification was achieved by silica gel column chromatography. the polymers were precipitated from methanol and were collected by membrane filtration and dried in vacuum oven. The colors of **P5**, **P6** and **P7** as solid and in solution were green, navy blue and navy blue while their yields were 38, 67 and 90%, respectively.

4.4.2. Characterization of the copolymers

The electrochemical and optical properties of **P5**, **P6**, **P7** were studied using cyclic voltammetry and UV-vis spectroscopy, respectively. The oxidation potentials of all the polymers were determined under the same experimental conditions to estimate the HOMO energy levels. The LUMO energy levels of the polymers were calculated from the difference between optical band gaps and the HOMO energy levels of the polymers whereas the optical bandgaps of all the polymers were obtained from the onsets of their optical absorption spectra in solid state.

4.4.2.1.Optical properties of copolymers

The UV-Vis spectra of **P5**, **P6**, **P7** were recorded both in solution and as thin films. The thin films were prepared by coating their chloroform solutions on glass plates. The onset absorption wavelengths (λ_{onset}) in the spectra of the thin films were used to calculate the optical band gaps (E_g^{opt}) according to the following equation.

$$E_g^{opt} = hc/\lambda_{onset} = 1240/\lambda_{onset} \qquad (1)$$

Where E_g^{opt} is the optical band gap of the polymers, h is the Planck constant (6.63×10^{-34} m^2kg/s), c is the speed of light (3×10^8 m/s) and λ_{onset} is the onset of optical absorption.

The optical absorption spectra of the polymers **P5**, **P6** and **P7** in chloroform solution and as thin films are shown in Figure 8. Two absorption maxima arising from the π-π* transitions of the polymer backbones and intramolecular charge transfer (ICT) from the donors to the acceptor units are observed in the spectra of the polymers. The absorption maxima at shorter wavelengths are due to the π-π* transitions while the longer wavelength absorption maxima are due to intramolecular charge transfer from donor to the acceptor.[47]

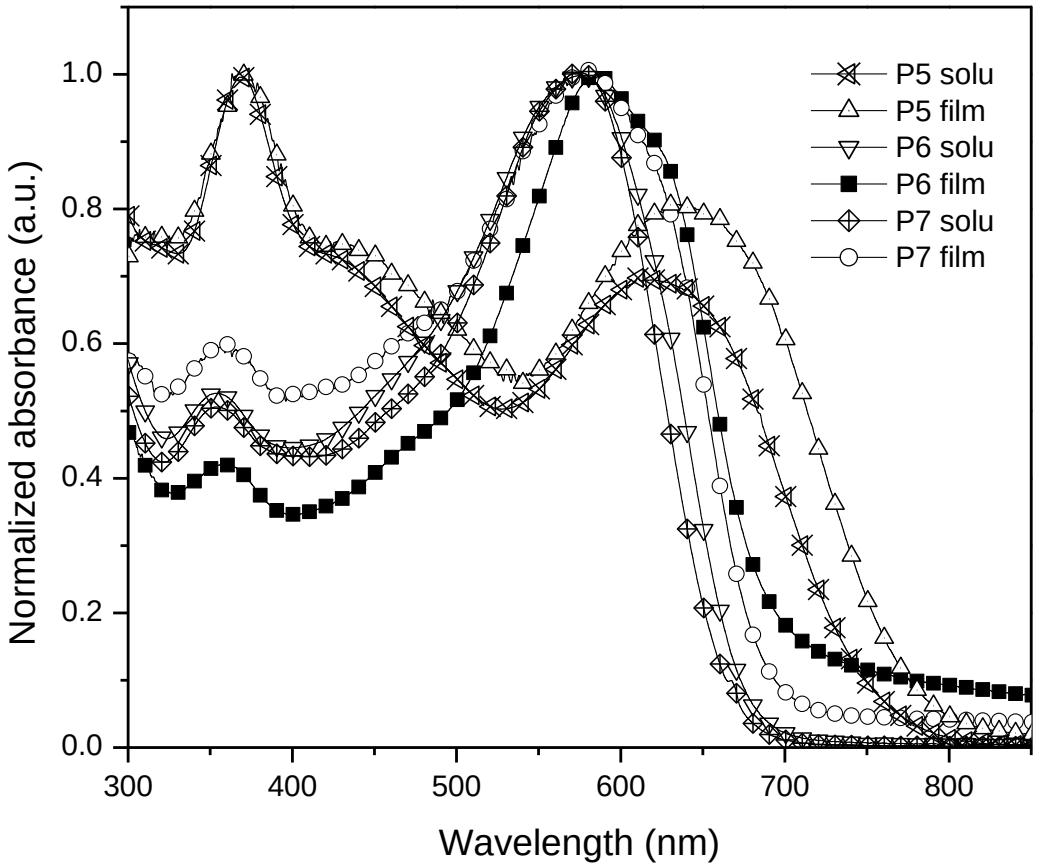

Figure 8: UV-Vis absorption spectra of **P5**, **P6** and **P7** in chloroform solutions and as thin films.

The thin film spectra of **P5**, **P6** and **P7** each showed two absorption maxima at 371 and 636, 359 and 584, and 359 and 581 nm, respectively. The thin film absorptions for all the polymers are red-shifted due to the intermolecular unsaturated bond interactions.[47, 45] However, **P5** is more red-shifted than the other two, because the thiadiazole group is more electron withdrawing than the triazole group.[66] The onsets of absorption in the thin film spectra of **P5**, **P6** and **P7** are 770, 689 and 693 nm and the corresponding E_g^{opt} are 1.61, 1.80 and 1.82 eV, respectively. Table 11 gives a summary of the optical properties of the copolymers.

Table 11: The optical properties of polymers **P5**, **P6** and **P7**

Copolymers	λ_{max} (nm) in solution	λ_{max} (nm) in film	λ_{onset} (nm)	E_g^{opt} (eV)
P5	369, 616	371, 636	770	1.61
P6	353, 576	359, 584	689	1.80
P7	353, 575	359, 581	683	1.82

4.4.2.2.Electrochemical properties of the copolymers

The electrochemical properties of **P5**, **P6** and **P7** were studied by cyclic voltammetry (CV), a technique that is used to determine the oxidation and reduction potential values of the polymers. These values could be used to determine the bandgap between the HOMO and LUMO of the polymers.[67] Generally, the oxidation process corresponds to the removal of electron from the HOMO energy level, while the reduction corresponds to an electron addition to the LUMO energy level of the polymer. As such, the HOMO and LUMO energy levels of the polymers could be determined from the onset potentials of oxidation (E_{ox}) and optical bandgaps, respectively. The onset potential of oxidation can be correlated to the HOMO according to the empirical relationship proposed by Bredas e*t al*.[64]

$$E_{HOMO} = -(E_{ox} + 4.4)\ (eV) \quad (2)$$

$$E_{LUMO} = (E_{HOMO} + E_g^{opt}) \quad (3)$$

The onset potentials are determined from the intersection of the two tangents drawn at the rising current and baseline charging current of the CV traces.

In a typical voltammetric experiment, potential is applied using a three-electrode system with platinum disk as the working electrode, platinum wire as the counter or auxiliary electrode and silver wire as the reference electrode. The current response is measured using the working electrode and counter electrode. Polymer films of **P5**, **P6** and **P7** were dissolved in chloroform and coated on platinum working electrode which was immersed in a supporting electrolyte of 0.1 M tetrabutylammoniumtetrafluoroborate (Bu_4NF_4B) in acetonitrile and were measured at a scanning rate of 100 mV/*s*.

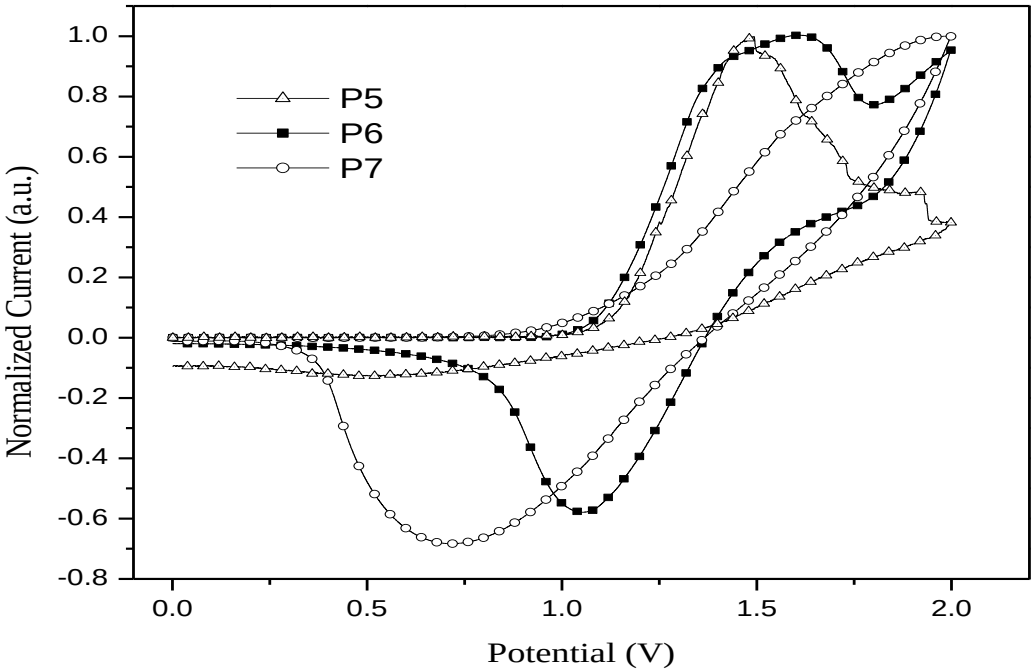

Figure 9: Cyclic voltammograms of the oxidation of **P5**, **P6** and **P7**

As shown in Figure 9, the oxidation potentials of **P5**, **P6** and **P7** occurred at 1.09, 1.05 and 0.90 V which correspond to HOMO energy levels of -5.49, -5.45 and -5.30 eV, respectively. The LUMO energy levels of **P5**, **P6** and **P7** were calculated to be -3.88, -3.65 and -3.48 eV, respectively, from their HOMO energy levels and their optical band gaps. Figure 10 shows the energy levels of the polymers.

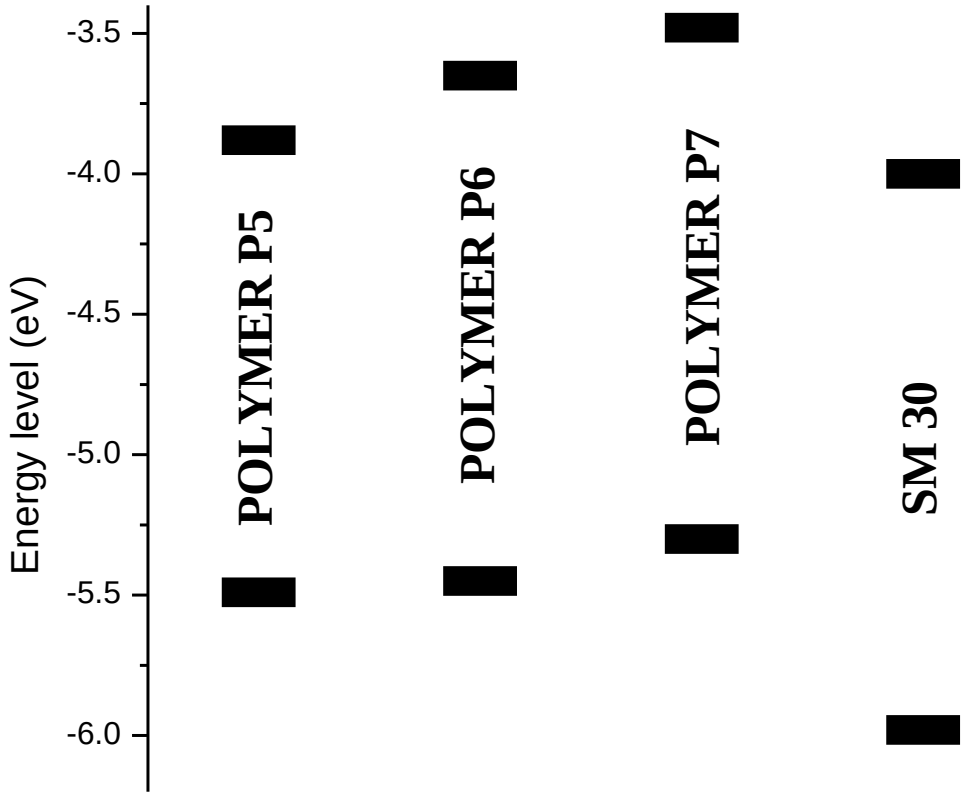

Figure 10: Energy level diagram of **P5**, **P6**, **P7** and **SM 30**

4.5. Synthesis of PDI-based acceptor 11,11'-(9,9'-spirobi[fluorene]-2,7-diyl)bis(2,8-bis(2-ethylhexyl)-1*H*-pyrido[3',4',5':4,5]naphtho[2,1,8-*cde*]pyrido[3',4',5':4,5]naphtho[8,1,2-*ghi*]isoindole-1,3,7,9(2*H*,5*H*,8*H*)-tetraone) (30)

The synthesis of compound **30** was started with perylene-3,4,9,10-tetracarboxylic dianhydride (**1**) following the reported procedures.[57, 68, 58] Thus, compound **22** was aminated with 1-amino-2-ethylhexane (**23**) as shown in Scheme 8 to furnish **24**. Compound **24** was obtained in 86% yield as a red pink powder. Then compound **24** was converted to **25** through nitration reaction with fuming nitric acid as depicted in Scheme 9. Compound **25** was obtained in 66% yield as a red powder. The structures of **24** and **25** were confirmed by ^{1}H and ^{13}C NMR spectra.

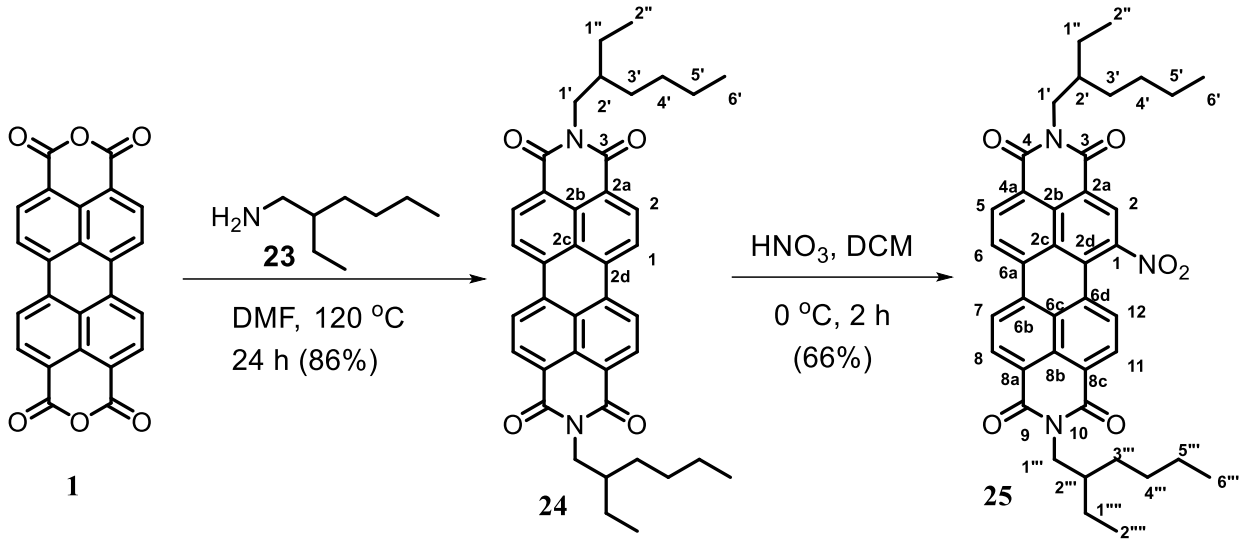

Scheme 8: Synthesis of compounds **24** and **25**

The ^{1}H NMR spectrum (Table 12) of compound **24** clearly showed that it is a symmetrical compound and that it was diaminated. Thus, two proton resonances were observed in the aromatic region and five signals in the aliphatic region. The doublets at δ 8.59 and 7.48 are due to H-1 and H-2, respectively. The multiplet at δ 4.15 and the broad singlet at δ 1.98 are due to H-1' and H-2', respectively. The broad overlapping peaks between δ 1.42 and 1.35 are due to the methylene protons of the side chains and the two methyl signals appeared as overlapping triplets at δ 0.98 and 0.92.

The ^{13}C NMR spectrum (Table 13) of compound **24** showed a total of fifteen carbon signals, seven of which appeared in the aromatic region and eight in aliphatic region. The most downfield signal at δ 163.6 is due to the carbonyl carbon. The signals at δ 131.3 and 123.0 are aromatic methine carbons confirmed by the upward appearance of the signals in the DEPT-135 spectrum. The remaining signals in the aromatic region are due to quaternary carbon atoms. The aliphatic region of the DEPT-135 spectrum showed one methine, five methylene, and two methyl

carbon signals. In general, the ^{1}H and ^{13}C NMR data agree very well with the structure of compound **24**.

The ^{1}H NMR spectrum (Table 12) of compound **25** clearly showed the loss of symmetry of the starting material. Thus, seven proton resonances were observed in the aromatic region and four signals in the aliphatic region. The aromatic doublets at δ 8.74, 8.69, 8.65, 8.63, 8.55 and 8.16 are due to H-5, H-11, H-8, H-6, H-7 and H-12, respectively, while the singlet at δ 8.66 overlapping with the doublet at δ 8.65 is due to H-2. The multiplet at δ 4.15 and the broad singlet at δ 1.95 are due to H-1' and H-2', respectively. The broad overlapping peaks between δ 1.40 and 1.33 are due to the methylene protons of the side chains and the two methyl signals appeared as overlapping triplets at δ 0.97 and 0.92.

Table 12: The ^{1}H NMR (400.13 MHz, $CDCl_3$) data (δ_{ppm}) of compounds **24** and **25**

24	**25**
8.59 (*d*, *J* = 7.6 Hz, 4H, H-1) 8.48 (*d*, *J* = 8.0 Hz, 4H, H-2) 4.15 (*m*, 4H, H-2') 1.42-1.35 (unresolved, 16H, H-3', 4', 5', 1") 0.98 & 0.92 (overlapping triplets, 12H, H-6', H-2")	8.74 (*d*, *J* = 8.0 Hz, 1H, H-6) 8.69 (*d*, *J* = 8.0 Hz, 1H, H-5) 8.66 (*s*, 1H, H-2) 8.65 (*d*, *J* = 7.2, 1H, H-11) 8.63 (*d*, *J* = 8.4 Hz, 1H, H-7) 8.55 (*d*, *J* = 8.4,1H, H-8) 8.16 (*d*, *J* = 8.0, 1H, H-12) 4.15-4.14 (unresolved, 4H, H-1', H-1"') 1.95 (unresolved, 2H, H-2', H-2"') 1.40-1.33 (unresolved, 16H, H-1", 1"",((3, 4, 5)'),"") 0.97 (*t*, *J* = 7.2 Hz, 6H, H-2", H-2"") 0.92 (*t*, *J* = 6.8 Hz, 6H, H-6', H-6"')

The ^{13}C NMR spectrum (Table 13) of compound **25** showed a total of thirty-seven carbon signals, twenty-four of which appeared in the carbonyl and aromatic region and twelve in the aliphatic region. The most downfield signals are due to the four carbonyl carbons. Seven of the methine carbons are in the aromatic region as confirmed by the upward appearance of the signals in the DEPT-135 spectrum. The remaining signals in the aromatic region are due to quaternary carbon atoms. The aliphatic region of the DEPT-135 spectrum showed two methine, six overlapping methylene, and three methyl carbon signals with one overlap. In general, the ^{1}H and ^{13}C NMR data agree very well with the structure of compound **25**.

Table 13: The ^{13}C-NMR (100.6 MHz, $CDCl_3$) data (δ_{ppm}) of compounds **24** and **25**

Carbon	**24**	Carbon	**25**
3, 4	163.6	3	163.3
2a	134.3	4	163.0
2	131.3	10	162.9
2b	129.3	9	162.1
2c	126.2	1	147.5
2d	123.2	2d	135.4
1	123.0	2	132.8
1’	44.4	2a	132.8
2’	38.0	5	131.4
1”	30.8	11	131.2
3’	28.7	4a	129.2
4’	24.1	8c	129.1
5’	23.1	8a	128.8
2”	14.1	12	127.9
6’	10.7	2b	127.4
		2c	126.5
		8	126.3
		8b	126.3
		6d	124.8
		6	124.5
		7	124.0
		6c	124.0
		6b	123.8
		6a	123.0
		1’	44.6
		1”’	44.5
		2’	38.0
		2”’	37.9
		1”, 1””	30.7
		3’	28.7
		3”’	28.7
		4’, 4”’	24.0
		5’	23.1
		5”’	23.1
		2”, 2””	14.1
		6”	10.6
		6”’	10.6

Compound **25** was transformed to compound **26** by modified Cadogan[68] reaction with PPh_3 in refluxing *o*-DCB as shown in Scheme 9. The first attempt to conduct the reaction in

DMF did not give the desired product. Compound **26** was obtained in 89% yield as a red powder. Due to its poor solubility, not even proton NMR analysis was possible.

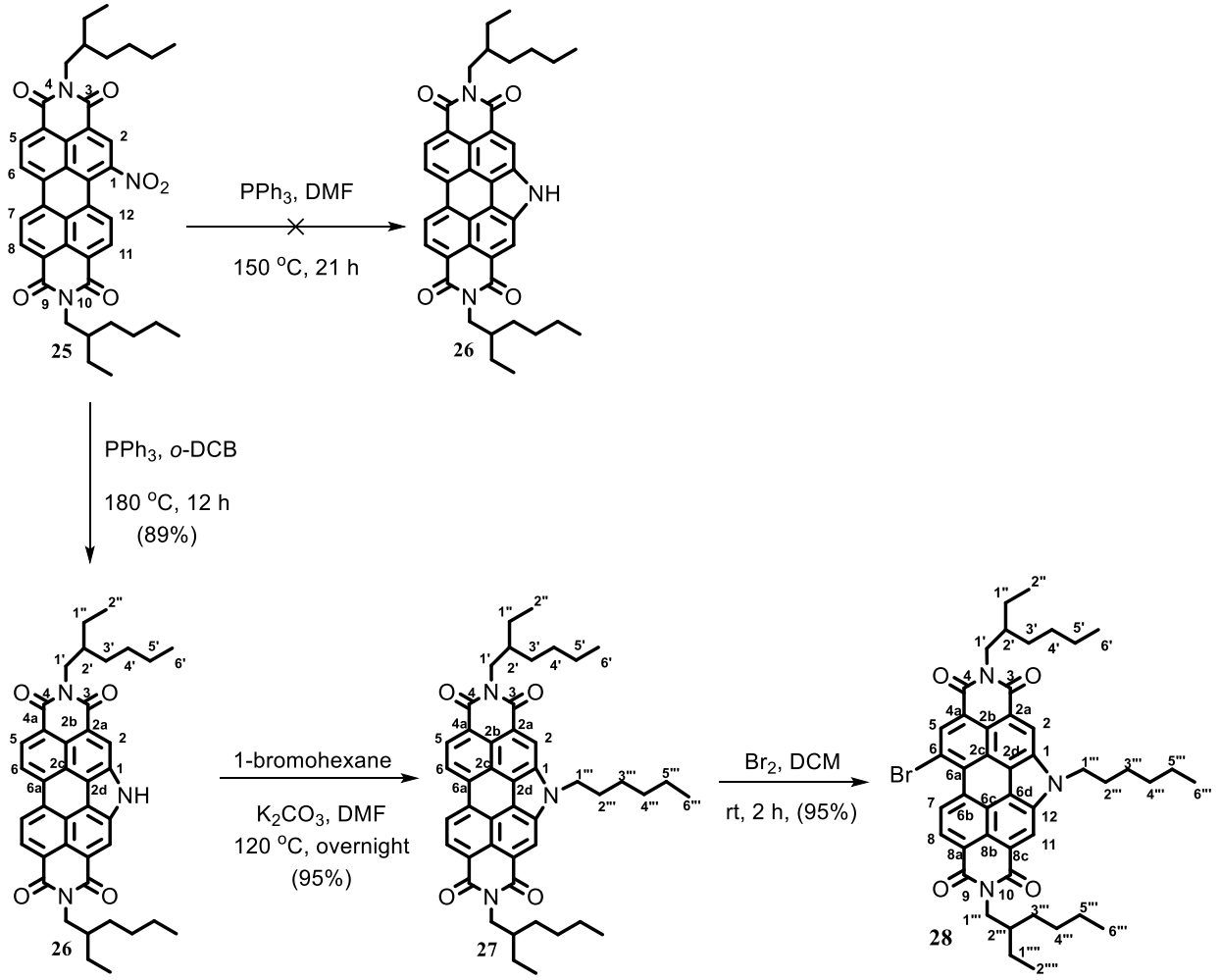

Scheme 9: Synthesis of compounds **26**, **27** and **28**

Compound **26** was then alkylated with 1-bromohexane in the presence of potassium carbonate in DMF to afford compound **27** in 95% yield as a red power whose structure was confirmed via ^{1}H and ^{13}C NMR spectra.

Compound **27** then underwent bromination with molecular bromine in DCM to give compound 2**8** in 95% yield as a dark red powder whose structure was confirmed via ^{1}H and ^{13}C NMR spectra.

The ^{1}H NMR spectrum (Table 14) of compound **27** clearly showed that it is a symmetrical compound. Thus, three proton resonances were observed in the aromatic region and eight signals in the aliphatic region. The singlet at δ 8.60 belongs to H-2 while the doublets at δ 8.45 and 8.42 (J = 8.0 Hz) are due to H-5 and H-6, respectively, which couple with each other. The multiplet at δ 4.22 corresponds to H-1'. The quintets at δ 2.11 and 2.0 correspond to H-2' and H-2"', respectively. The broad unresolved methylene proton signals at δ 1.47-1.39 integrating for 22 protons belong to H-(3, 4, 5)', 1" and (3, 4, 5)"'. The triplets at δ 1.01, 0.94 and 0.87 are due to methyl protons at C-2", C-6' and C-6"', respectively.

The ^{13}C NMR spectrum (Table 15) of compound **27** showed a total of twenty-six carbon signals, two of which appeared in the carbonyl region, ten in the aromatic region and fourteen in the aliphatic region where seven of them are due to quaternary carbon atoms. The two most downfield signals at δ 165.0 and 163.7 are due to carbonyl carbons corresponding to C-3 and 4. The signals at δ 126.9, 123.0 and 118.0 are due to aromatic methine carbons as confirmed by the upward appearance of the signals in the DEPT-135 spectrum. The remaining signals in the aromatic region are due to quaternary carbon atoms. The aliphatic region of the DEPT-135 spectrum showed one methine, ten methylene, and three methyl carbon signals. In general, the ^{1}H and ^{13}C NMR data agree very well with the structure of compound **27**.

The ^{1}H NMR spectrum (Table 14) of compound **28** clearly showed that it has an unsymmetrical structure. Thus, five proton resonances were observed in the aromatic region and

seven signals in the aliphatic region. The aromatic doublets at δ 9.17 and 8.16 (J = 8 Hz) couple with each other and correspond to H-8 and H-7, respectively. The three singlets at δ 8.58, 8.51 and 8.23 correspond to H-5, H-2 and H-11, respectively. The signal at δ 4.73 belongs to H-1’’’’ while the unresolved multiplet from δ 4.27- 4.07, accounting for two protons, belongs to H-1’ and H-1’’’, respectively. The three unresolved signals at δ 2.11, 2.01 and 1.92 accounting for 2H, 1H and 1H belong to methylene protons H-2’’’’, H-2’ and H-2’’’, respectively. The broad unresolved signal around δ 1.42, accounting for 22H of methylene protons, is assigned to H-(3, 4, 5)’,’’’, H-(1)’’,’’’’ and H-(3, 4, 5)’’’’. Finally, the broad unresolved signals around δ 1.03 and 0.90, accounting for 15H of methyl protons, belong to H-6’,2’’, 6’’’’, 6’’’ and 6’’’’.

The ^{13}C NMR spectrum (Table 15) of compound **28** showed a total of forty-five carbon signals, four of which appeared in the carbonyl region, twenty in the aromatic region and twenty-one in the aliphatic region. In the aromatic region five of the signals at δ 133.1, 126.2, 125.9, 117.3 and 117.2 were due to methine carbons while the remaining fifteen signals were quaternary carbons. The aliphatic region of the DEPT-135 spectrum showed one signal due to methine, fifteen due to methylene and the remaining five due to methyl carbons. In general, the ^{1}H and ^{13}C NMR data agree very well with the structure of compound **28**.

Table 14: The ^{1}H NMR (400.13 MHz, $CDCl_3$) data (δ_{ppm}) of compounds **27** and **28**

27	**28**
8.60 (*s*, 2H, H-2) 8.45 (*d*, *J* = 8.0 Hz, 2H, H-5) 8.42 (*d*, *J* = 8.0, 2H, H-6) 4.72 (*t*, *J*= 7.2 Hz, 2H, H-1”’) 4.22 (*m*, 4H, H-1’) 2.11 (*quin*, 2H, H-2’) 2.00 (*m*, 2H, H-2”’) 1.47-1.39 (unresolved, 22H, H-(3, 4, 5)’, 1”, (3, 4, 5)”’ 1.01 (*t*, *J* = 7.2 Hz, 6H, H-2”) 0.94 (*t*, *J* = 7.2 Hz, 6H, H-6’) 0.87 (*t*, *J* = 7.2 Hz, 3H, H-6”’)	9.17 (*d*, *J* = 8.0 Hz, 1H, H-8) 8.58 (*s*, 1H, H-2) 8.51 (*s*, 1H, H-11) 8.23 (*s*, 1H, H-5) 8.16 (*d*, *J* = 8.0 Hz, 1H, H-7) 4.73 (*t*, *J* = 6.8 Hz, 2H, H-1””’) 4.27-4.07 (unresolved, 4H, H-1’, 1”’) 2.11 (unresolved, 2H, H-2””’) 2.01 (unresolved, 1H, H-2’) 1.92 (unresolved, 1H, H-2”’) 1.42 (unresolved, 22H, H-(3, 4, 5)’,”’, H-1”, 1””, H-(3, 4, 5)””’ 1.03-0.90 (unresolved, 15H, H-(6)’, ”, ”’, ””’, H-2””)

Table 15: The ^{13}C-NMR (100.6 MHz, $CDCl_3$) data (δ_{ppm}) of compounds **27**, **28** and **30**

Carbon	**27**	Carbon	**28**	Carbon	**30**
C-3	165.0	C-3	164.7	3	165.4
C-4	163.7	C-10	164.3	4	165.4
C-1	134.1	C-4	163.3	10	164.1
C-2a	131.7	C-9	162.2	9	163.8
C-2	126.9	C-1	133.6	12	150.8
C-4a	123.7	C-12	133.5	1	147.3
C-5	123.0	C-2	133.1	10a	142.4
C-2b	121.8	C-2a	130.7	2a	141.8
C-2c	121.1	C-4a	128.7	8a	141.5
C-2d	120.8	C-8a	126.2	4a	134.6
C-6a	118.4	C-8c	126.0	2e	134.2
C-6	118.0	C-2d	123.0	2d	133.1
C-1”’	46.8	C-6d	122.0	7	131.2
C-1’	44.5	C-2b	121.9	2b	130.1
C-2’	38.2	C-8b	121.8	2	128.7
C-2”’	31.5	C-2c	121.2	8b	128.7
C-3’	31.3	C-8b	121.1	11	128.3
C-3”’	30.9	C-2c	121.0	5	128.0
C-4’	28.8	C-8b	120.6	6c	127.7
C-4”’	26.8	C-6a	120.3	8	127.7
C-1”	24.1	C-7	117.3	18	127.2
C-5’	23.1	C-8	117.2	14	125.0
C-5”’	22.4	C-6b	117.1	2c	124.1
C-2”	14.1	C-6	116.9	15	123.9
C-6’	13.9	C-1”””’	46.9	6b	123.5
C-6”’	10.7	C-1’	44.6	6a	122.7
		C-1”’	44.5	19	122.5
		C-2’	38.3	6	122.5
		C-2”’	38.2	13	122.0
		C-2”””’	31.4	16	121.9
		C-3’	31.3	17	120.9
		C-3”’	30.9	24	120.8
		C-1”	30.8	20	120.0
		C-3”””’	28.8	23	119.4
		C-4’	28.7	21, 22	117.9
		C-4”’, 4”””’	26.9	25	66.2
		C-5’	24.2	1”””’	46.8
		C-5”’	24.1	1”’	44.5
		C-5”””’	23.2	1’	44.4
		C-5”’	23.1	2’, 2”’	38.2
		C-2””	22.5	2”””’	31.4
		C-2”	14.2	1””	31.4
		C-6”””’	14.0	1”	30.9

	C-6’’’	10.7	3’’’’’	29.7
	C-6’	10.6	3’’’	28.8
			3’	28.7
			4’’’’’	26.8
			4’’’	26.8
			4’	24.2
			5’’’’’	23.2
			5’’’	23.1
			5’	22.5
			2’’’’	14.2
			2’’	14.2
			6’’’’’	13.9
			6’’’	13.9
			6’	10.8

Compound **28** reacted with the organoboron ester 2,7-bis(4,4,5,5-tetramethyl-1,3,2-dioxaborolan-2-yl)-9,9'-spirobi[fluorene] (**29**) in the presence of $Pd(PPh_3)_4$ as catalyst, K_2CO_3 as base and dry DMF as a solvent to afford pink-red small molecule **30** as depicted in Scheme 10.

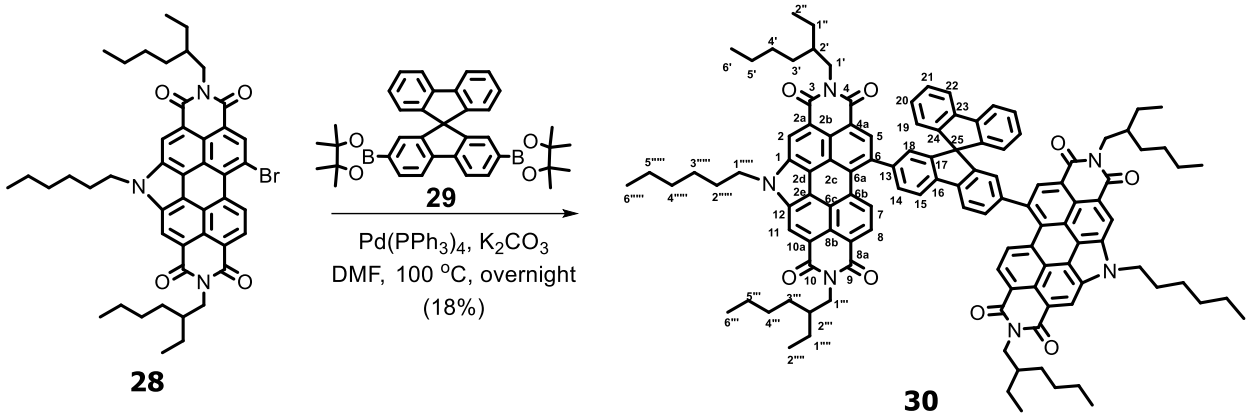

Scheme 10: Synthesis of small molecule **30**

The ^{1}H NMR spectrum (Table 16) of compound **30** showed 18 proton resonances, twelve of which are aromatic while six belong to the aliphatic region. There were four singlets, six doubles and two triplets in the aromatic region. Most of the signals in the aliphatic region were unresolved.

Table 16: The ^{1}H NMR (400.13 MHz, $CDCl_3$) data (δ_{ppm}) of compound **30**

30
8.93 (*s*, 2H, H-11)
8.87 (*s*, 2H, H-2)
8.69 (*s*, 2H, H-5)
8.47 (*d*, *J* = 8.0 Hz, 2H, H-7)
8.35 (*d*, *J* = 8.8 Hz, 2H, H-8)
8.00 (*d*, *J* = 8.4 Hz, 2H, H-14)
7.90 (*d*, *J* = 7.2 Hz, 2H, H-15)
7.45 (*d*, *J* = 7.2 Hz, 2H, H-19)
7.33 (*t*, *J* = 7.6 Hz, 2H, H-20)
7.21 (*d*, *J* = 7.6 Hz, 2H, H-22)
7.13 (*t*, *J* = 7.2, 7.2 Hz, H-21)
7.09 (*s*, 2H, H-18)
4.84 (*t*, *J* = 6.8 Hz, 4H, H-1’’’’’)
4.23 (unresolved, 8H, H-1’)
2.16 (unresolved, 4H, H-2’’’’’)
2.02-2.01 (unresolved, 4H, H-2’)
1.45-1.27 (unresolved, 44H, H-(3, 4, 5)’,’’’,’’’’’, (1)’’,’’’’
0.99-0.86 (unresolved, 30H, H-(2’’, 2’’’’, 6’, 6’’’, 6’’’’’)

The ^{13}C NMR spectrum (Table 15) of compound **30** showed a total of fifty-seven carbon signals with four in the carbonyl, thirty-one in the aromatic and twenty-two in the aliphatic regions. Twenty-four signals were due to aromatic quaternary carbons, while eleven signals belonged to aromatic methine carbons with one overlap. The aliphatic region had one quaternary, one methine, fifteen methylene and five methyl carbon resonances. In general, the ^{1}H and ^{13}C NMR data agree with the structure of compound **30**.

4.5.1. Optical and electrochemical property of PDI-based small molecule 30

The UV-Vis spectra of small molecule **30** (Figure 11) showed absorptions between 400-600 nm with two absorption maxima at 554 and 513 nm due to 0-0 and 0-1 electronic transitions, respectively, typical of PDI molecules.[57, 58] The thin-film absorption is red-shifted as a consequence of greater intermolecular interactions in the solid state. The onset of absorption in the thin film spectrum is 625 nm which gives a bandgap of 1.98 eV.

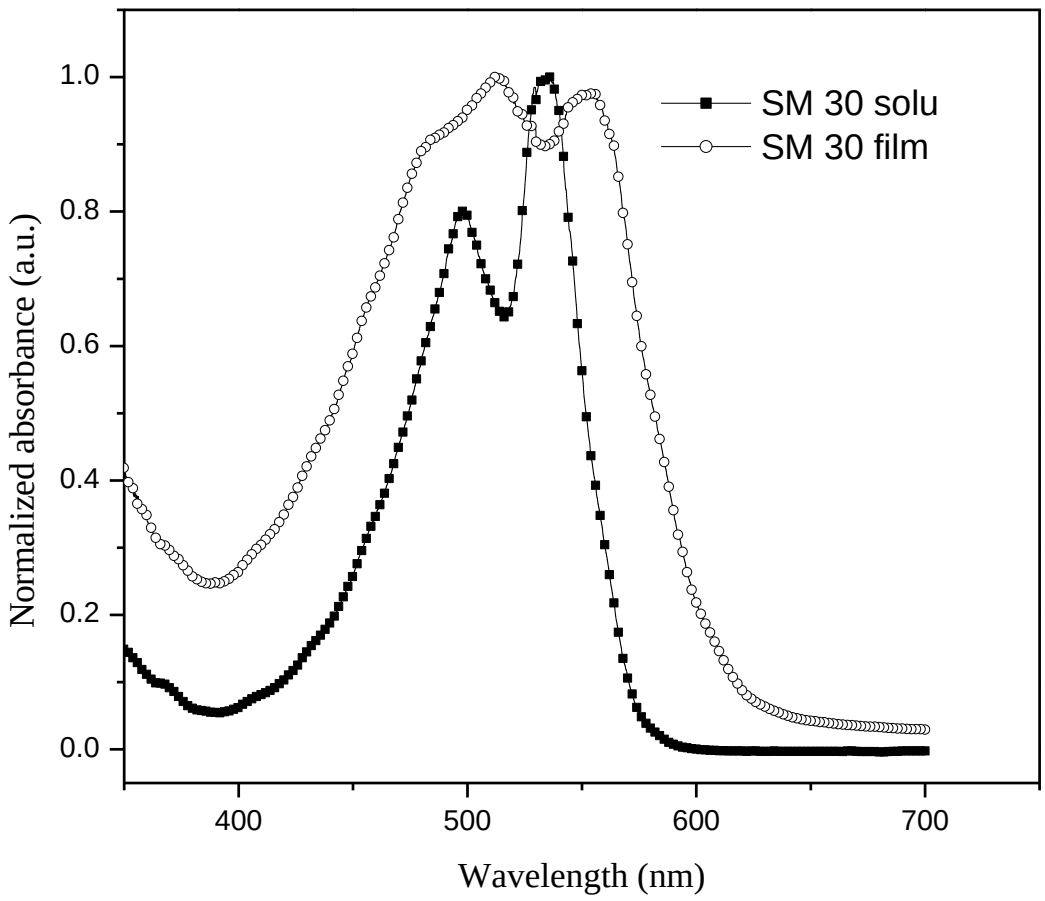

Figure 11: UV-Vis absorption spectrum of small molecule (SM) **30** in solution and as thin film

The electrochemical analysis (Figure 12) of small molecule **30** gave an onset oxidation potential of 1.58 V which corresponds to a HOMO energy level of -5.98 eV. The LUMO energy level was calculated to be -4.00 eV from the HOMO energy level and the optical bandgap. The energy level of small molecule **30** is shown in Figure 10.

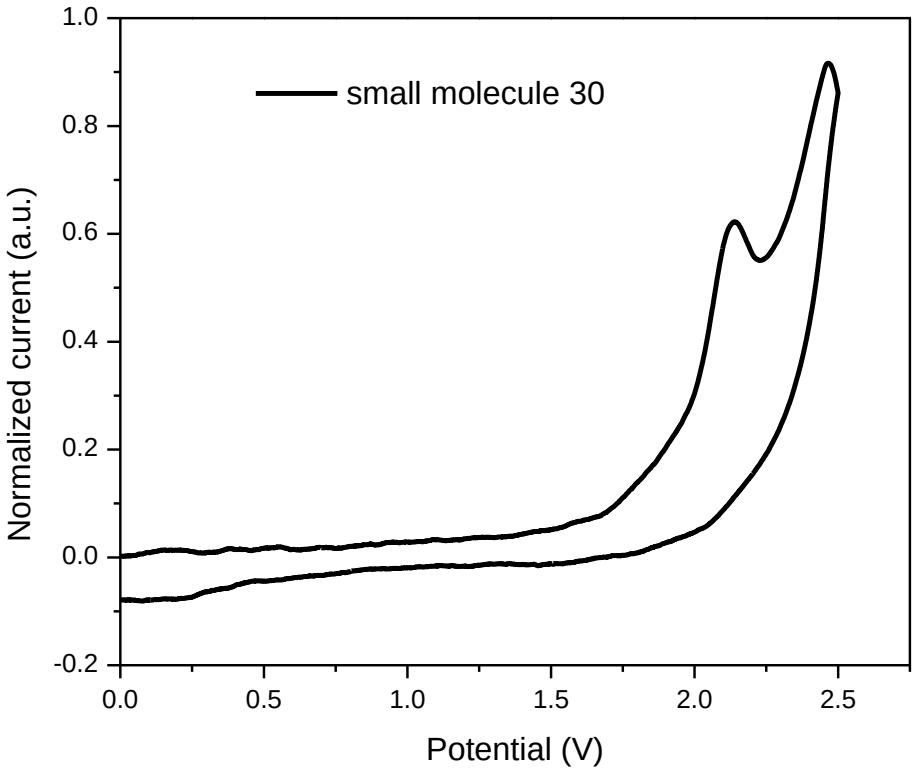

Figure 12: Cyclic voltammogram of small molecule **30**

5. CONCLUSION

Conjugated polymers have been studied in great detail due to their potential applications in various organic electronic devices. In this regard benzotriazole- and benzothiadiazole-based materials have been investigated extensively because of their many attractive properties. In addition, in recent years, nonfullerene acceptors have been researched to overcome the drawbacks of fullerene-based acceptors while possessing their great qualities. PDI-based acceptors have shown potential in replacing fullerene-based acceptors. In the course of this work, three acceptor monomers were synthesized starting from 2,5-dibromothiophene and a small

molecule acceptor was synthesized from perylene-3,4,9,10-tetracarboxylic dianhydride. The monomers were copolymerized with benzodithiophene-based donor monomer to afford three pyrrolobenzotriazoledione- and pyrrolobenzothiadiazoledione-containing copolymers. The polymerization reactions were conducted using the palladium-catalyzed Stille polymerization technique. The resulting polymers had good solubility in chloroform. The optical bandgaps of **P5**, **P6** and **P7** were estimated from their thin-film UV-Vis absorption spectra to be 1.61, 1.80 and 1.82 eV, respectively. The HOMO and LUMO levels of **P5**, **P6** and **P7** were determined to be -5.49 and -3.88, -5.45 and -3.65, and -5.30 and -3.48 eV, respectively. On the other hand, the PDI-based small molecule **30** exhibited an optical band gap of 1.98 eV with HOMO and LUMO energy levels of -5.98 and -4.00 eV, respectively. The physical properties of all the polymers and the small molecule along with their possible application in organic solar cell devices will be studied in collaboration with laboratories specializing in characterization of polymers.

6. EXPERIMENTAL SECTION

6.1. Materials and Methods

All the intermediates, the monomers and small molecule acceptor prepared in the course of this work were purified mainly by silica gel column chromatography but also by recrystallization or filtration and characterized by NMR spectrometry, UV-Vis spectrometry and cyclic voltammetry. ^{1}H NMR, ^{13}C NMR and DEPT-135 spectra where recorded on a Bruker Avance 400 MHz spectrometer at 400.13 and 100.6 MHz, respectively, with $CDCl_3$ and DMSO-d_6 as solvents. ^{1}H and ^{13}C chemical shifts (δ) are reported in ppm downfield from the tetramethylsilane (TMS) reference using the residual protonated solvent resonance as an internal standard. The coupling constants are reported in hertz (Hz). Splitting patterns are designated as *s* (singlet), *d* (doublet), *t* (triplet), *m* (multiplet), *p* (pentate) or *quin* (quintet). Analytical thin layer chromatographic experiments were performed on Merck 0.25 mm silica gel 60 F_{254} pre-coated plates on aluminum. Visualization was accomplished by an ultraviolet lamp (254 and 365 nm). Column chromatography was conducted using silica gel as a stationary phase using different kinds of solvents as eluents. All starting materials were purchased from commercial sources (Aldrich, Fisher, Fuka) and were used without further purification. The polymers were purified by Soxhlet extraction using methanol and diethyl ether. The high molecular weight polymers were extracted with chloroform and *o*-DCB. The chloroform and *o*-DCB solutions of the polymers were further purified by passing them through short columns of silica gel. Purified polymers were collected by membrane filtration (PTFE 0.45 μm). Cyclic voltammetric (CV) measurements were carried out on CH-Instruments 650A Electrochemical Workstation. UV-Vis absorption spectra were recorded on a Perkin-Elmer Lamda 950 UV-Vis-NIR spectrometer and T60 UV-Visible spectrophotometer.

6.2. Reagents

The following chemicals were used: acetic anhydride, 2,5-dibromothiophene, 2-(tributylstannyl)thiophene, tri(*o*-tolyl)phosphine, tris(dibenzyideneacetone)dipalladium(0), toluene, sodium hydroxide, *N*-thionyl aniline, trimethylsilyl chloride, pyridine, fuming nitric acid, fuming sulfuric acid, dimethyl acetylenedicarboxylate, *o*-xylene, xylene, ethanol, methanol, *n*-octylamine, acetic acid, iron, tin chloride, concentrated hydrochloric acid, sodium nitrite, potassium carbonate, DMF, 1-bromo-2-ethylhexane, 1-bromooctane, $MgSO_4$, Na_2SO_4, chloroform, NBS, dichloromethane, 2-ethyl-1-hexylamine, 2-bromothiphene, dimethylsulfoxide, petroleum ether, hexane, *o*-DCB, bromine, concentrated sulfuric acid, isopropanol, diethyl ether, *n*-pentane, 4,8-bis(5-(2-ethylhexyl)thieno[3,2-*b*]thiophen-2-yl)benzo[1,2-*b*:4,5-*b'*]dithiophene-2,6-diyl)bis(trimethylstannane), perylene-3,4,9,10-tetracarboxylic dianhydride, and 2,7-bis(4,4,5,5-tetramethyl-1,3,2-dioxaborolan-2-yl)-9,9'-spirobi[fluorene].

6.3. Synthetic procedures

6.3.1. Synthesis of 2,5-dibromo-3,4-dinitrothiophene (6)[62]

2,5-Dibromothiophene (**5**) (22.4 g, 92.7 mmol) was added slowly into an ice cold solution of conc. H_2SO_4 (30 mL), fuming H_2SO_4 (66 mL) and fuming HNO_3 (41 mL) while monitoring the reaction mixture temperature not to exceed 20 ^oC. After complete addition, the reaction was allowed to proceed for 20 h at room temperature. After TLC monitoring indicated complete consumption of the reactant, the reaction mixture was slowly poured into ice. The precipitate was filtered and washed with water several times to afford compound **6** (17.4, 56.4%) which was a pale yellow powder. ^{13}C NMR (100.6 MHz, $CDCl_3$) δ(ppm): 140.7 and 113.4.

6.3.2. Synthesis of 2,5-bis(2-thienyl)-3,4-dinitrothiophene (7)[62]

Under nitrogen atmosphere, 2,5-dibromo-3,4-dinitrothiophene (**6**) (14.0 g, 42.2 mmol), Pd $(PPh_3)_2Cl_2$ (0.59 g, 0.84 mmol) and dried toluene (152 mL) were refluxed and 2-tributylstannylthiophene was added drop-wise and allowed to react overnight. After TLC monitoring (1:1 *n*-pentane/toluene) indicated complete consumption of the reactant, the cooled reaction mixture was concentrated via rotary evaporator, and the resulting brown residue was slurried with *n*-pentane, filtered and washed with *n*-pentane several times. The crude solid was further purified on silica gel with chloroform which removed the trace metal impurity. A brown powder **7** (12.7 g, 88.8 %) was obtained. ^{1}H NMR (400.13 MHz, $CDCl_3$) δ(ppm): 7.64 (*dd*, *J* = 1.2, 5.2 Hz, 2H), 7.57 (*dd*, *J* = 1.2, 4.0 Hz, 2H), 7.20 (*dd*, *J* = 4.0, 5.2 Hz, 2H); ^{13}C NMR (100.6 MHz, $CDCl_3$) δ(ppm): 136.0, 133.9, 131.3, 131.2, 128.4 and 128.1.

6.3.3. Synthesis of 2,5-bis(2-thienyl)-3,4-diaminothiophene (8)[62]

Under nitrogen atmosphere, 2,5-bis(2-thienyl)-3,4-dinitrothiophene (**7**) (12.0 g, 35.5 mmol) was dissolved in a mixture of anhydrous ethanol (120 mL) and concentrated HCl (250 mL). A solution of anhydrous $SnCl_2$ (135 g, 712 mmol) in ethanol (250 mL) was added and stirred at 30 ^oC for 25 h when reaction progress monitoring by TLC (hexane: DCM, 1:1(v/v)) indicated completion of reaction. The reaction mixture was poured into 25% NaOH (860 mL) whose filtrate was extracted with toluene (1,030 mL). The organic layer was dried with Na_2SO_4 and solvent removed with rotary evaporator to give a brown cake (9.62 g, 97 %). ^{1}H NMR (400.13 MHz, $CDCl_3$) δ(ppm): 7.30 (*dd*, *J* = 1.2, 4.8 Hz, 2H), 7.14-7.10 (unresolved, 4H), 3.76 (*s*, 4H); ^{13}C NMR (100.6 MHz, $CDCl_3$) δ(ppm): 136.0, 133.7, 127.8, 125.4, 124.0 and 123.9.

6.3.4. Synthesis of 4,6-di(2-thienyl)-thiano[3,4-*c*][1,2,5]-thiadiazole (9)[63]

Under nitrogen atmosphere, *N*-thionyl aniline (20.5 g, 147 mmol) was added into a stirred solution of 2,5-bis(2-thienyl)-3,4-diaminothiophene (**8**) (9.4 g, 33.8 mmol) and dry pyridine (137 mL). Then TMSCl (27.4 g, 247 mmol) was added dropwise while being cooled with ice-water bath. After 72 h the starting was completely consumed as indicated by TLC in chloroform. The reaction mixture was poured into DCM (1250 mL) and washed with 1 N HCl (860) and washed with water several times. The organic phase was dried in Na_2SO_4 and solvent removed by rotary evaporator. A fluffy royal blue compound (**9**) (10.1 g, 97%) was obtained in good purity. ^{1}H NMR (400.13 MHz, $CDCl_3$) δ(ppm): 7.58 (*dd*, *J* = 1.2, 3.6 Hz, 2H), 7.35 (*dd*, *J* = 1.2, 5.2 Hz, 2H), 7.12 (*dd*, *J* = 3.6, 5.0 Hz, 2H); ^{13}C NMR (100.6 MHz, $CDCl_3$) δ(ppm): 156.3, 135.0, 128.3, 125.5, 124.3 and 112.4.

6.3.5. Synthesis of dimethyl-4,7-di(2-thienyl)-2,1,3-benzothiadiazole-5,6-dicarboxylate (11)[47]

Under nitrogen atmosphere, dimethyl acetylenedicarboxylate (**10**) (9.25 g, 65.1 mmol) was added slowly into a mixture of *o*-xylene (124 mL) and 4,6-di(2-thienyl)-thiano[3,4-*c*][1,2,5]-thiadiazole (**9**) (9.95 g, 32.4 mmol) and refluxed. TLC monitoring (chloroform) indicated complete consumption of the starting material after 5 h. The reaction mixture was concentrated using rotary evaporator and dried in vacuum oven. The crude brown solid was loaded on silica gel and eluted with chloroform and further purified by recrystallization with ethanol and then with isopropanol to furnish brown crystals (**11**) (10 g, 74.0 %). ^{1}H NMR (400.13 MHz, $CDCl_3$) δ(ppm): 7.62 (*dd*, *J* = 0.8, 5.2 Hz, 2H), 7.45 (*dd*, *J* = 1.2, 3.6 Hz, 2H), 7.22 (*dd*, *J* = 3.6, 5.0 Hz, 2H), 3.79 (*s*, 6H); ^{13}C NMR (100.6 MHz, $CDCl_3$) δ(ppm): 168.0, 153.6, 135.0, 132.0, 129.7, 128.9, 127.2, 126.2 and 53.0.

6.3.6. Synthesis of 4,7-di(2-thienyl)-2,1,3-benzothiadiazole-5,6-dicarboxylic acid (12)[50]

Dimethyl-4,7-di(2-thienyl)-2,1,3-benzothiadiazole-5,6-dicarboxylate (**11**) (6.0 g, 14.4 mmol) was suspended in ethanol (250 mL). 20% aqueous NaOH (200 mL) was added drop-wise. After refluxing for 24 h, the reaction content was brought to room temperature and concentrated HCl was added drop-wise until pH was near 1. The reaction was allowed to continue overnight at room temperature and then filtered and washed with water. The dried compound **12** was yellow (4.86 g, 87%). ^{1}H NMR (400.13 MHz, DMSO-d_6) δ(ppm): 7.87 (*dd*, *J* = 1.2, 3.6 Hz, 2H), 7.47 (*dd*, *J* = 1.2, 5.2 Hz, 2H), 7.25 (*dd*, *J* = 3.6, 5.0 Hz, 2H); ^{13}C NMR (100.6 MHz, DMSO-d_6) δ(ppm): 168.9, 153.1, 135.3, 133.6, 130.2, 129.8, 127.7 and 124.3.

6.3.7. Synthesis of 4,7-di(2-thienyl)-2,1,3-benzothiadiazole-5,6-dicarboxylic anhydride (13)[47]

Compound **12** (4.39 g, 11.3 mmol) and acetic anhydride (37.8 g, 370 mmol) were added into xylene (110 mL), and the mixture refluxed for 36 h. After the solvent was removed by rotary evaporator, the crude solid was recrystallized in ethanol which gave red crystals **13** in very poor yield, so the filtrate was dried and combined with the precipitate in the next reaction. ^{1}H NMR (400.13 MHz, DMSO-d_6) δ(ppm): 7.78 (*dd*, 1.2, 5.2 Hz, 2H), 7.46 (*dd*, 0.8, 3.2 Hz, 2H), 7.21 (*dd*, *J* = 3.6, 4.8 Hz, 2H); ^{13}C NMR (100.6 MHz, DMSO-d_6) δ(ppm): 168.9, 153.1, 135.3, 133.7, 130.0, 129.5, 127.5 and 124.3.

6.3.8. Synthesis of *N*-octyl-4,7-di(2-thienyl)-2,1,3-benzothiadiazole-5,6-dicarboxylic imide (14)[50]

Under nitrogen atmosphere, compound **13** (4 g, 10.8 mmol) and glacial acetic acid (180 mL) were refluxed and 1-aminooctane (3.44g, 26.6 mmol) was added drop-wise. After reacting

overnight acetic anhydride (80 mL) was added and refluxed overnight. After TLC analysis (chloroform) showed complete consumption of starting material, the solvent was removed via rotary evaporator. The crude solid was extracted with DCM and washed with 1 M HCl. The organic phase was dried in Na_2SO_4 and the solvent removed by rotary evaporator. The solid was recrystallized in isopropanol to give orange crystals **14** (4.95g, 95%). ^{1}H NMR (400.13 MHz, $CDCl_3$) δ(ppm): 7.92 (*dd*, *J* = 1.2, 3.6 Hz, 2H), 7.73 (*dd*, *J* = 1.2, 5.2 Hz, 2H), 7.29 (*dd*, *J* = 3.6, 5.0 Hz, 2H), 3.74 (*t*, *J* = 7.2 Hz, 2H), 1.71 (*quin*, 2H), 1.34-1.28 (unresolved 10H), 0.89 (*t*, *J* = 7.2 Hz, 3H); ^{13}C NMR (100.6 MHz, $CDCl_3$) δ(ppm): 165.8, 156.5, 133.3, 131.6, 130.3, 127.0, 126.9, 126.6, 38.9, 31.8, 29.2, 28.3, 27.0, 22.7, and 14.1.

6.3.9. Synthesis of *N*-octyl-4,7-di(5-bromo-2-thienyl)-2,1,3-benzothiadiazole-5,6-dicarboxylic imide (15)[50]

Under inert atmosphere, compound **14** (0.9 g, 1.86 mmol) was dissolved in THF (85 mL). *N*-bromosuccinimide (0.66 g, 3.72 mmol) was added in the dark and allowed to react overnight at room temperature. TLC monitoring (petroleum ether/ethyl acetate 15:1 v/v) indicated presence of starting material in which additional NBS was added (0.066 g) in several portions until a total of 3.59 g (20 mmol) NBS dibrominated the starting material. The reaction mixture was extracted with DCM and washed with distilled water and brine solution. The organic phase was dried in Na_2SO_4 and the solvent removed by rotary evaporator. The crude solid was passed through silica gel with 1:1 solution of chloroform/petroleum ether. Compound **15** was dark red powder (0.98 g, 82%). ^{1}H NMR (400.13 MHz, $CDCl_3$) δ(ppm): 7.82 (*d*, *J* = 4.0 Hz, 2H), 7.23 (*d*, *J* = 4.0 Hz, 2H), 3.74 (*t*, *J* = 7.2 Hz, 2H), 1.71 (*quin*, 2H), 1.34-1.27 (unresolved, 10H), 0.88 (*t*, *J* = 6.8 Hz, 3H); ^{13}C NMR (100.6 MHz, $CDCl_3$) δ(ppm): 165.6, 155.9, 134.1, 133.1, 129.8, 126.3, 125.9, 118.7, 39.0, 31.8, 29.2, 28.3, 27.0, 22.6 and 14.1.

6.3.10. Synthesis of 4,8-di(thien-2-yl)-1*H*-6-octyl-5*H*-pyrrolo[2,4-*f*]benzotriazole-5,7-(6*H*)-dione (17)[47, 69]

Under nitrogen atmosphere, compound **14** (4 g, 8.30 mmol) and iron powder (15.5 g, 278 mmol) and glacial acetic acid (145 mL) were refluxed overnight. When TLC monitoring (chloroform) indicated consumption of starting material after 24 h, the reaction content was cooled. The reaction content was filtered and washed with chloroform. The filtrate was concentrated to the volume of the acetic acid and the resulting solution containing the intermediate **16** was cooled in an ice bath to which a solution of $NaNO_2$ (3.28 g, 21.2 mmol) in water (30 mL) was added drop-wise. Then the reaction was allowed to continue overnight. When TLC monitoring (chloroform) showed complete reaction of starting material, the reaction content was extracted with DCM and washed with distilled water several times. The organic phase was dried with Na_2SO_4, the solvent removed with rotary evaporator and further dried in vacuum oven. The crude product containing compound **17** was pale yellow with trace colored impurities (3.66 g, 95%). NMR analysis showed the presence of the symmetrically and unsymmetrically protonated triazole functionality and was used in the next reaction step without further purification.

6.3.11. Synthesis of 2-(2-ethylhexyl)-6-octyl-4,8-di(thiophen-2-yl)[1,2,3]triazolo[4,5-*f*]isoindole-5,7-(2*H*,6*H*)-dione (18)[69]

Under nitrogen atmosphere, compound **17** (2.0 g, 4.30 mmol), K_2CO_3 (3.33 g, 24.1 mmol) and dry DMF (45 mL) were stirred and heated to 80 ^oC when 1-bromo-2-ethylhexane was added drop-wise. The reaction continued overnight and TLC analysis (10:1 petroleum ether/ethyl acetate) indicated completion of reaction, so reaction content was cooled and extracted with DCM. The organic phase was dried with Na_2SO_4 and the solvent was removed with rotary evaporator. The crude oily substance was passed through silica gel with 10:1 petroleum ether/

ethyl acetate to give a light orange gummy compound **18** (1.76 g, 71%). ^{1}H NMR (400.13 MHz, $CDCl_3$) δ(ppm): 8.14 (*dd*, *J* = 1.2, 3.8 Hz, 2H), 7.67 (*dd*, *J* = 0.8, 5.0 Hz, 2H), 7.27 (*dd*, *J* = 4.0, 5.0 Hz, 2H), 4.69 (*d*, *J* = 6.8 Hz, 2H), 3.73 (*t*, *J* = 7.6 Hz, 2H), 2.25 (*m*, 1H), 1.71 (*m*, 2H), 1.38-1.28 (unresolved, 18H), 1.00 (*t*, *J* = 7.2 Hz, 3H), 0.95-0.87 (unresolved, 6H); ^{13}C NMR (100.6 MHz, $CDCl_3$) δ(ppm): 166.6, 145.7, 133.0, 132.2, 129.7, 126.8, 125.0, 123.8, 60.3, 40.4, 38.5, 31.8, 30.6, 29.2, 29.2, 28.4, 27.1, 24.0, 23.0, 22.7, 14.1, 14.1 and 10.6

6.3.12. Synthesis of 4,8-bis(5-bromothiophen-2-yl)-2-(2-ethylhexyl)-6-octyl-[1,2,3]triazolo[4,5-f]isoindole-5,7(2*H*,6*H*)-dione (19)[69]

Under nitrogen atmosphere, compound **18** (1.78 g, 3.05 mmol) was dissolved in 1:1 v/v chloroform/acetic acid (70 mL) and chilled in ice water bath in the dark. *N*-bromosuccinimide (1.09 g, 6.10 mmol) was added gradually. The reaction was allowed to proceed overnight at room temperature. A total of 1.45 g of NBS was used to complete the dibromination. The reaction content was extracted with DCM and washed with brine solution. The organic phase was dried with Na_2SO_4 and the solvent removed via rotary evaporator. The crude gummy substance was passed through silica with 12:1 petroleum ether/ethyl acetate and the relatively pure fraction was recrystallized with ethanol to give a leathery bright yellow compound **19** (1.28 g, 57%). %). ^{1}H NMR (400.13 MHz, $CDCl_3$) δ(ppm): 8.04 (*d*, *J* = 4.0 Hz, 2H), 7.21 (*d*, *J* = 4.0 Hz, 2H), 4.70 (*d*, *J* = 6.8 Hz, 2H), 3.71 (*t*, *J* = 7.6 Hz, 2H), 2.23 (*m*, 1H), 1.69 (*quin*, 2H), 1.36-1.27 (unresolved, 18H), 1.00 (*t*, *J* = 7.2 Hz, 3H), 0.93 (*t*, *J* = 7.2 Hz, 3H), 0.88 (*t*, 3H); ^{13}C NMR (100.6 MHz, $CDCl_3$) δ(ppm): 166.5, 145.2, 134.0, 133.8, 129.8, 123.9, 123.5, 118.0, 60.4, 40.5, 38.6, 31.8, 30.6, 29.2, 28.4, 27.0, 24.0, 23.0, 22.6, 14.1, and 10.6.

6.3.13. Synthesis of 2-(octyl)-6-octyl-4,8-di(thiophen-2-yl)[1,2,3]triazolo[4,5-*f*]isoindole-5,7-(2*H*,6*H*)-dione (20)[69]

Under nitrogen atmosphere, compound **17** (1.4 g, 3.01 mmol), K_2CO_3 (2.33 g, 16.9 mmol) and dry DMF (35 mL) were stirred and heated to 80 ^oC when 1-bromooctane was added drop-wise. The reaction continued overnight and TLC analysis (10:1 petroleum ether/ethyl acetate) indicated completion of reaction, so reaction content was cooled. The content was extracted with DCM and the organic phase dried with Na_2SO_4. The solvent was removed with rotary evaporator. The crude oily substance was passed through silica gel with 12:1 petroleum ether/ ethyl acetate to give a light orange gummy compound **20** (1.15 g, 66%). ^1H NMR (400.13 MHz, $CDCl_3$) δ(ppm): 8.11 (*dd*, *J* = 0.8, 3.6 Hz, 2H), 7.67 (*dd*, *J* = 1.2, 5.0 Hz, 2H), 7.27 (*dd*, *J* = 4.0, 5.2 Hz, 2H), 4.74 (*t*, *J* = 7.2 Hz, 2H), 3.72 (*t*, *J* = 7.2 Hz, 2H), 2.15 (*quin*, 1H), 1.71 (*quin*, 2H), 1.39-1.28 (unresolved, 20H), 0.90-0.89 (unresolved, 6H); ^{13}C NMR (100.6 MHz, $CDCl_3$) δ(ppm): 166.5, 145.8, 132.9, 132.0, 129.6, 126.7, 124.9, 123.8, 57.4, 38.5, 31.8, 31.7, 29.8, 29.2, 29.1, 29.0, 28.9, 28.4, 27.0, 26.5, 22.6 and 14.0.

6.3.14. Synthesis of 4,8-bis(5-bromothiophen-2-yl)-2,6-dioctyl-[1,2,3]triazolo[4,5-*f*]isoindole-5,7(2*H*,6*H*)-dione (21)[69]

Under nitrogen atmosphere, compound **20** (1.15 g, 1.99 mmol) was dissolved in 1:1 v/v chloroform/acetic acid (36 mL) and chilled in ice water bath in the dark. *N*-bromosuccinimide (0.71 g, 3.98 mmol) was added gradually. The reaction was allowed to proceed overnight at room temperature. A total of 1.32 g of NBS was used to complete the dibromination. The reaction content was extracted with DCM and washed with brine solution. The organic phase was dried with Na_2SO_4 and the solvent removed via rotary evaporator. The crude oily substance was passed through silica with 12:1 petroleum ether/ethyl acetate and the relatively pure fraction

was recrystallized with ethanol to give a light yellow-orange compound **21** (1.28 g, 57%). ^{1}H NMR (400.13 MHz, $CDCl_3$) δ(ppm): 8.03 (*d*, *J* = 4.0 Hz, 2H), 7.20 (*d*, *J* = 4.0 Hz, 2H), 4.74 (*t*, *J* = 7.2 Hz, 2H), 3.69 (*t*, *J* = 7.2 Hz, 2H), 2.15 (*quin*, 1H), 1.68 (*quin*, 2H), 1.41-1.30 (unresolved, 20H), 0.90-0.88 (unresolved, 6H); ^{13}C NMR (100.6 MHz, $CDCl_3$) δ(ppm): 166.4, 145.2, 134.0, 133.7, 129.8, 123.8, 123.4, 118.0, 57.5, 38.6, 31.8, 31.7, 29.8, 29.2, 29.2, 28.9, 28.3, 27.0, 26.5, 22.7 and 14.1.

6.3.15. Synthesis of P5

Under nitrogen atmosphere, compound **15** (128 mg, 0.200 mmol), (4,8-bis(5-(2-ethylhexyl)thieno[3,2-*b*]thiophen-2-yl)benzo[1,2-*b*:1,2-*b'*]dithiophene-2,6-)bis (trimethylstannane) (203 mg, 0.200 mmol), tris(dibenzylideneacetone)dipalladium ($Pd_2(dba)_3$) (3.66 mg, 4 µmol) and tri(*o*-tolyl)phosphine (P(*o*-tolyl)$_3$ (4.9 mg, 16 µmol) were placed in a 50-mL two-necked round-bottomed flask. The content of the flask was evacuated and purged with nitrogen three times after which dry toluene (9 mL) was added. The mixture was evacuated and purged twice after which it was vigorously stirred and heated to 80 ^{o}C in a pre-heated oil bath at 60 ^{o}C. After 35 min, the end-capping 2-bromothiophene (0.2 mL) was added and allowed to react for 30 min. Then the second end-capping 2-tributylstannylthiophene (0.4 mL) was added and reacted for 30 min. Then the reaction mixture was cooled and precipitated from methanol (200 mL). The polymer was filtered through a thimble and underwent Soxhlet extraction with methanol and diethyl ether which removed impurities and chloroform whose extraction was concentrated and passed through silica gel with chloroform as eluent and precipitated from methanol. The precipitate was collected through membrane filtration and dried in vacuum oven at 40 ^{o}C to afford copolymer **P5** (0.090 g, 38%) as a dark green solid.

6.3.16. Synthesis of P6

Under nitrogen atmosphere, compound **19** (147 mg, 0.200 mmol), (4,8-bis(5-(2-ethylhexyl)thieno[3,2-*b*]thiophen-2-yl)benzo[1,2-b:1,2-*b*']dithiophene-2,6-)bis (trimethylstannane) (203 mg, 0.200 mmol), tris(dibenzylideneacetone)dipalladium ($Pd_2(dba)_3$) (3.66 mg, 4 µmol) and tri(*o*-tolyl)phosphine (P(*o*-tolyl)$_3$ (4.9 mg, 16 µmol) were placed in a 50-mL two-necked round-bottomed flask. The content of the flask was evacuated and purged with nitrogen three times after which dry toluene (9 mL) was added. The mixture was evacuated and purged twice after which it was vigorously stirred and heated to 90 ^oC in a pre-heated oil bath at 60 ^oC. After 50 min, the end-capping 2-bromothiophene (0.2 mL) was added and allowed to react for 30 min. Then the second end-capping 2-tributylstannylthiophene (0.4 mL) was added and reacted for 30 min. Then the reaction mixture was cooled and precipitated from methanol (200 mL). The polymer was filtered through a thimble and underwent Soxhlet extraction with methanol and diethyl ether which removed impurities and chloroform whose extraction was concentrated and passed through silica gel with chloroform as eluent and precipitated from methanol. The polymers remaining in the thimble were dissolved in a minimum amount of *o*-DCB heated at 60 ^oC which was loaded onto silica gel with *o*-DCB as eluent and precipitated from methanol. The chloroform and *o*-DCB precipitates were separately collected through membrane filtration and dried in vacuum oven at 40 ^oC to afford **P6** (0.17 g, 67%) as a navy blue solid.

6.3.17. Synthesis of P7

Under nitrogen atmosphere, compound **21** (147 mg, 0.200 mmol), (4,8-bis(5-(2-ethylhexyl)thieno[3,2-*b*]thiophen-2-yl)benzo[1,2-*b*:1,2-*b*']dithiophene-2,6-)bis (trimethylstannane) (203 mg, 0.200 mmol), tris(dibenzylideneacetone)dipalladium ($Pd_2(dba)_3$)

(3.66 mg, 4 µmol) and tri(*o*-tolyl)phosphine (P(*o*-tolyl)$_3$ (4.9 mg, 16 µmol) were placed in a 50-mL two-necked round-bottomed flask. The content of the flask was evacuated and purged with nitrogen three times after which dry toluene (9 mL) was added. The mixture was evacuated and purged twice after which it was vigorously stirred and heated to 90 ^{o}C in a pre-heated oil bath at 60 ^{o}C. After 20 min, the end-capping 2-bromothiophene (0.2 mL) was added and allowed to react for 20 min. Then the second end-capping 2-tributylstannylthiophene (0.4 mL) was added and reacted for 20 min. Then the reaction mixture was cooled and precipitated from methanol (200 mL). The polymer was filtered through a thimble and underwent Soxhlet extraction with methanol and diethyl ether which removed impurities and chloroform whose extraction was concentrated and passed through silica gel with chloroform as eluent and precipitated from methanol. No significant amount of polymers remained in the thimble. The chloroform precipitate was collected through membrane filtration and dried in vacuum oven at 40 ^{o}C to afford copolymer **P7** (0.227 g, 90%) as a navy blue solid.

6.3.18. Synthesis of 2,9-bis(2-ethylhexyl)anthra[2,1,9-*def*:6,5,10-*d′e′f′*]diisoquinoline-1,3,8,10(2*H*,9*H*)-tetraone (24)[57]

Under nitrogen atmosphere, perylene-3,4,9,10-tetracarboxylic dianhydride (**1**) (1.0 g, 2.5 mmol) was dissolved in DMF (50 mL) to which 2-ethyl-6-hexylamine (**23**) (0.79 g, 6.1 mmol) was added once it reached 120 ^{o}C. After reacting for 9 h, TLC analysis indicated completion of reaction and content was cooled. The reaction mixture was filtered and washed with distilled water several times. The solid product was dried in vacuum oven to give compound **24** which was a red powder (1.37 g, 86%). ^{1}H NMR (400.13 MHz, $CDCl_3$) δ(ppm): 8.59 (*d*, *J* = 7.6 Hz, 4H), 8.48 (*d*, *J* = 8.0, Hz, 4H), 4.15 (*m*, 4H), 1.98 (*m*, 2H), 1.42-1.35 (unresolved, 16H), 0.98-

0.92 (unresolved, 12H); ^{13}C NMR (100.6 MHz, $CDCl_3$) δ(ppm): 163.6, 134.3, 131.3, 129.3, 126.2, 123.2, 123.0, 44.4, 38.0, 30.8, 28.7, 24.1, 23.1, 14.1 and 10.7.

6.3.19. Synthesis of 2,9-bis(2-ethylhexyl)-5-nitroanthra[2,1,9-*def*:6,5,10-*d'e'f'*]diisoquinoline-1,3,8,10(2*H*,9*H*)-tetraone (25)[57]

Compound **24** (0.70 g, 1.14 mmol) was treated with fuming nitric acid (1.51 g, 24.0 mmol) at 0 ^{o}C. After 2 h, TLC analysis indicated consumption of the reactant, and the reaction content was quenched in distilled water (500 mL) and extracted with DCM. The organic layer was dried in Na_2SO_4 and the solvent removed using rotary evaporator. The crude solid was purified on silica gel using 3:1 DCM/hexane to give a compound **25** which was light red. (0.48 g, 66%). ^{1}H NMR (400.13 MHz, $CDCl_3$) δ(ppm): 8.74 (*d*, *J* = 8.0 Hz, 1H), 8.69 (*d*, *J* = 8.0 Hz, 1H), 8.66 (*s*, 1H), 8.65 (*d*, *J* = 7.2 Hz, 1H), 8.63 (*d*, *J* = 8.4 Hz, 1H), 8.55 (*d*, *J* = 8.4 Hz, 1H), 8.16 (*d*, *J* = 8.0 Hz, 1H), 4.15-4.14 (unresolved, 4H), 1.95 (unresolved, 2H), 1.40-1.35 (unresolved, 16H), 0.97 (*t*, *J* = 7.2 Hz, 6H), 0.92 (t, J = 6.8 Hz, 6H); ^{13}C NMR (100.6 MHz, $CDCl_3$) δ(ppm): 163.3, 163.0, 162.9, 162.1, 147.5, 135.4, 132.8, 132.8, 131.4, 131.2, 129.3, 129.2, 128.8, 127.9, 127.4, 126.5, 126.3, 126.3, 124.8, 124.5, 124.0, 124.0, 123.8, 123.3, 123.0, 44.6, 44.5, 38.0, 37.9, 30.7, 28.7, 28.7, 24.0, 23.1, 23.1, 14.1, 10.6 and 10.6.

6.3.20. Synthesis of 2,8-bis(2-ethylhexyl)-1*H*-pyrido[3',4',5':4,5]naphtho[2,1,8-*cde*]pyrido[3',4',5':4,5]naphtho[8,1,2-*ghi*]isoindole-1,3,7,9(2*H*,5*H*,8*H*)-tetraone (26)[68]

Under nitrogen atmosphere, compound **25** (2.0 g, 3.03 mmol), triphenylphospine (2.0 g, 7.63 mmol) and *o*-DCB were stirred and heated to 180 ^{o}C overnight. After 19 h, TLC analysis indicated the completion of reaction, the content was cooled. The reaction content was precipitated into hexane and filtered and washed with hexane several times. The crude solid was dissolved in chloroform until most of the product mixture was dissolved. Then the solution was

filtered gravitationally on a filter paper. The precipitate on the filter paper was washed with chloroform several times and then dried in vacuum oven. Compound **26** was a poorly soluble red powder (1.7 g, 89%) that did not dissolve enough even for ^{1}H NMR analysis.

6.3.21. Synthesis of 2,8-bis(2-ethylhexyl)-5-hexyl-1*H*-pyrido[3',4',5':4,5]naphtho[2,1,8-*cde*]pyrido[3',4',5':4,5]naphtho[8,1,2-*ghi*]isoindole-1,3,7,9(2*H*,5*H*,8*H*)-tetraone (27)[57]

Under nitrogen atmosphere, compound **26** (3.0 g, 4.78 mmol), potassium carbonate (1.2 g, 8.60 mmol) and dry DMF (90 mL) were stirred and heated to 120 ^{o}C. Then 1-bromohexane (1.65 g, 9.96 mmol) was added drop-wise. The reaction proceeded overnight after which TLC analysis showed complete consumption of the reactant. The cooled reaction content was washed in 1 M HCl and extracted with DCM and the organic phase was dried in Na_2SO_4. The solvent was removed using rotary evaporator. The crude solid was slurred in methanol, filtered and washed with methanol. Then it was dried in vacuum oven. Compound **27** was a red crystalline (3.24 g, 95%). ^{1}H NMR (400.13 MHz, $CDCl_3$) δ(ppm): 8.60 (*s*, 2H), 8.45 (*d*, *J* = 8.0 Hz, 2H), 8.42 (*d*, *J* = 8.0 Hz, 2H), 4.72 (*t*, *J* = 7.2 Hz, 2H), 4.22 (*m*, 4H), 2.11 (*quin*, 2H), 2.00 (*m*, 2H), 1.47-1.39 (unresolved, 22H), 1.01 (*t*, *J* = 7.2 Hz, 6H), 0.94 (*t*, *J* = 7.2 Hz, 6H), 0.87 (*t*, *J* = 7.2 Hz, 3H); ^{13}C NMR (100.6 MHz, $CDCl_3$) δ(ppm): 165.0, 163.7, 134.1, 131.7, 126.9, 123.7, 123.0, 121.8, 121.1. 120.8, 118.4, 118.0, 46.8, 44.5, 38.2, 31.5, 31.3, 30.9, 28.8, 26.8, 24.1, 23.1, 22.4, 14.1, 13.9 and 10.7.

6.3.22. Synthesis of 11-bromo-2,8-bis(2-ethylhexyl)-5-hexyl-1*H*-pyrido[3',4',5':4,5]naphtho[2,1,8-*cde*]pyrido[3',4',5':4,5]naphtho[8,1,2-*ghi*]isoindole-1,3,7,9(2*H*,5*H*,8*H*)-tetraone (28)[57]

Compound **27** (0.50 g, 0.702 mmol) was dissolved in DCM (30 mL) and chilled in ice-water bath in the dark. Molecular bromine (1.81 g, 34.9 mmol) was placed in an addition funnel with a

top layer of DCM and added drop-wise. Once all the bromine was added, the ice-water bath was removed and reaction allowed to proceed for 2 h at room temperature. When TLC analysis indicated complete consumption of reactant, the reaction mixture's excess bromine was treated with $Na_2S_2O_5$ (5%) followed by extraction with DCM and washing several times with distilled water. The organic phase was dried in Na_2SO_4 and the solvent removed using rotary evaporator. The crude solid was slurried with methanol and filtered and washed with methanol. The solid product was dried in vacuum oven giving compound **28** which was a dark red crystalline (0.54 g, 95%). ^{1}H NMR (400.13 MHz, $CDCl_3$) δ(ppm): 9.17 (*d*, *J* = 8.0 Hz, 1H), 8.58 (*s*, 1H), 8.51 (*s*, 1H), 8.23 (*s*, 1H), 8.16 (*d*, *J* = 8.4 Hz, 1H), 4.73 (*t*, *J* = 6.8 Hz, 2H), 4.27-4.07 (unresolved, 4H), 2.11 (unresolved, 2H), 2.01 (unresolved, 1H), 1.92 (unresolved, 1H), 1.42 (unresolved, 22H), 1.03-0.90 (unresolved, 15H); ^{13}C NMR (100.6 MHz, $CDCl_3$) δ(ppm): 164.7, 164.3, 163.3, 162.2, 133.6, 133.5, 133.1, 130.7, 128.7, 126.2, 125.9, 123.0, 122.0, 121.9, 121.8, 121.2, 121.1, 121.0, 120.6, 120.3, 117.3, 117.2, 117.1, 116.9, 46.9, 44.6, 44.5, 38.2, 38.2, 31.4, 31.3, 30.9, 30.8, 28.8, 28.7, 26.9, 24.2, 24.1, 23.2, 23.1, 22.5, 14.2, 14.0, 10.7 and 10.6.

6.3.23. Synthesis of 11,11'-(9,9'-spirobi[fluorene]-2,7-diyl)bis(2,8-bis(2-ethylhexyl)-5-hexyl-1*H*-pyrido[3',4',5':4,5]naphtho[2,1,8-*cde*]pyrido[3',4',5':4,5]naphtho[8,1,2-*ghi*]isoindole-1,3,7,9(2*H*,5*H*,8*H*)-tetraone) (30)[70]

Compound **28** (0.10 g, 126 µmol), organoboron ester **29** (35.1 mg, 61.5 µmol), $Pd(PPh_3)_4$ (6.0 mg, 5.0 µmol), and K_2CO_3 (35 mg, 252 µmol) were placed in a round-bottomed flask, evacuated and purged with nitrogen. Then, 6 mL dry DMF which was evacuated and purged with nitrogen was added and stirred. Then, the reaction was allowed to react overnight and stopped when TLC monitoring in chloroform indicated consumption of starting material. The reaction product was passed through silica gel with 1:1 chloroform/petroleum ether and further purified using

preparative TLC with 10:1 petroleum ether/ethyl acetate and then with 1:1 petroleum ether/chloroform. A pink-red small molecule (**30**) (0.020 g,18%) was very low in yield. ^{1}H NMR (400.13 MHz, $CDCl_3$) δ(ppm): 8.93 (*s*, 2H), 8.87 (*s*, 2H), 8.69 (*s*, 2H), 8.47 (*d*, *J* = 8.0 Hz, 2H), 8.35 (*d*, *J* = 8.8 Hz, 2H), 8.00 (*d*, *J* = 8.4 Hz, 2H), 7.90 (*d*, *J* = 7.9 Hz, 2H), 7.45 (*d*, *J* = 7.2 Hz, 2H), 7.33 (*t*, *J* = 7.6 Hz, 2H), 7.21 (*d*, *J* = 7.6 Hz, 2H), 7.13 (*t*, *J* = 7.2 Hz, 2H), 7.09 (*s*, 2H), 4.84 (*t*, *J* = 6.8 Hz, 4H), 4.23 (unresolved, 8H), 2.16 (unresolved, 4H), 2.02-2.01 (unresolved, 4H) 1.45-1.27 (unresolved, 44H), 0.99-0.86 (unresolved, 30H); ^{13}C NMR (100.6 MHz, $CDCl_3$) δ(ppm): 165.4, 165.4, 164.1, 163.8, 150.8, 147.3, 142.4, 141.8, 141.5, 134.6, 134.2, 133.1, 131.2, 130.1, 128.7, 128.7, 128.3, 128.0, 127.7, 127.7, 127.2, 125.0, 124.1, 123.9, 123.5, 122.7, 122.5, 122.5, 122.0, 121.9, 120.9, 120.8, 120.0, 119.4, 117.9, 66.2, 46.8, 44.5, 44.4, 38.2, 31.4, 31.4, 30.9, 29.7, 28.8, 28.7, 26.8, 26.8, 24.2, 23.2, 23.1, 22.5, 14.2, 14.2, 13.9, 13.9, and 10.8.

7. References

1. Lu, L.; Zheng, T.; Wu, Q.; Schneider, A. M.; Zhao, D.; Yu, L., Recent Advances in Bulk Heterojunction Polymer Solar Cells. *Chemical Reviews* **2015,** *115* (23), 12666-12731.
2. Zhang, Z.; Liu, Y.; Zhang, J.; Feng, S.; Wu, L.; Gong, X.; Xu, X.; Chen, X.; Bo, Z., Enhancing the efficiency of polymer solar cells by incorporation of 2, 5-difluorobenzene units into the polymer backbone via random copolymerization. *ACS applied materials & interfaces* **2017,** *9* (28), 23775-23781.
3. Haque, S.; Ardila-Rey, J.; Umar, Y.; Rahman, H.; Mas'ud, A.; Muhammad-Sukki, F.; Albarracín, R., Polymeric Materials for Conversion of Electromagnetic Waves from the Sun to Electric Power. *Polymers* **2018,** *10* (3), 307.
4. Zhou, Y.; Zhu, K., Perovskite Solar Cells Shine in the "Valley of the Sun". *ACS Energy Letters* **2016,** *1* (1), 64-67.
5. Holliday, S.; Li, Y.; Luscombe, C. K., Recent advances in high performance donor-acceptor polymers for organic photovoltaics. *Progress in Polymer Science* **2017,** *70*, 34-51.
6. Evans, D., *A Bird's eye View on the Synthesis and Practical Application of Conducting Polymers*. 2018; Vol. 67.
7. Kukreti, K.; Rathod, A. P. S.; Kumar, B. In *Recent advancements and overview of organic solar cell*, 2016 International Conference on Computing, Communication and Automation (ICCCA), 29-30 April 2016; 2016; pp 1539-1544.
8. Vivek, K.; Agrawal, G., Organic Solar Cells: Principles Mechanism and Recent Developments. *hypothesis* **2014,** *17*, 18.
9. Dou, L.; You, J.; Hong, Z.; Xu, Z.; Li, G.; Street, R. A.; Yang, Y., 25th anniversary article: a decade of organic/polymeric photovoltaic research. *Advanced materials* **2013,** *25* (46), 6642-6671.
10. Notarianni, M.; Liu, J.; Vernon, K.; Motta, N., Synthesis and applications of carbon nanomaterials for energy generation and storage. *Beilstein journal of nanotechnology* **2016,** *7*, 149.
11. Zhou, H.; Yang, L.; You, W., Rational Design of High Performance Conjugated Polymers for Organic Solar Cells. *Macromolecules* **2012,** *45* (2), 607-632.
12. Zhang, S.; Ye, L.; Hou, J., Breaking the 10% Efficiency Barrier in Organic Photovoltaics: Morphology and Device Optimization of Well-Known PBDTTT Polymers. *Advanced Energy Materials* **2016,** *6* (11), 1502529.
13. Lin, Z.; Chang, J.; Zhang, C.; Chen, D.; Wu, J.; Hao, Y., Enhanced Performance and Stability of Polymer Solar Cells by In Situ Formed AlOx Passivation and Doping. *The Journal of Physical Chemistry C* **2017,** *121* (19), 10275-10281.
14. Gao, Y.; Liu, M.; Zhang, Y.; Liu, Z.; Yang, Y.; Zhao, L., *Recent Development on Narrow Bandgap Conjugated Polymers for Polymer Solar Cells*. 2017; Vol. 9, p 39.
15. Lu, L.; Zheng, T.; Wu, Q.; Schneider, A. M.; Zhao, D.; Yu, L., Recent Advances in Bulk Heterojunction Polymer Solar Cells. *Chem Rev* **2015,** *115* (23), 12666-731.
16. Sun, C.; Pan, F.; Bin, H.; Zhang, J.; Xue, L.; Qiu, B.; Wei, Z.; Zhang, Z.-G.; Li, Y., A low cost and high performance polymer donor material for polymer solar cells. *Nature Communications* **2018,** *9* (1), 743.
17. Arbouch, I.; Karzazi, Y.; Hammouti, B., *Organic photovoltaic cells: Operating principles, recent developments and current challenges – review*. 2014; Vol. 72, p 73-84.

18. Scharber, M. C.; Sariciftci, N. S., Efficiency of bulk-heterojunction organic solar cells. *Progress in Polymer Science* **2013,** *38* (12), 1929-1940.
19. Kawashima, K.; Tamai, Y.; Ohkita, H.; Osaka, I.; Takimiya, K., High-efficiency polymer solar cells with small photon energy loss. *Nature Communications* **2015,** *6*, 10085.
20. Nielsen, C. B.; Ashraf, R. S.; Treat, N. D.; Schroeder, B. C.; Donaghey, J. E.; White, A. J.; Stingelin, N.; McCulloch, I., 2, 1, 3-Benzothiadiazole-5, 6-Dicarboxylic Imide–A Versatile Building Block for Additive-and Annealing-Free Processing of Organic Solar Cells with Efficiencies Exceeding 8%. *Advanced Materials* **2015,** *27* (5), 948-953.
21. Kranthiraja, K.; Gunasekar, K.; Cho, W.; Park, Y. G.; Lee, J. Y.; Shin, Y.; Kang, I.-N.; Song, M.; Chae, K. H.; Kim, B.; Jin, S.-H., Influential effects of π-spacers, alkyl side chains, and various processing conditions on the photovoltaic properties of alkylselenyl substituted benzodithiophene based polymers. *Journal of Materials Chemistry C* **2015,** *3* (4), 796-808.
22. Li, W.; Yan, L.; Zhou, H.; You, W., A general approach toward electron deficient triazole units to construct conjugated polymers for solar cells. *Chemistry of Materials* **2015,** *27* (18), 6470-6476.
23. Kim, I.-B.; Jang, S.-Y.; Kim, Y.-A.; Kang, R.; Kim, I.-S.; Ko, D.-K.; Kim, D.-Y., The Effect of Fluorine Substitution on the Molecular Interactions and Performance in Polymer Solar Cells. *ACS applied materials & interfaces* **2017,** *9* (28), 24011-24019.
24. Lee, D.; Stone, S. W.; Ferraris, J. P., A novel dialkylthio benzo [1, 2-b: 4, 5-b′] dithiophene derivative for high open-circuit voltage in polymer solar cells. *Chemical Communications* **2011,** *47* (39), 10987-10989.
25. Xu, S.; Feng, L.; Yuan, J.; Zhang, Z.-G.; Li, Y.; Peng, H.; Zou, Y., Hexafluoroquinoxaline based polymer for nonfullerene solar cells reaching 9.4% efficiency. *ACS applied materials & interfaces* **2017,** *9* (22), 18816-18825.
26. Ji-Hoon, K.; Sebastian, W.; Baek, P. J.; Jessica, W.; Myungkwan, S.; Cheol, Y. S.; Hwan, J. I.; Ji-Seon, K.; Do-Hoon, H., Optimization and Analysis of Conjugated Polymer Side Chains for High-Performance Organic Photovoltaic Cells. *Advanced Functional Materials* **2016,** *26* (10), 1517-1525.
27. Heckler, I.; Kesters, J.; Defour, M.; Madsen, M.; Penxten, H.; D'Haen, J.; Van Mele, B.; Maes, W.; Bundgaard, E., The Influence of Conjugated Polymer Side Chain Manipulation on the Efficiency and Stability of Polymer Solar Cells. *Materials* **2016,** *9* (3), 181.
28. Liu, T.; Pan, X.; Meng, X.; Liu, Y.; Wei, D.; Ma, W.; Huo, L.; Sun, X.; Lee, T. H.; Huang, M., Alkyl Side-Chain Engineering in Wide-Bandgap Copolymers Leading to Power Conversion Efficiencies over 10%. *Advanced Materials* **2017,** *29* (6), 1604251.
29. Gong, X.; Li, G.; Wu, Y.; Zhang, J.; Feng, S.; Liu, Y.; Li, C.; Ma, W.; Bo, Z., Enhancing the Performance of Polymer Solar Cells by Using Donor Polymers Carrying Discretely Distributed Side Chains. *ACS applied materials & interfaces* **2017,** *9* (28), 24020-24026.
30. Zhu, D.; Zhu, Q.; Gu, C.; Ouyang, D.; Qiu, M.; Bao, X.; Yang, R., Alkoxyl Side Chain Substituted Thieno[3,4-c]pyrrole-4,6-dione To Enhance Photovoltaic Performance with Low Steric Hindrance and High Dipole Moment. *Macromolecules* **2016,** *49* (16), 5788-5795.
31. Wang, Q.; Zhang, S.; Xu, B.; Ye, L.; Yao, H.; Cui, Y.; Zhang, H.; Yuan, W.; Hou, J., Effectively Improving Extinction Coefficient of Benzodithiophene and Benzodithiophenedione-based Photovoltaic Polymer by Grafting Alkylthio Functional Groups. *Chemistry–An Asian Journal* **2016,** *11* (19), 2650-2655.

32. Cui, C.; Wong, W.-Y.; Li, Y., Improvement of open-circuit voltage and photovoltaic properties of 2D-conjugated polymers by alkylthio substitution. *Energy & Environmental Science* **2014,** *7* (7), 2276-2284.
33. Bin, H.; Gao, L.; Zhang, Z.-G.; Yang, Y.; Zhang, Y.; Zhang, C.; Chen, S.; Xue, L.; Yang, C.; Xiao, M., 11.4% Efficiency non-fullerene polymer solar cells with trialkylsilyl substituted 2D-conjugated polymer as donor. *Nature communications* **2016,** *7*, 13651.
34. Bin, H.; Yang, Y.; Peng, Z.; Ye, L.; Yao, J.; Zhong, L.; Sun, C.; Gao, L.; Huang, H.; Li, X., Effect of Alkylsilyl Side-Chain Structure on Photovoltaic Properties of Conjugated Polymer Donors. *Advanced Energy Materials* **2018,** *8* (8), 1702324.
35. Deng, Y.; Li, W.; Liu, L.; Tian, H.; Xie, Z.; Geng, Y.; Wang, F., Low bandgap conjugated polymers based on mono-fluorinated isoindigo for efficient bulk heterojunction polymer solar cells processed with non-chlorinated solvents. *Energy & Environmental Science* **2015,** *8* (2), 585-591.
36. Salim, T.; Lek, J. Y.; Bräuer, B.; Fichou, D.; Lam, Y. M., Polymer nanofibers: preserving nanomorphology in ternary blend organic photovoltaics. *Physical Chemistry Chemical Physics* **2014,** *16* (43), 23829-23836.
37. O'Hara, K. A.; Ostrowski, D. P.; Koldemir, U.; Takacs, C. J.; Shaheen, S. E.; Sellinger, A.; Chabinyc, M. L., Role of Crystallization in the Morphology of Polymer: Non-fullerene Acceptor Bulk Heterojunctions. *ACS applied materials & interfaces* **2017,** *9* (22), 19021-19029.
38. Yao, H.; Yu, R.; Shin, T. J.; Zhang, H.; Zhang, S.; Jang, B.; Uddin, M. A.; Woo, H. Y.; Hou, J., A Wide Bandgap Polymer with Strong π–π Interaction for Efficient Fullerene-Free Polymer Solar Cells. *Advanced Energy Materials* **2016,** *6* (15), 1600742.
39. Liuyuan, L.; Zhiming, C.; Qin, H.; Lei, Y.; Rui, Z.; Feng, L.; P., R. T.; Fei, H.; Yong, C., High-Performance Polymer Solar Cells Based on a Wide-Bandgap Polymer Containing Pyrrolo[3,4-f]benzotriazole-5,7-dione with a Power Conversion Efficiency of 8.63%. *Advanced Science* **2016,** *3* (9), 1600032.
40. Yao, H.; Ye, L.; Zhang, H.; Li, S.; Zhang, S.; Hou, J., Molecular design of benzodithiophene-based organic photovoltaic materials. *Chemical reviews* **2016,** *116* (12), 7397-7457.
41. Zara, Z.; Iqbal, J.; BiBi, S.; Sadaf, S.; Eliasson, B., Designing Benzodithiophene-Based Donor Materials with Favorable Photovoltaic Parameters for Bulk Heterojunction Organic Solar Cells. *ChemistrySelect* **2017,** *2* (20), 5628-5639.
42. B., N. C.; Shahid, A. R.; D., T. N.; C., S. B.; E., D. J.; P., W. A. J.; Natalie, S.; Iain, M., 2,1,3-Benzothiadiazole-5,6-Dicarboxylic Imide – A Versatile Building Block for Additive- and Annealing-Free Processing of Organic Solar Cells with Efficiencies Exceeding 8%. *Advanced Materials* **2015,** *27* (5), 948-953.
43. Li, H.; Sun, S.; Mhaisalkar, S.; Zin, M. T.; Lam, Y. M.; Grimsdale, A. C., A high voltage solar cell using a donor–acceptor conjugated polymer based on pyrrolo[3,4-f]-2,1,3-benzothiadiazole-5,7-dione. *Journal of Materials Chemistry A* **2014,** *2* (42), 17925-17933.
44. Yang, Y.; Jia, B.; Wang, J.; Lau, T.-K.; Lu, X.; Zhan, X.; Chen, X., A new random D-A copolymer based on two different benzotriazole units as co-acceptors for polymer solar cells. *Polymer* **2018,** *139*, 123-129.
45. Yao, B.; Zhou, X.; Ye, X.; Zhang, J.; Yang, D.; Ma, D.; Wan, X., 2,1,3-Benzothiadiazole-5,6-dicarboxylic imide based low-bandgap polymers for solution processed photodiode application. *Organic Electronics* **2015,** *26*, 305-313.

46. Yu, J.; Ornelas, J. L.; Tang, Y.; Uddin, M. A.; Guo, H.; Yu, S.; Wang, Y.; Woo, H. Y.; Zhang, S.; Xing, G.; Guo, X.; Huang, W., 2,1,3-Benzothiadiazole-5,6-dicarboxylicimide-Based Polymer Semiconductors for Organic Thin-Film Transistors and Polymer Solar Cells. *ACS Applied Materials & Interfaces* **2017,** *9* (48), 42167-42178.
47. Lan, L.; Chen, Z.; Li, Y.; Ying, L.; Huang, F.; Cao, Y., Donor–acceptor conjugated polymers based on cyclic imide substituted quinoxaline or dibenzo[a,c]phenazine for polymer solar cells. *Polymer Chemistry* **2015,** *6* (43), 7558-7569.
48. Yum, S.; An, T. K.; Wang, X.; Lee, W.; Uddin, M. A.; Kim, Y. J.; Nguyen, T. L.; Xu, S.; Hwang, S.; Park, C. E.; Woo, H. Y., Benzotriazole-Containing Planar Conjugated Polymers with Noncovalent Conformational Locks for Thermally Stable and Efficient Polymer Field-Effect Transistors. *Chemistry of Materials* **2014,** *26* (6), 2147-2154.
49. Wang, T.-L.; Yang, C.-H.; Chuang, Y.-Y., A comparative study of the effect of fluorine substitution on the photovoltaic performance of benzothiadiazole-based copolymers. *RSC Advances* **2016,** *6* (53), 47676-47686.
50. Wang, L.; Cai, D.; Zheng, Q.; Tang, C.; Chen, S.-C.; Yin, Z., Low Band Gap Polymers Incorporating a Dicarboxylic Imide-Derived Acceptor Moiety for Efficient Polymer Solar Cells. *ACS Macro Letters* **2013,** *2* (7), 605-608.
51. Thompson, B. C.; Fréchet, J. M., Polymer–fullerene composite solar cells. *Angewandte chemie international edition* **2008,** *47* (1), 58-77.
52. Nielsen, C. B.; Holliday, S.; Chen, H.-Y.; Cryer, S. J.; McCulloch, I., Non-Fullerene Electron Acceptors for Use in Organic Solar Cells. *Accounts of Chemical Research* **2015,** *48* (11), 2803-2812.
53. Li, S.; Liu, W.; Li, C.-Z.; Lau, T.-K.; Lu, X.; Shi, M.; Chen, H., A non-fullerene acceptor with a fully fused backbone for efficient polymer solar cells with a high open-circuit voltage. *Journal of Materials Chemistry A* **2016,** *4* (39), 14983-14987.
54. Duan, Y.; Xu, X.; Li, Y.; Peng, Q., Recent development of perylene diimide-based small molecular non-fullerene acceptors in organic solar cells. *Chinese Chemical Letters* **2017,** *28* (11), 2105-2115.
55. Liu, J.; Chen, S.; Qian, D.; Gautam, B.; Yang, G.; Zhao, J.; Bergqvist, J.; Zhang, F.; Ma, W.; Ade, H.; Inganäs, O.; Gundogdu, K.; Gao, F.; Yan, H., Fast charge separation in a non-fullerene organic solar cell with a small driving force. *Nature Energy* **2016,** *1*, 16089.
56. Zhao, J.; Li, Y.; Lin, H.; Liu, Y.; Jiang, K.; Mu, C.; Ma, T.; Lin Lai, J. Y.; Hu, H.; Yu, D.; Yan, H., High-efficiency non-fullerene organic solar cells enabled by a difluorobenzothiadiazole-based donor polymer combined with a properly matched small molecule acceptor. *Energy & Environmental Science* **2015,** *8* (2), 520-525.
57. Hendsbee, A. D.; Sun, J.-P.; Law, W. K.; Yan, H.; Hill, I. G.; Spasyuk, D. M.; Welch, G. C., Synthesis, Self-Assembly, and Solar Cell Performance of N-Annulated Perylene Diimide Non-Fullerene Acceptors. *Chemistry of Materials* **2016,** *28* (19), 7098-7109.
58. Zhou, X.; Sun, Q.; Li, W.; Zhao, Y.; Luo, Z.; Zhang, F.; Yang, C., Isomeric small molecule acceptors based on perylene diimide and spirobifluorene for non-fullerene organic solar cells. *Dyes and Pigments* **2017,** *146*, 151-158.
59. Wadsworth, A.; Ashraf, R. S.; Abdelsamie, M.; Pont, S.; Little, M.; Moser, M.; Hamid, Z.; Neophytou, M.; Zhang, W.; Amassian, A., Highly efficient and reproducible nonfullerene solar cells from hydrocarbon solvents. *ACS Energy Letters* **2017,** *2* (7), 1494-1500.

60. Moussalem, C.; Segut, O.; Gohier, F. d. r.; Allain, M.; Frère, P., Facile access via green procedures to a material with the benzodifuran moiety for organic photovoltaics. *ACS Sustainable Chemistry & Engineering* **2014,** *2* (4), 1043-1048.
61. Tan, L.; Li, P.; Zhang, Q.; Izquierdo, R.; Chaker, M.; Ma, D., Toward Enhancing Solar Cell Performance: An Effective and "Green" Additive. *ACS applied materials & interfaces* **2018,** *10* (7), 6498-6504.
62. Li, P.; Fenwick, O.; Yilmaz, S.; Breusov, D.; Caruana, D. J.; Allard, S.; Scherf, U.; Cacialli, F., Dual functions of a novel low-gap polymer for near infra-red photovoltaics and light-emitting diodes. *Chemical Communications* **2011,** *47* (31), 8820-8822.
63. Steinberger, S.; Mishra, A.; Reinold, E.; Mena-Osteritz, E.; Müller, H.; Uhrich, C.; Pfeiffer, M.; Bäuerle, P., Synthesis and characterizations of red/near-IR absorbing A–D–A–D–A-type oligothiophenes containing thienothiadiazole and thienopyrazine central units. *Journal of Materials Chemistry* **2012,** *22* (6), 2701-2712.
64. Misra, A.; Kumar, P.; Srivastava, R.; Dhawan, S.; Kamalasanan, M.; Chandra, S., Electrochemical and optical studies of conjugated polymers for three primary colours. **2005**.
65. Wodyński, A.; Gryff-Keller, A.; Pecul, M., The influence of a presence of a heavy atom on 13C shielding constants in organomercury compounds and halogen derivatives. *Journal of chemical theory and computation* **2013,** *9* (4), 1909-1917.
66. Yau, C. P.; Fei, Z.; Ashraf, R. S.; Shahid, M.; Watkins, S. E.; Pattanasattayavong, P.; Anthopoulos, T. D.; Gregoriou, V. G.; Chochos, C. L.; Heeney, M., Influence of the Electron Deficient Co-Monomer on the Optoelectronic Properties and Photovoltaic Performance of Dithienogermole-based Co-Polymers. *Advanced Functional Materials* **2014,** *24* (5), 678-687.
67. Admassie, S.; Inganäs, O.; Mammo, W.; Perzon, E.; Andersson, M. R., Electrochemical and optical studies of the band gaps of alternating polyfluorene copolymers. *Synthetic metals* **2006,** *156* (7-8), 614-623.
68. Freeman, A. W.; Urvoy, M.; Criswell, M. E., Triphenylphosphine-Mediated Reductive Cyclization of 2-Nitrobiphenyls: A Practical and Convenient Synthesis of Carbazoles. *The Journal of Organic Chemistry* **2005,** *70* (13), 5014-5019.
69. Lan, L.; Chen, Z.; Hu, Q.; Ying, L.; Zhu, R.; Liu, F.; Russell, T. P.; Huang, F.; Cao, Y., High-Performance Polymer Solar Cells Based on a Wide-Bandgap Polymer Containing Pyrrolo [3, 4-f] benzotriazole-5, 7-dione with a Power Conversion Efficiency of 8.63%. *Advanced Science* **2016,** *3* (9), 1600032.
70. Lv, G.; Mai, W.; Jin, R.; Gao, L., Immobilization of dipyridyl complex to magnetic nanoparticle via click chemistry as a recyclable catalyst for Suzuki cross-coupling reactions. *Synlett* **2008,** *2008* (09), 1418-1422.

8. Appendices

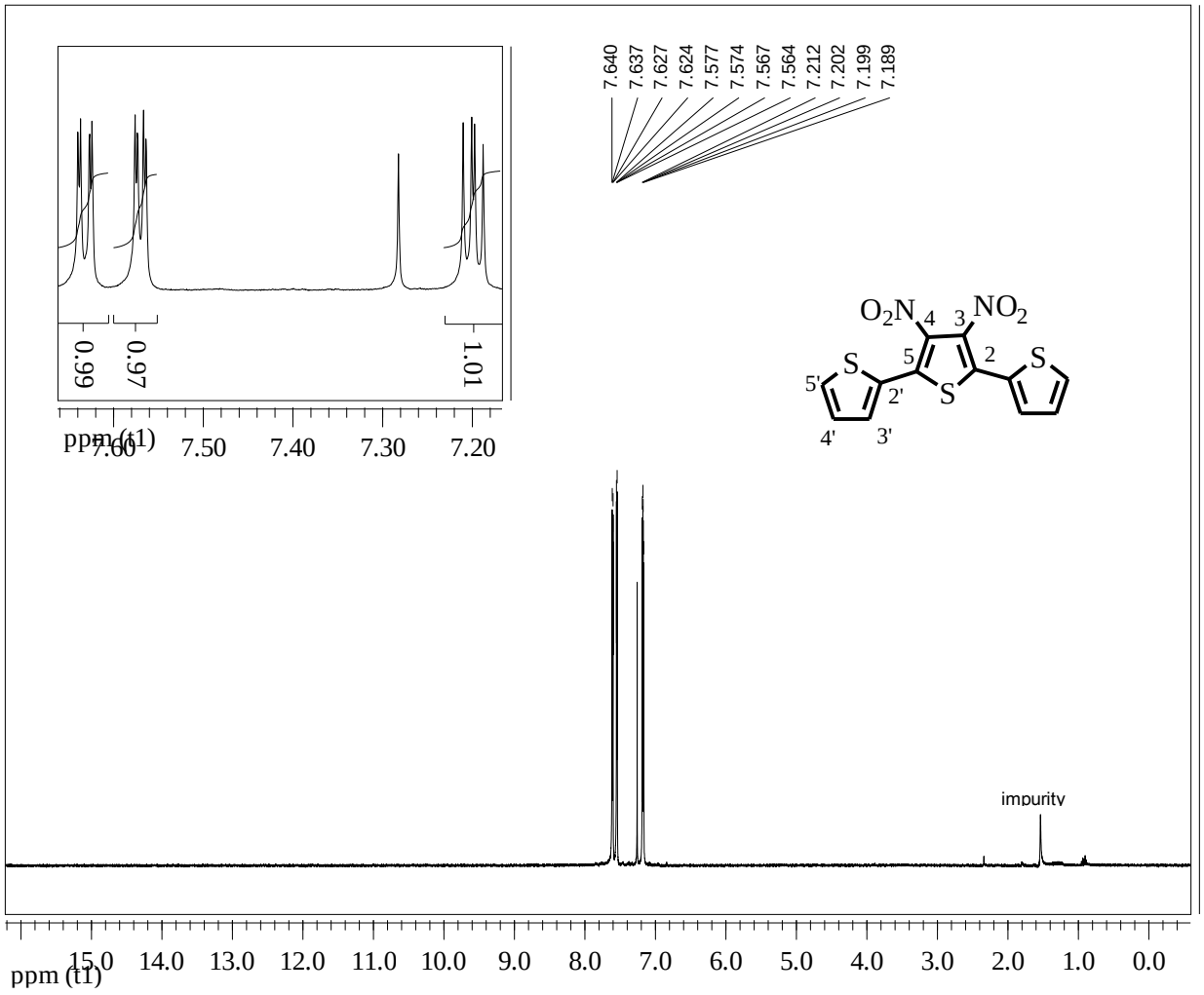

Appendix 1: ^{1}H NMR spectrum of 2,5-bis(2-thienyl)-3,4-dinitrothiophene (**7**).

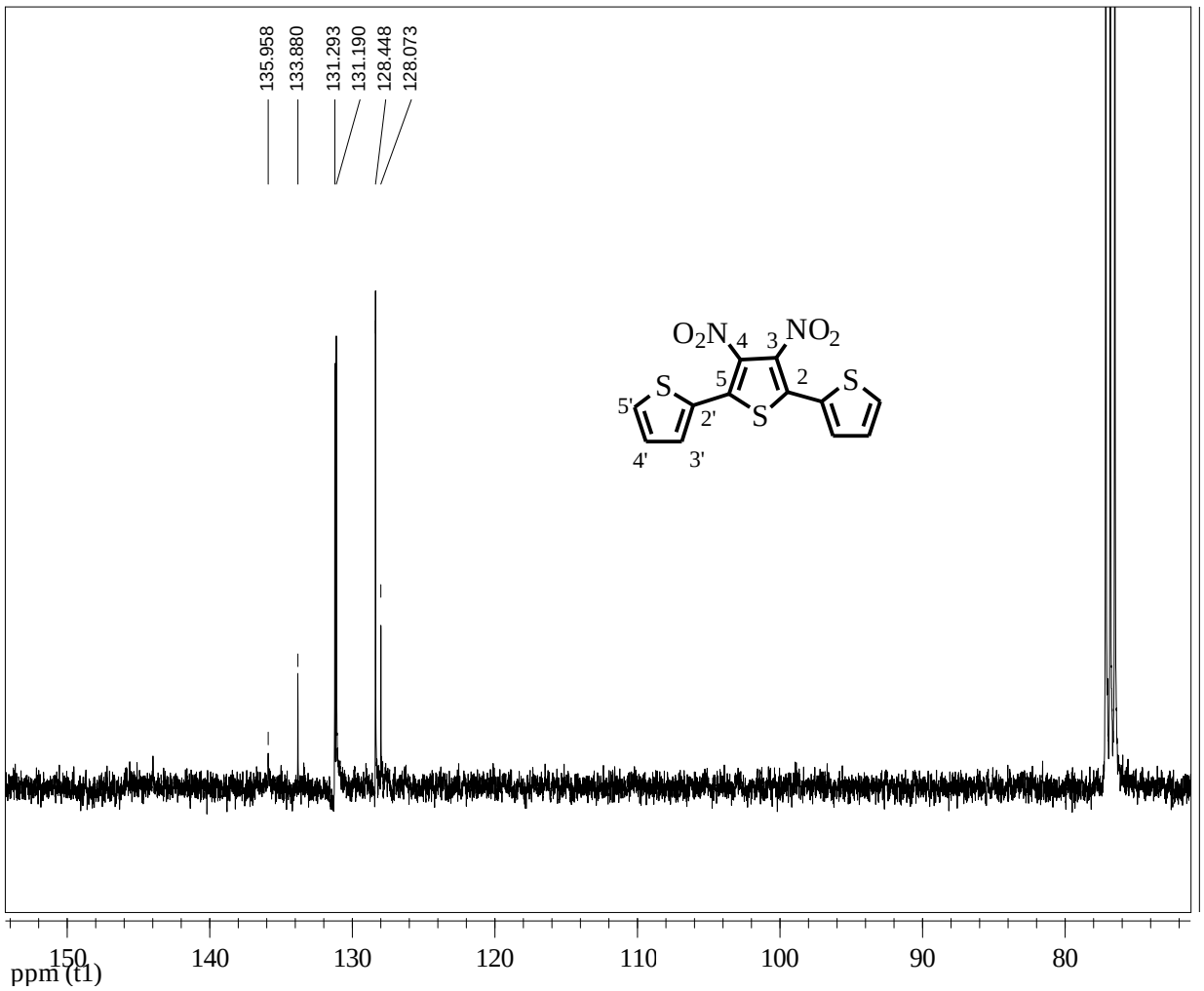

Appendix 2: ^{13}C NMR spectrum of 2,5-bis(2-thienyl)-3,4-dinitrothiophene (**7**).

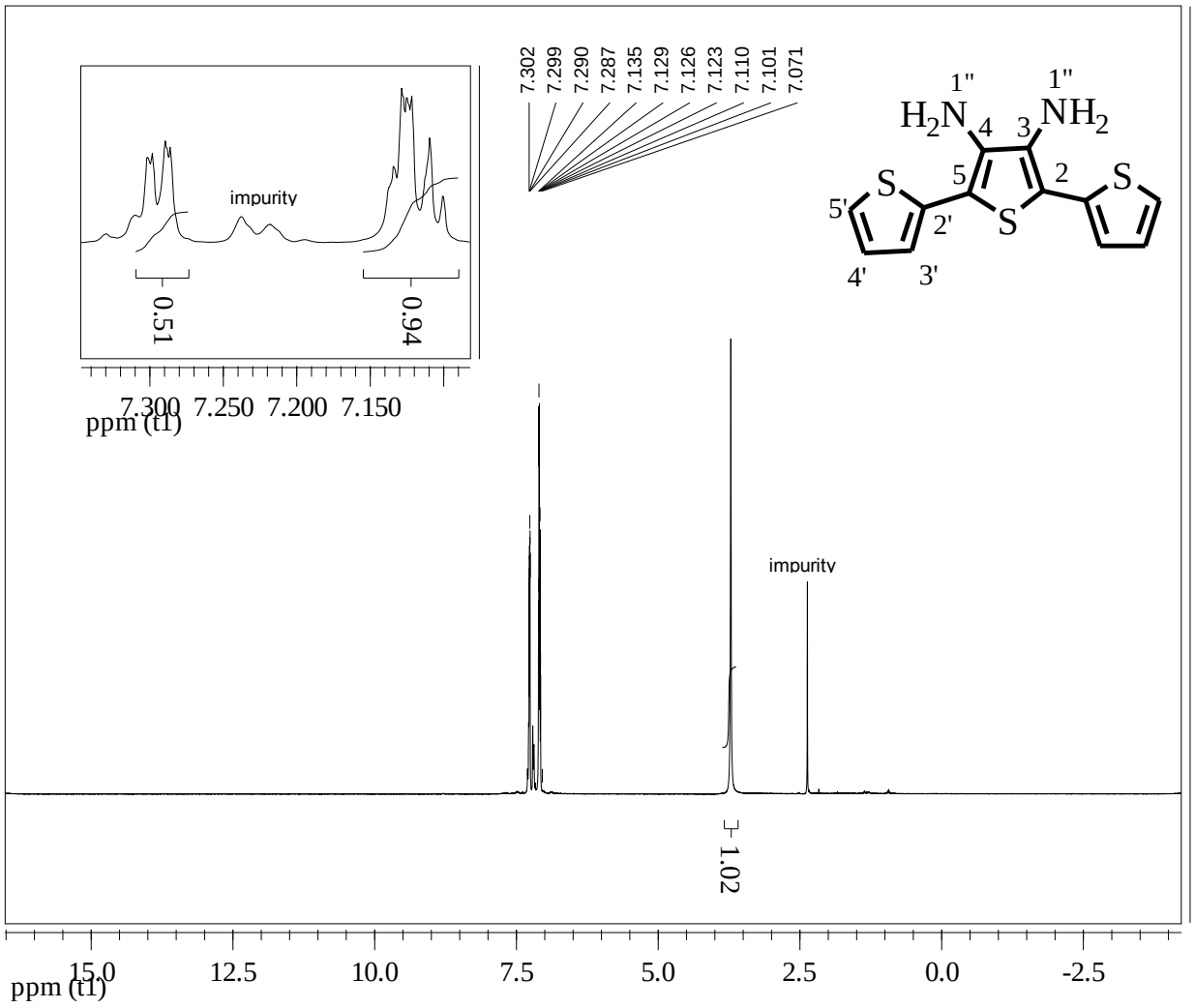

Appendix 3: ^{1}H NMR spectrum of 2,5-bis(2-thienyl)-3,4-diaminothiophene (**8**).

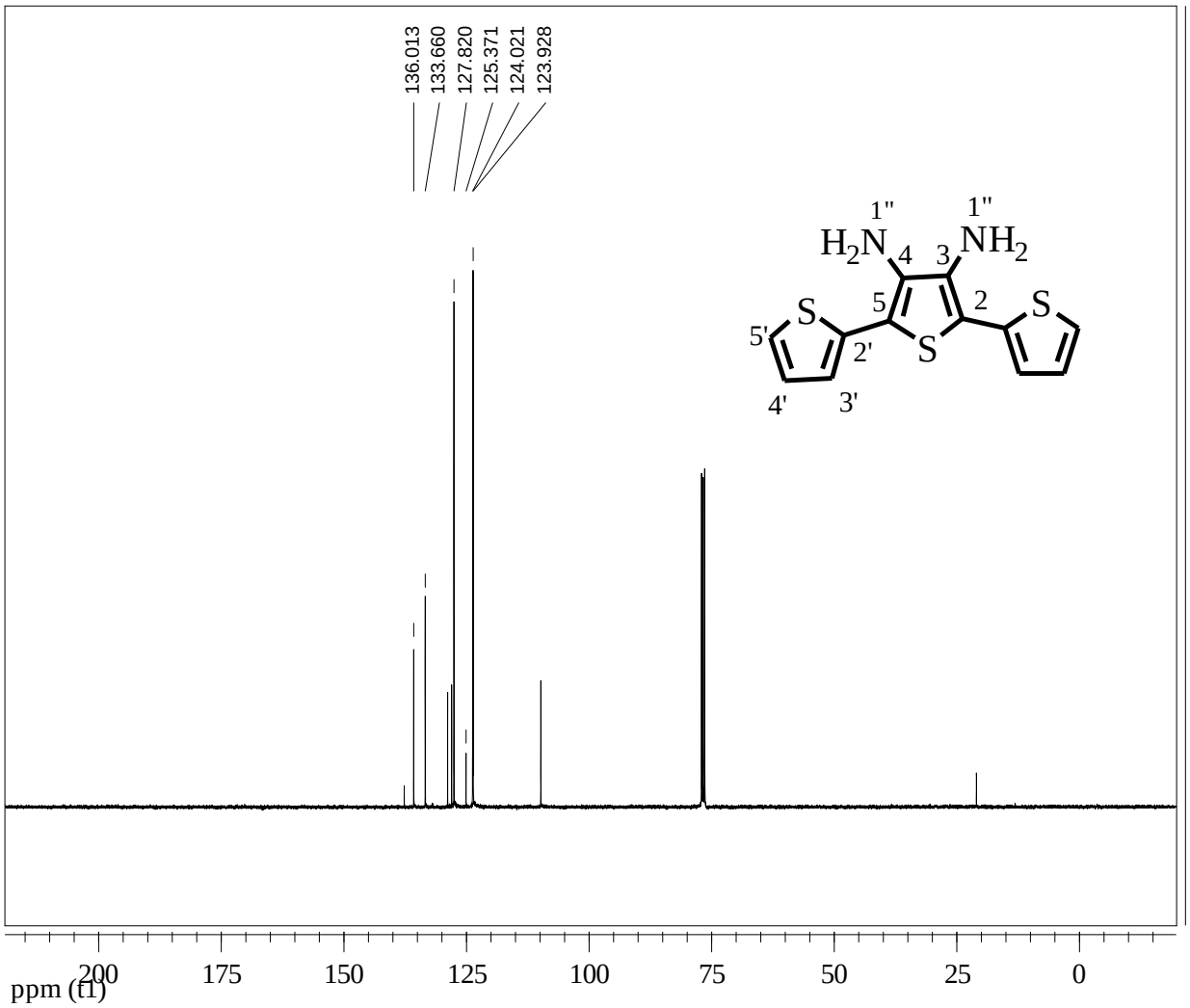

Appendix 4: ^{13}C NMR spectrum of 2,5-bis(2-thienyl)-3,4-diaminothiophene (**8**).

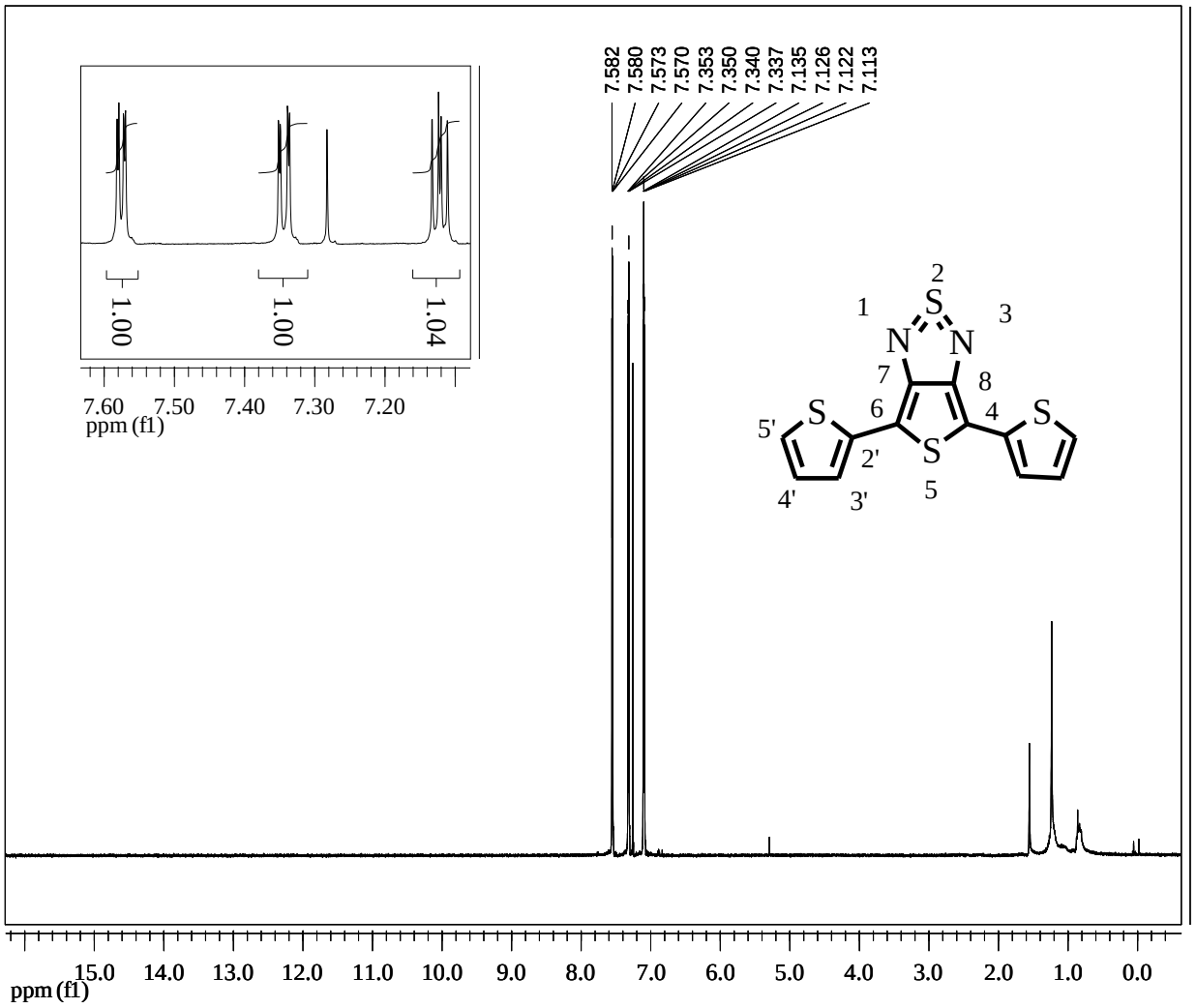

Appendix 5: ^{1}H NMR spectrum of 4,8-di(2-thienyl)-thieno[3,4-*c*]-thiadiazole (**9**).

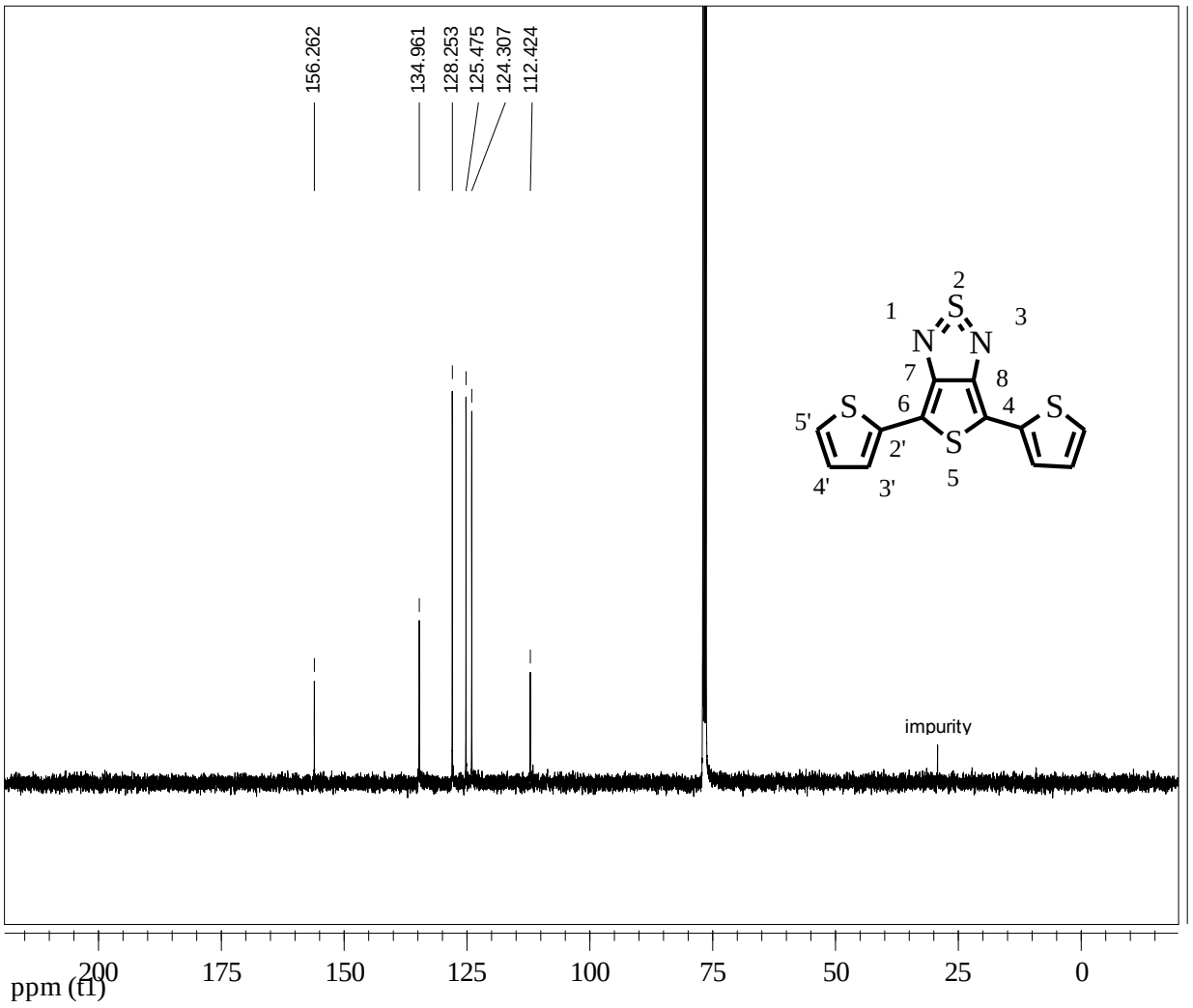

Appendix 6: ^{13}C NMR spectrum of 4,8-di(2-thienyl)-thieno[3,4-*c*]-thiadiazole (**9**).

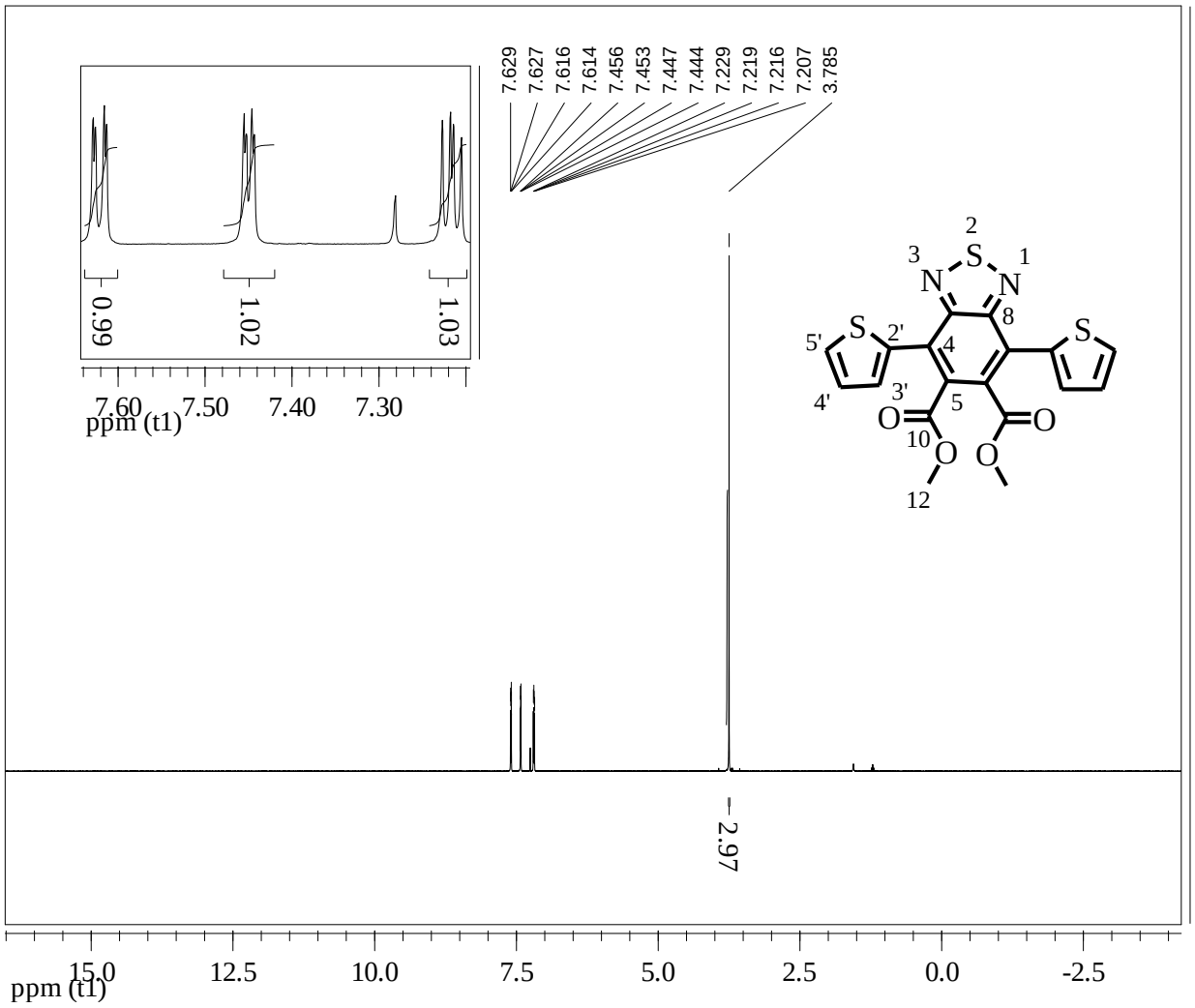

Appendix 7: ^{1}H NMR spectrum of dimethyl-4,7-di(2-thienyl)-2,1,3-benzothiadiazole-5,6-dicarboxylate (**11**).

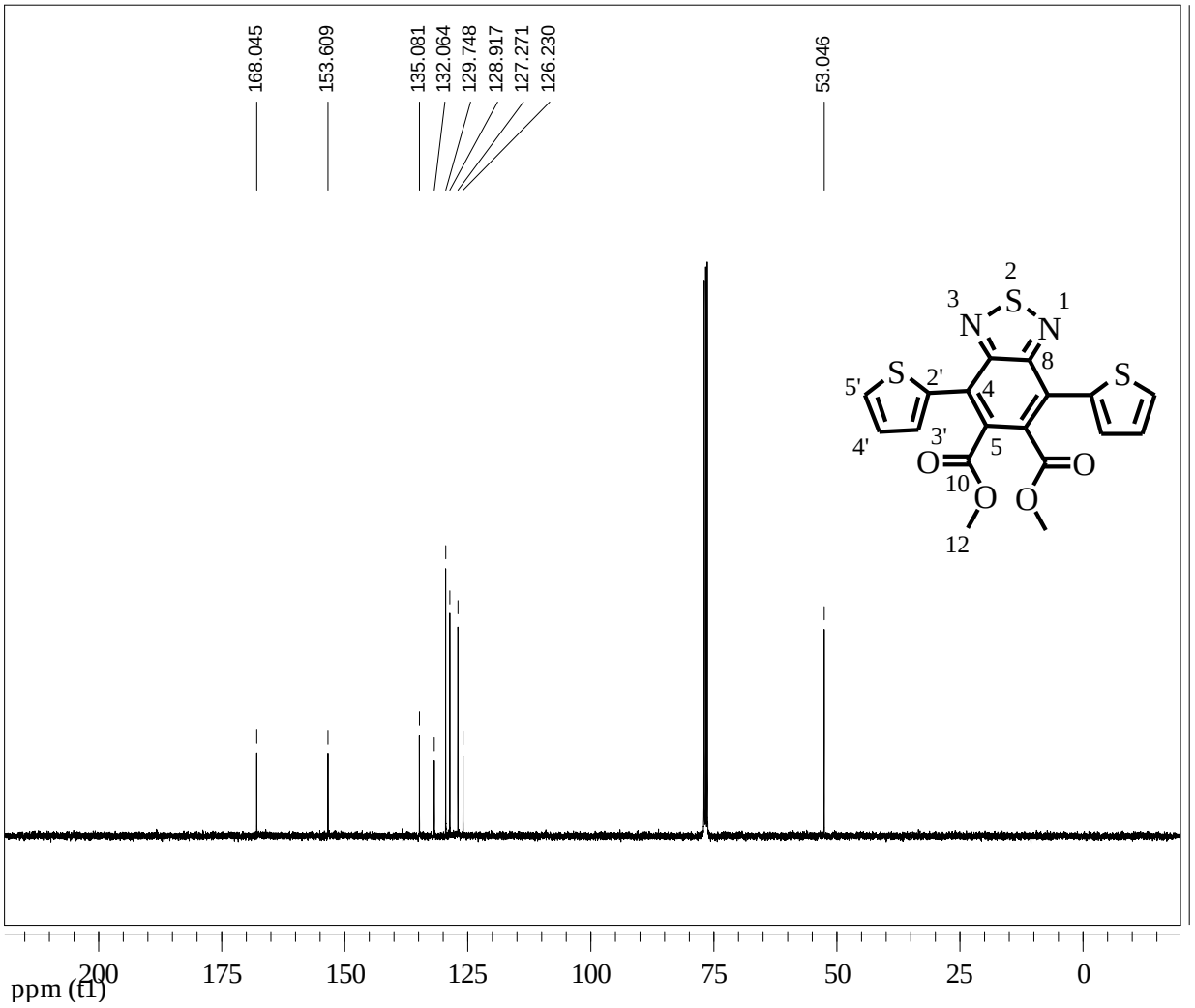

Appendix 8: ^{13}C NMR spectrum of dimethyl-4,7-di(2-thienyl)-2,1,3-benzothiadiazole-5,6-dicarboxylate (**11**).

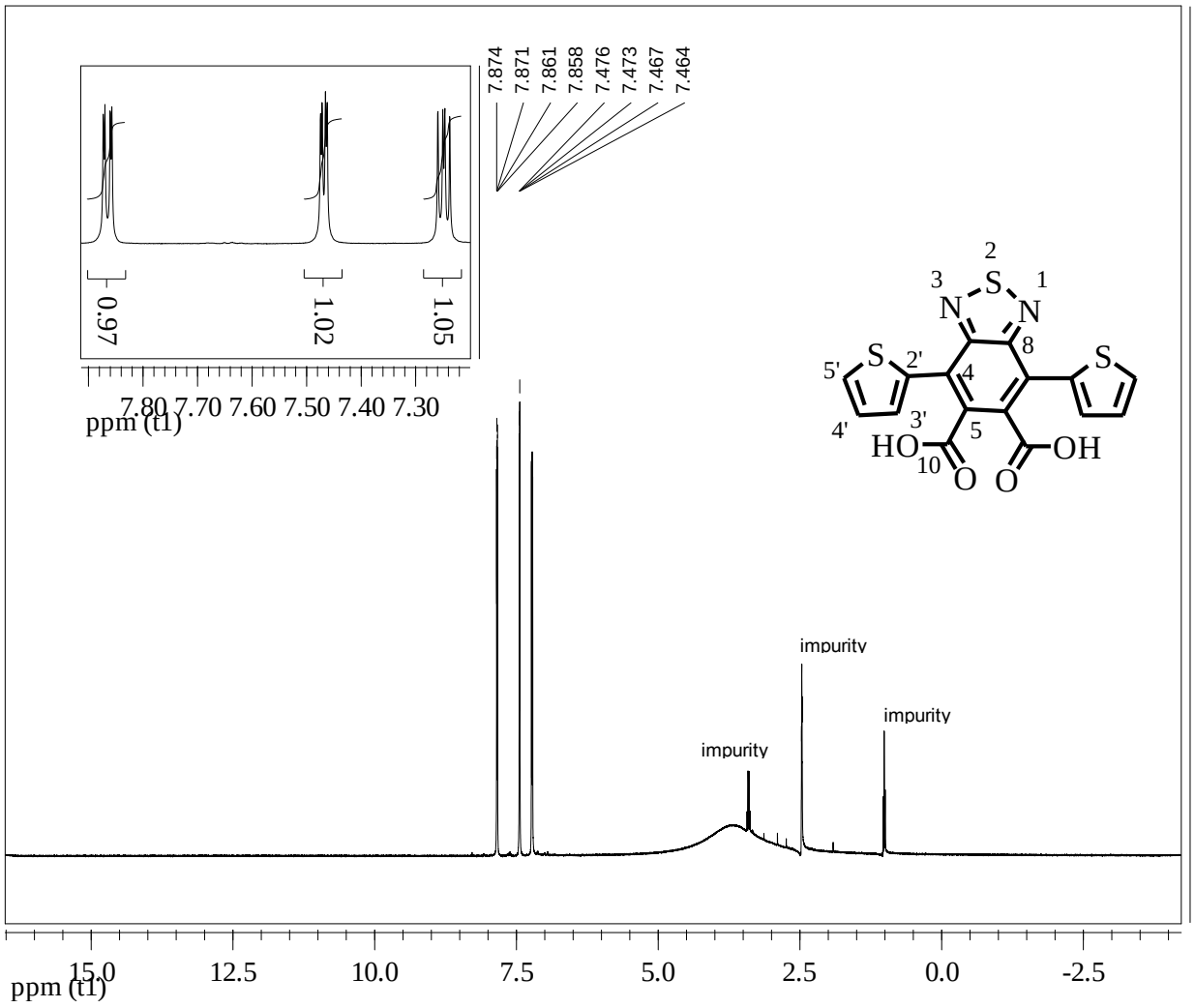

Appendix 9: ^{1}H NMR spectrum of 4,7-di(2-thienyl)-2,1,3-benzothiadiazole-5,6-dicarboxylic acid (**12**).

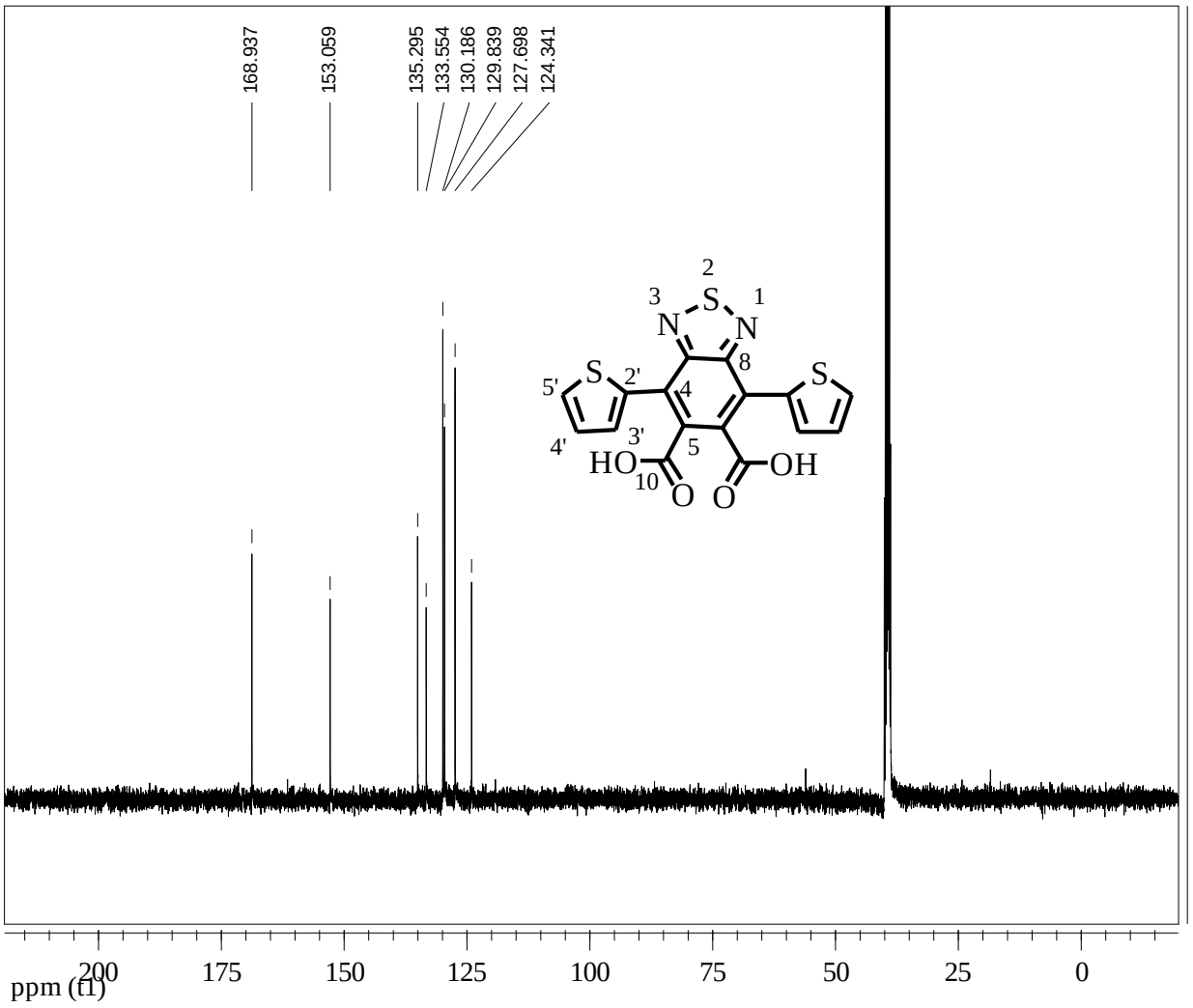

Appendix 10: ^{13}C NMR spectrum of 4,7-di(2-thienyl)-2,1,3-benzothiadiazole-5,6-dicarboxylic acid (**12**).

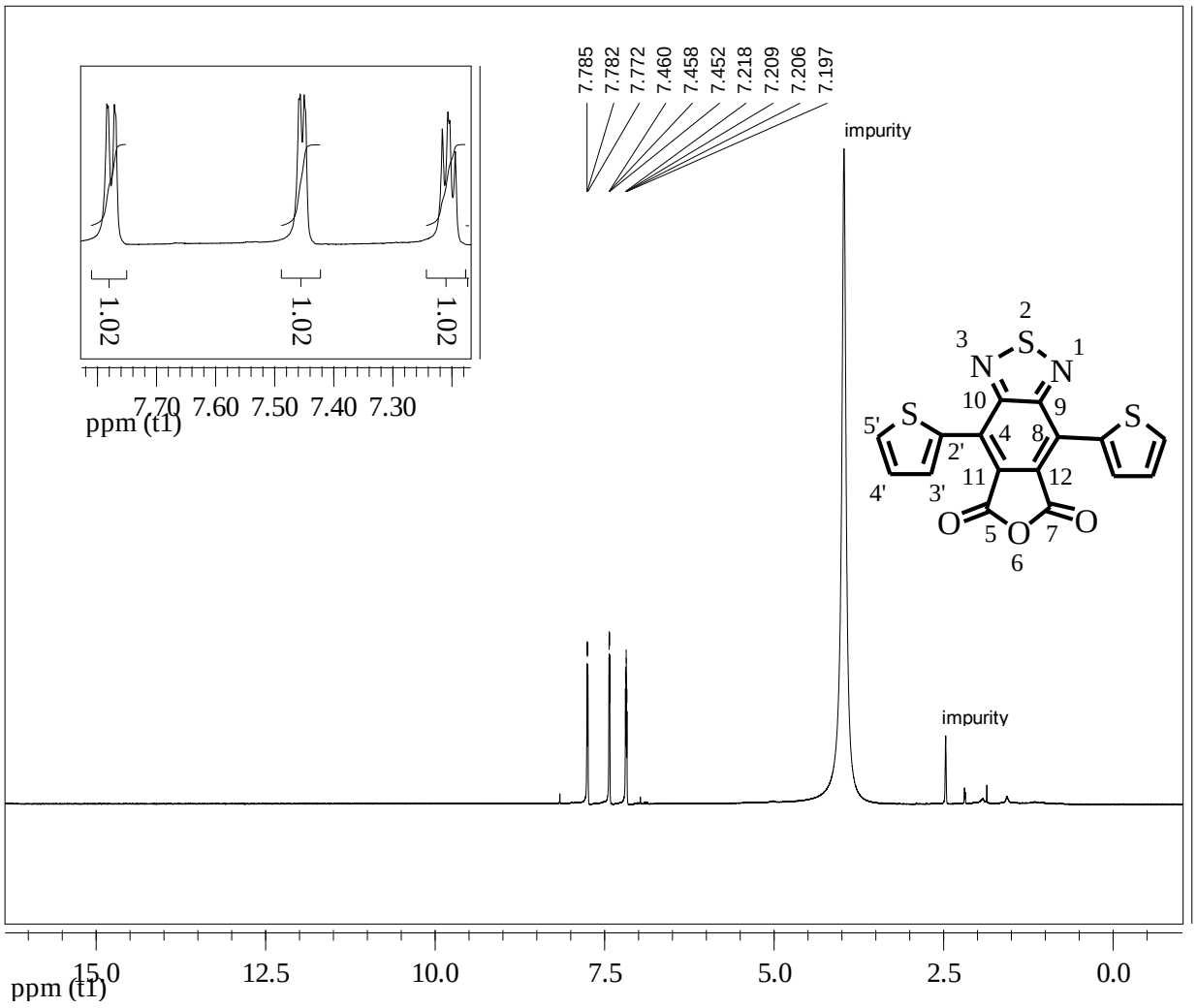

Appendix 11: ^{1}H NMR spectrum of 4,7-di(2-thienyl)-2,1,3-benzothiadiazole-5,6-dicarboxylic anhydride (**13**).

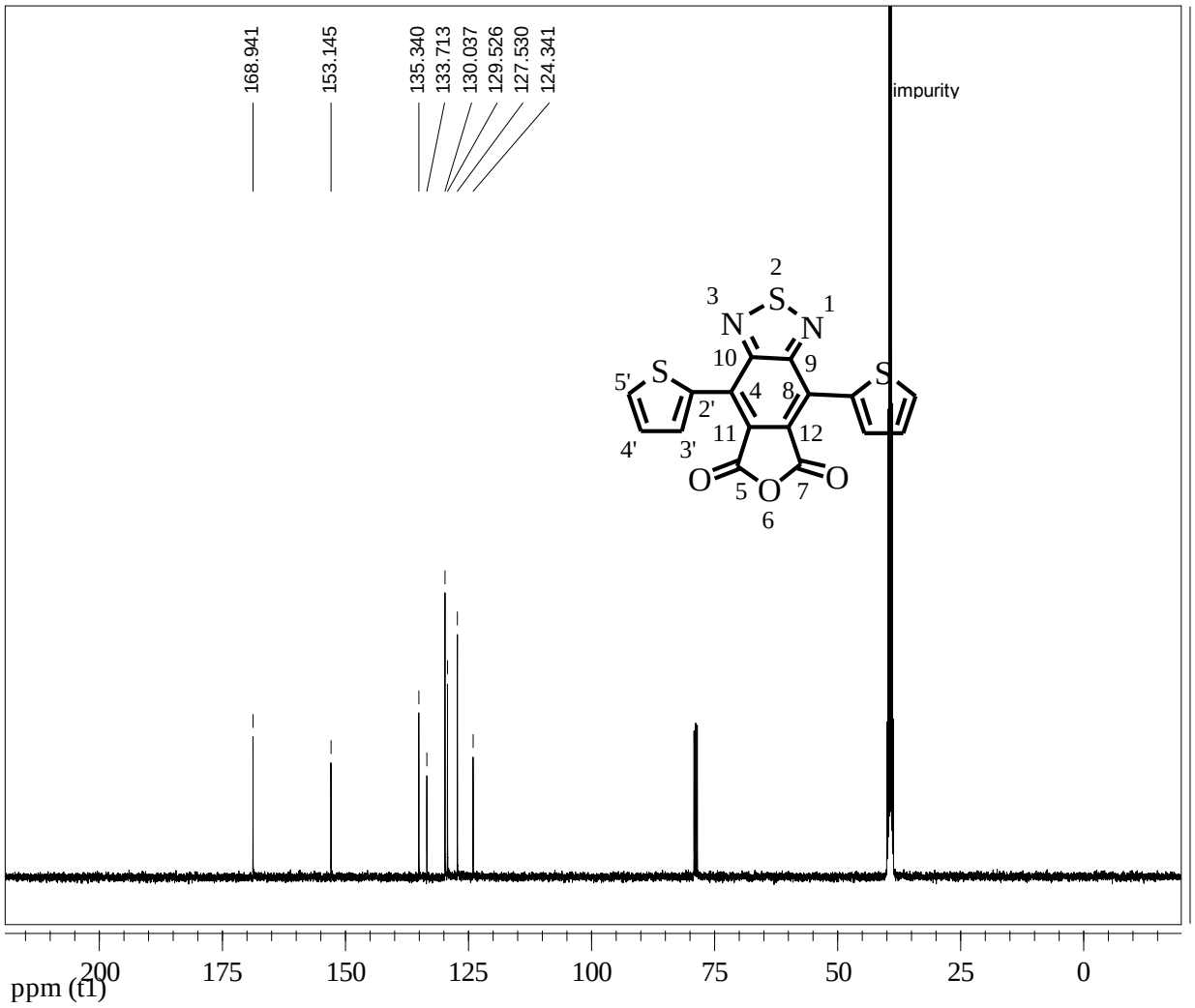

Appendix 12: ^{13}C NMR spectrum of 4,7-di(2-thienyl)-2,1,3-benzothiadiazole-5,6-dicarboxylic anhydride (**13**).

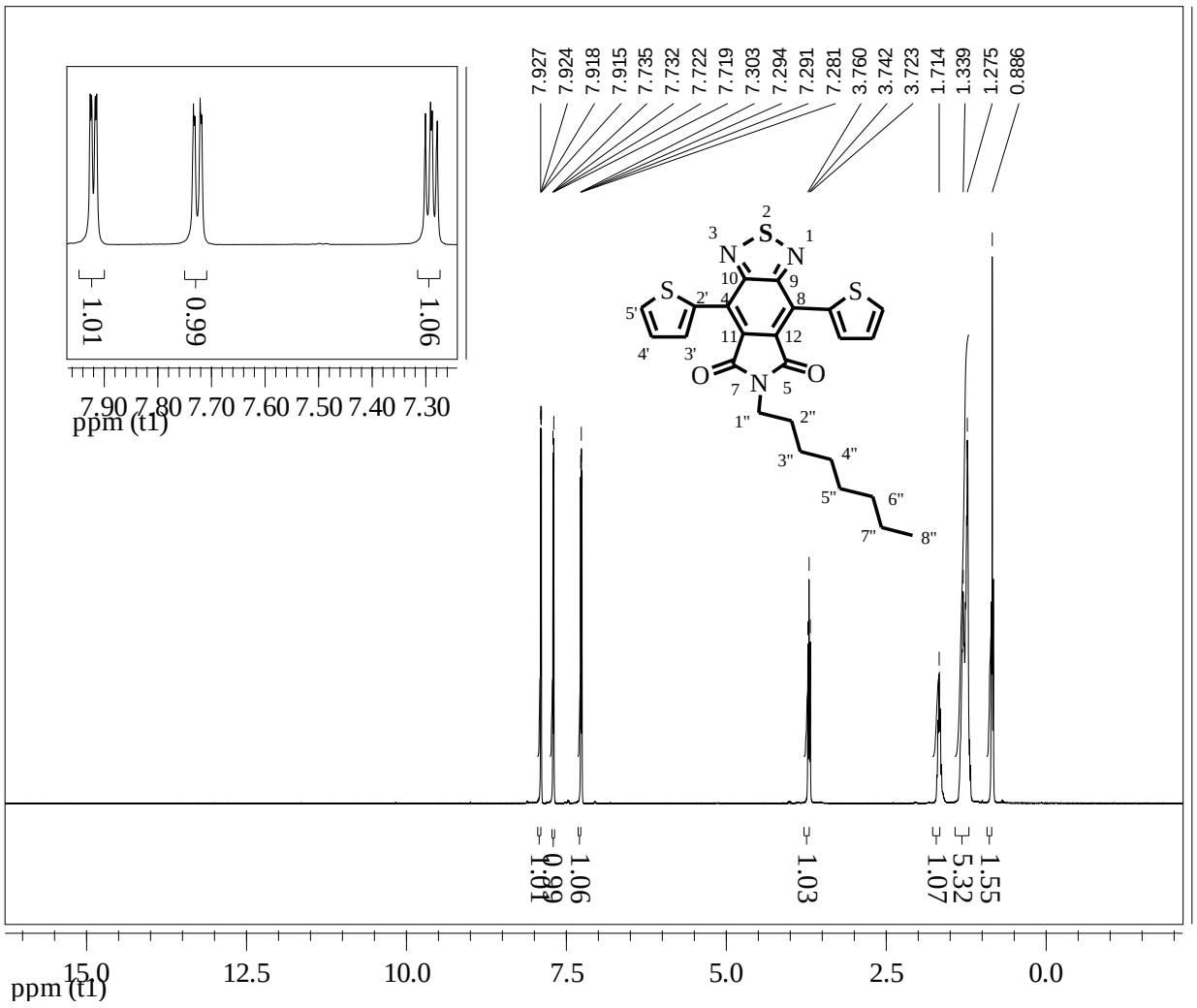

Appendix 13: ^{1}H NMR spectrum of *N*-octyl-4,7-di(thien-2-yl)-2,1,3-benzothiadiazole-5,6-dicarboxylic imide (**14**)

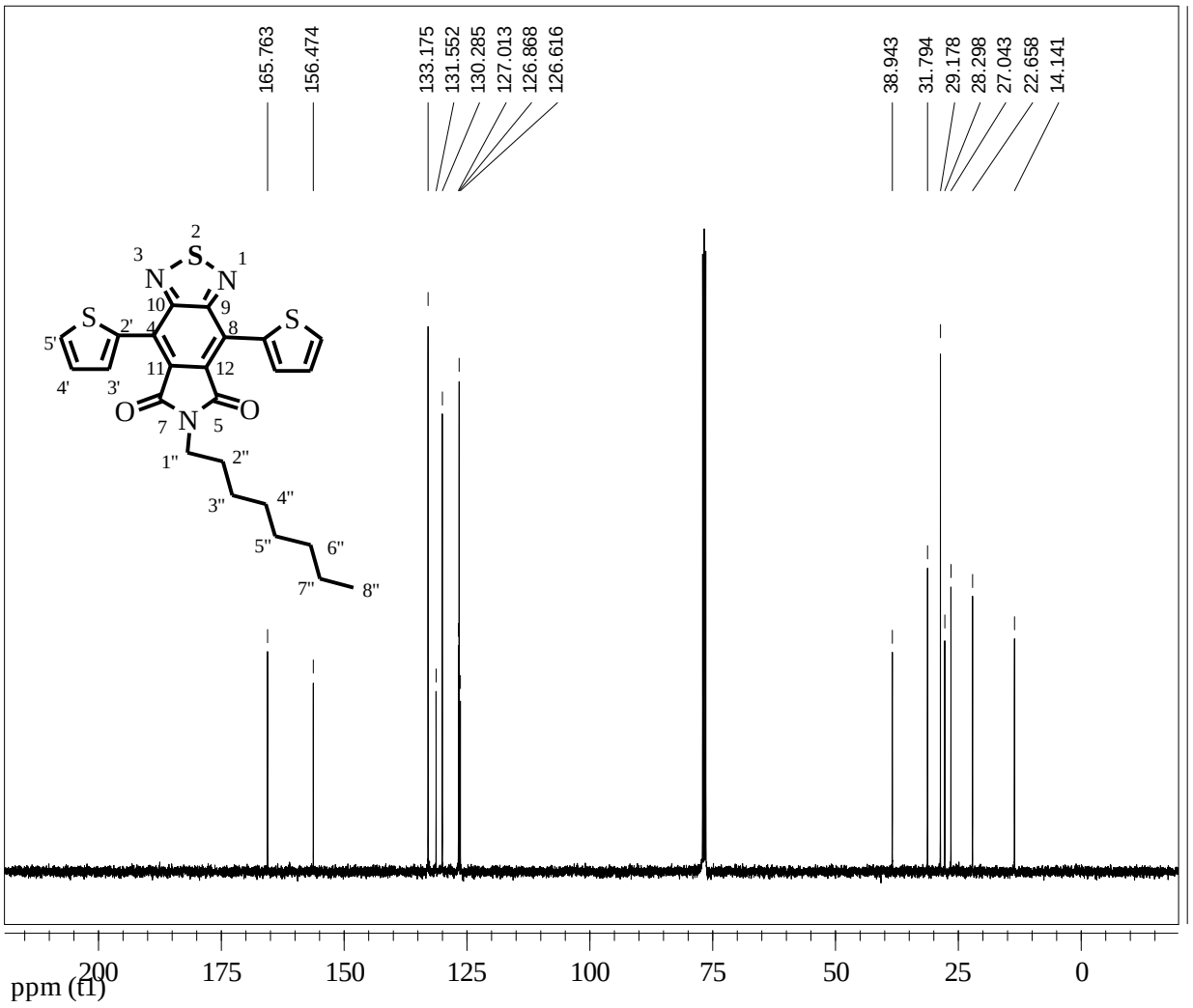

Appendix 14: ^{13}C NMR spectrum of *N*-octyl-4,7-di(thien-2-yl)-2,1,3-benzothiadiazole-5,6-dicarboxylic imide (**14**).

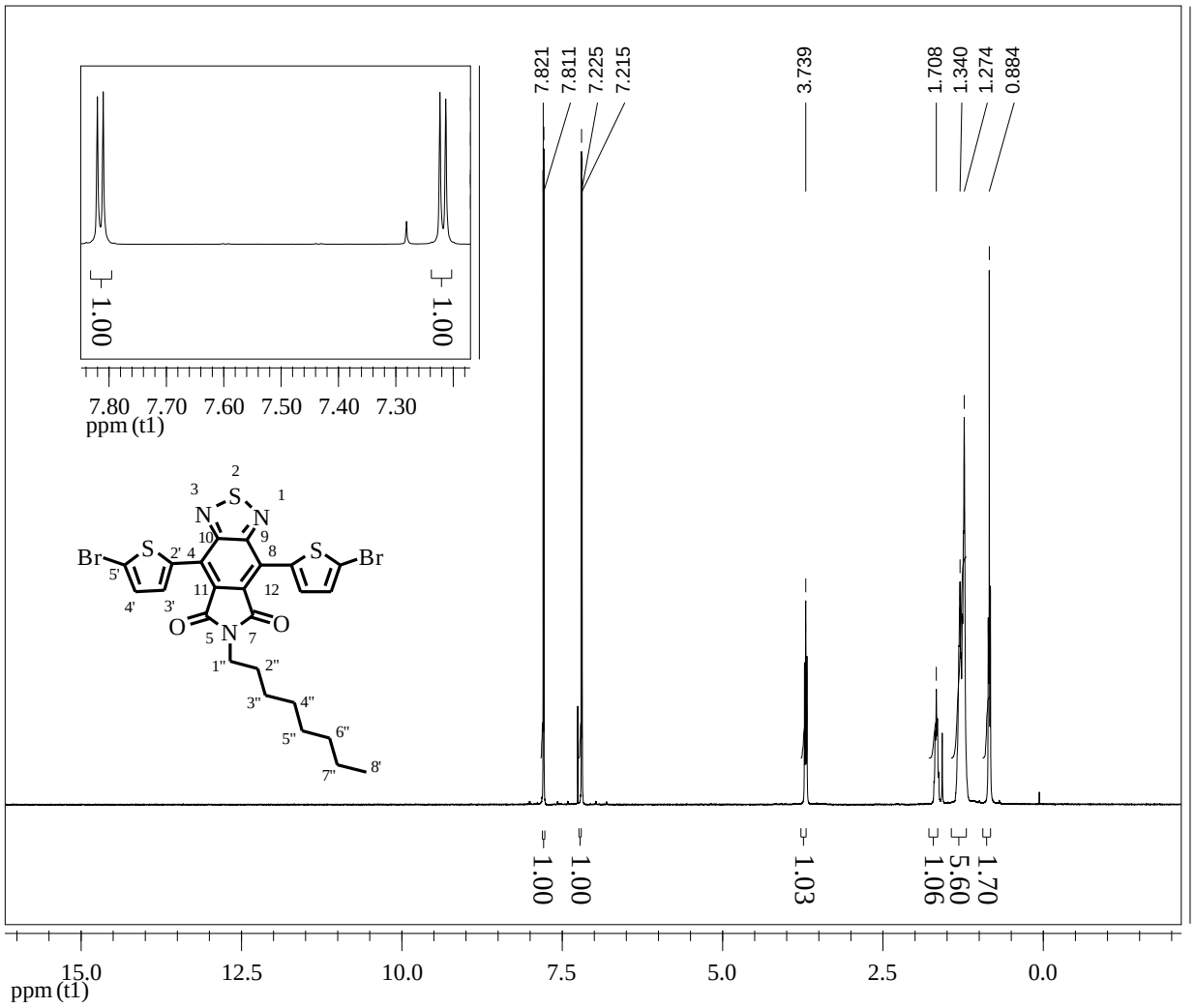

Appendix 15: ^{1}H NMR spectrum of *N*-octyl-4,7-di(5-bromo-2-thienyl)-2,1,3-benzothiadiazole-5,6-dicarboxylic imide (**15**).

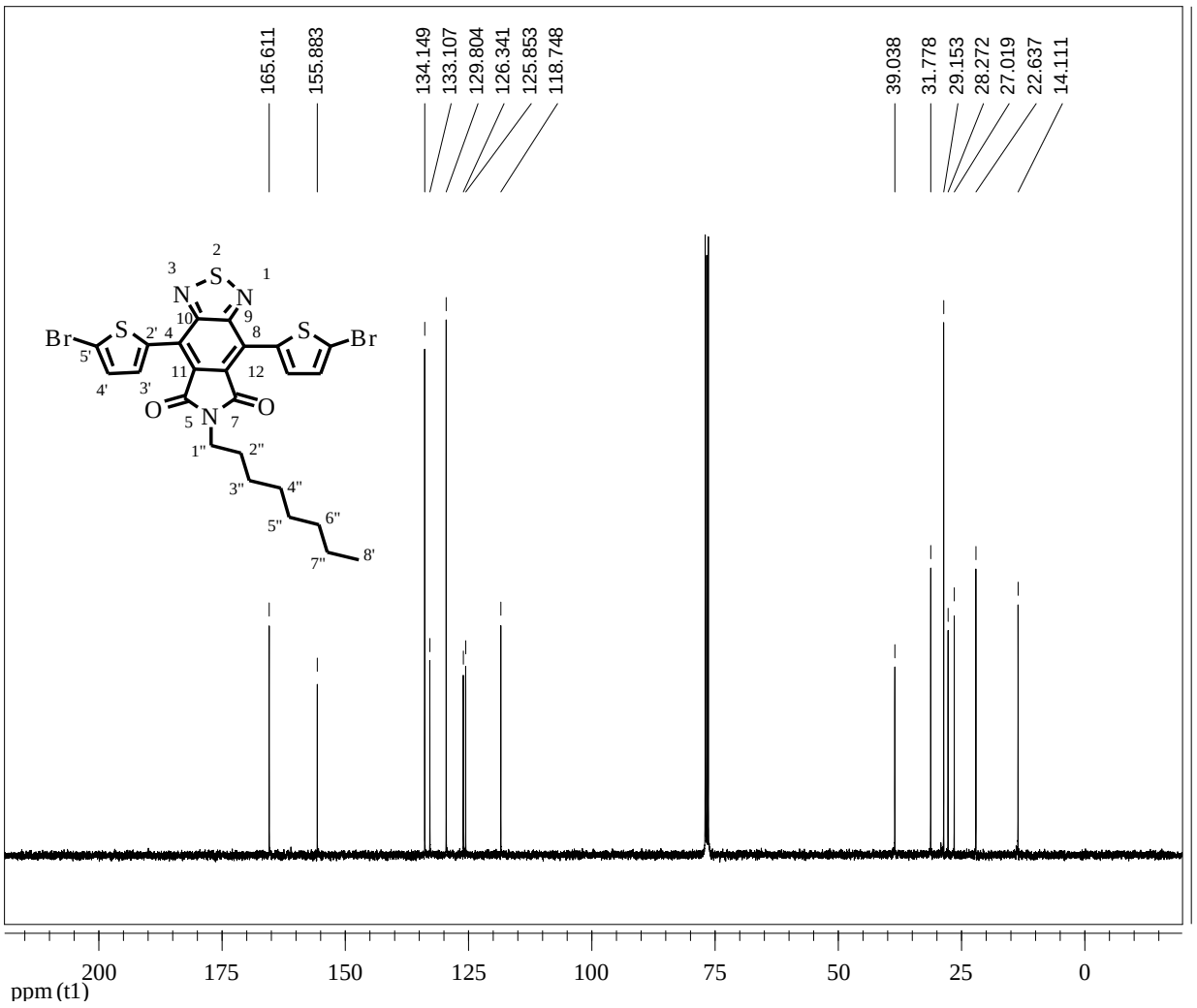

Appendix 16: ^{13}C NMR spectrum of *N*-octyl-4,7-di(5-bromo-2-thienyl)-2,1,3-benzothiadiazole-5,6-dicarboxylic imide (**15**).

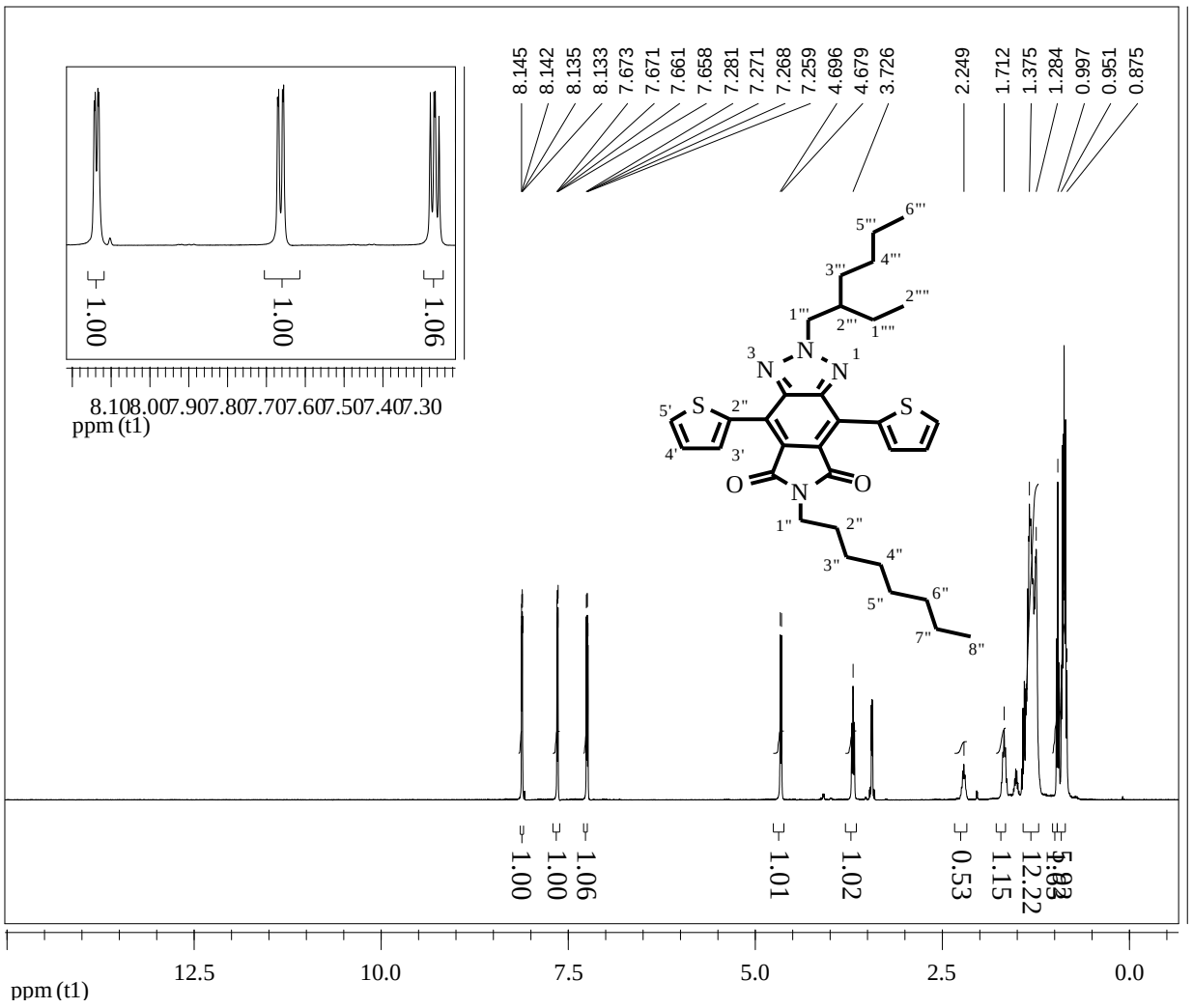

Appendix 17: ^{1}H NMR spectrum of 2-(2-ethylhexyl)-6-octyl-4,8-di(thien-2-yl)-[1,2,3]triazolo[4,5-*f*]isoindole-5,7-(2*H*,6*H*)-dione (**18**).

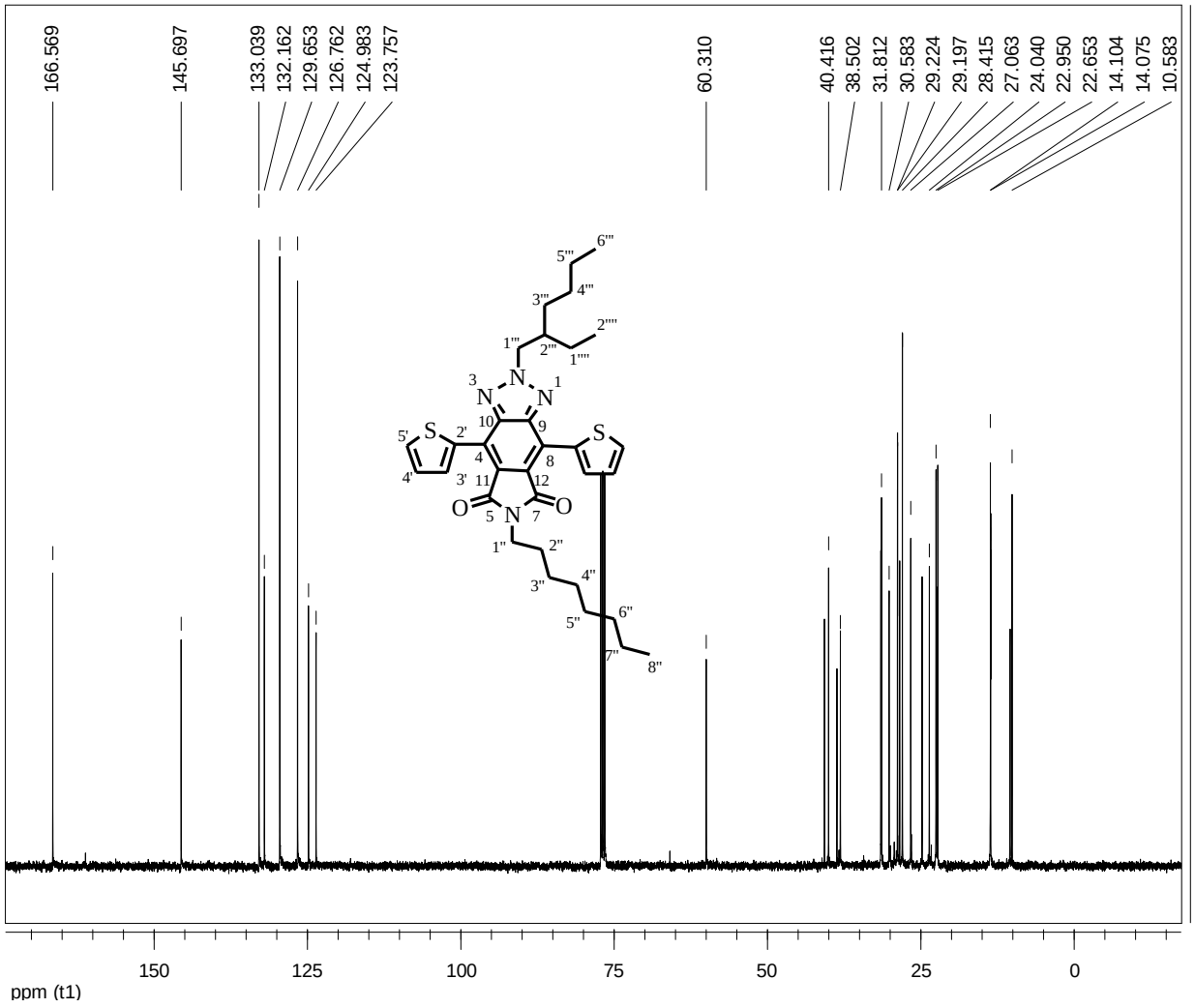

Appendix 18: ^{13}C NMR spectrum of 2-(2-ethylhexyl)-6-octyl-4,8-di(thien-2-yl)-[1,2,3]triazolo[4,5-*f*]isoindole-5,7-(2*H*,6*H*)-dione (**18**).

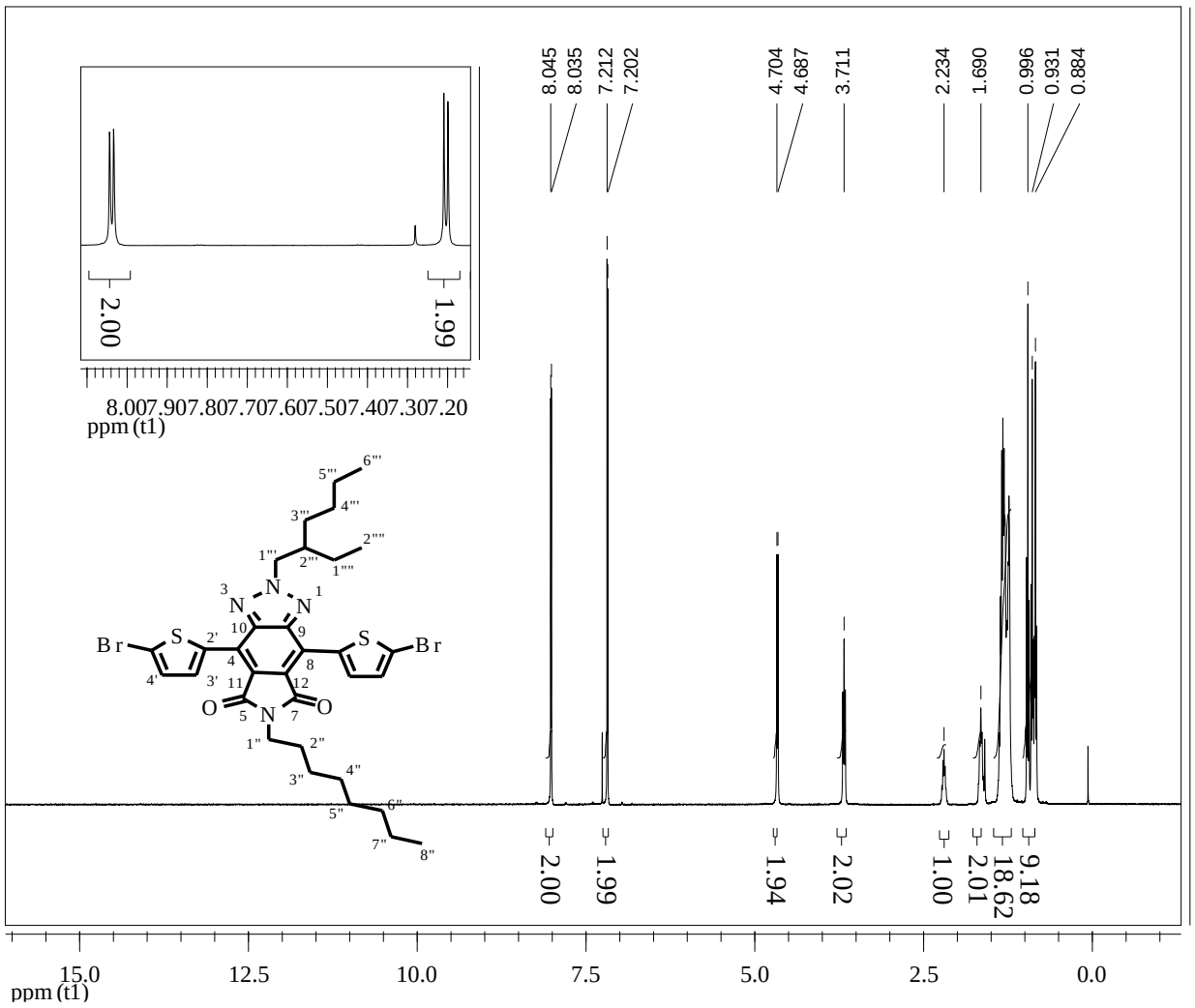

Appendix 19: ^{1}H NMR spectrum of 4,8-bis(5-bromothiophen-2-yl)-2-(2-ethylhexyl)-6-octyl-[1,2,3]triazolo[4,5-*f*]isoindole-5,7(2*H*,6*H*)-dione (**19**).

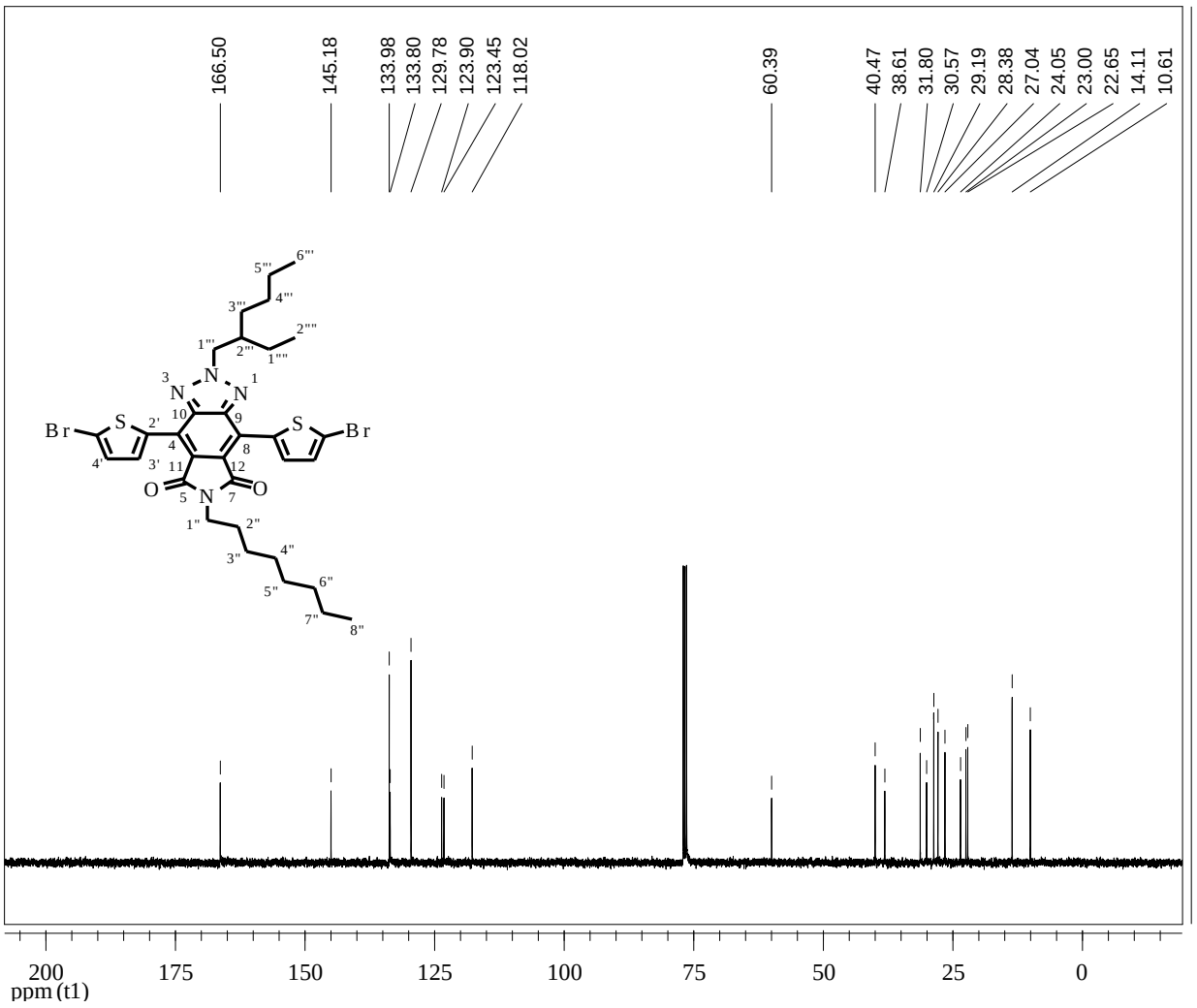

Appendix 20: ^{13}C NMR spectrum of 4,8-bis(5-bromothiophen-2-yl)-2-(2-ethylhexyl)-6-octyl-[1,2,3]triazolo[4,5-*f*]isoindole-5,7(2*H*,6*H*)-dione (**19**).

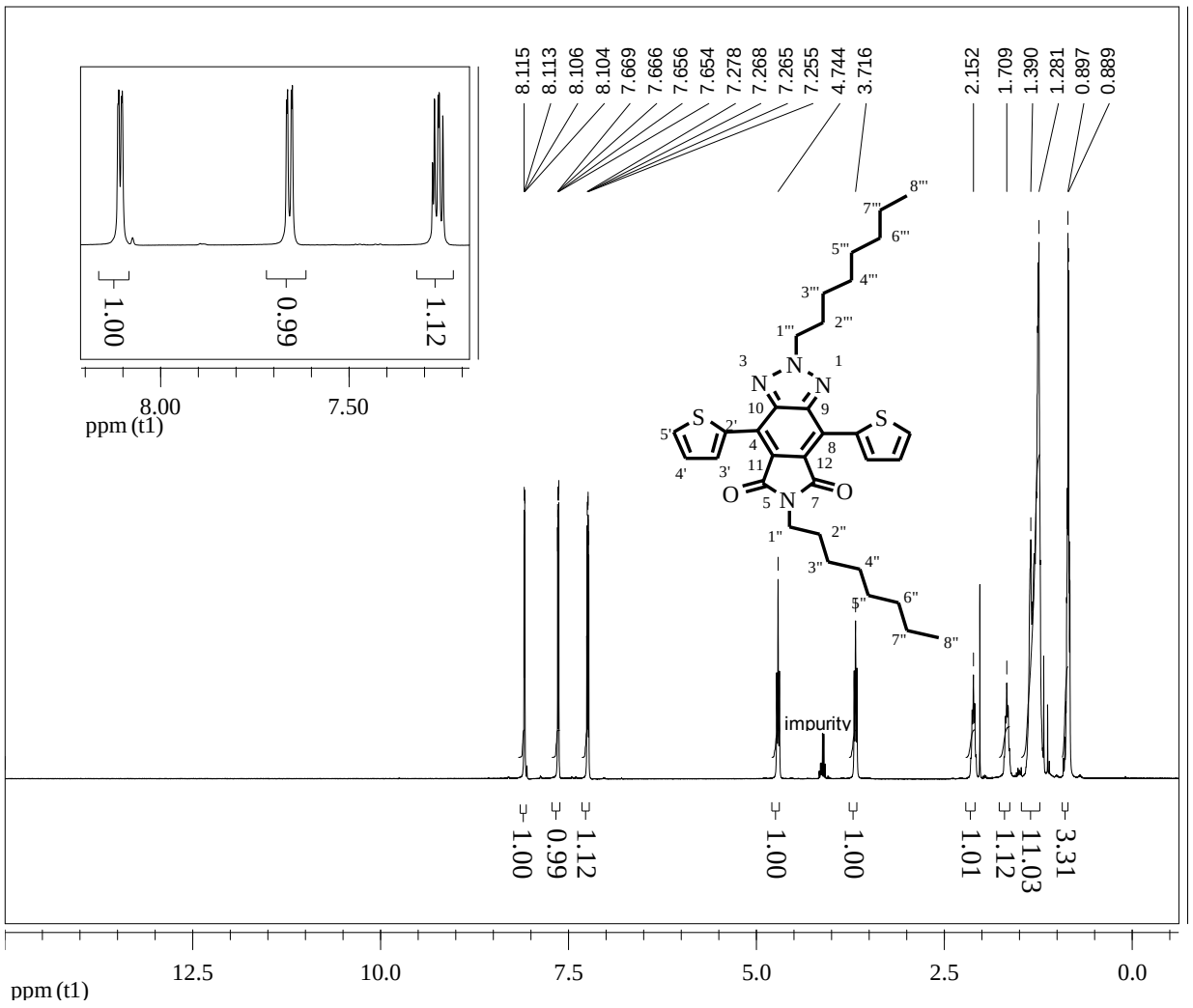

Appendix 21: ^{1}H NMR spectrum of 2-(octyl)-6-octyl-4,8-di(thiophen-2-yl)[1,2,3]triazolo[4,5-*f*]isoindole-5,7-(2*H*,6*H*)-dione (**20**).

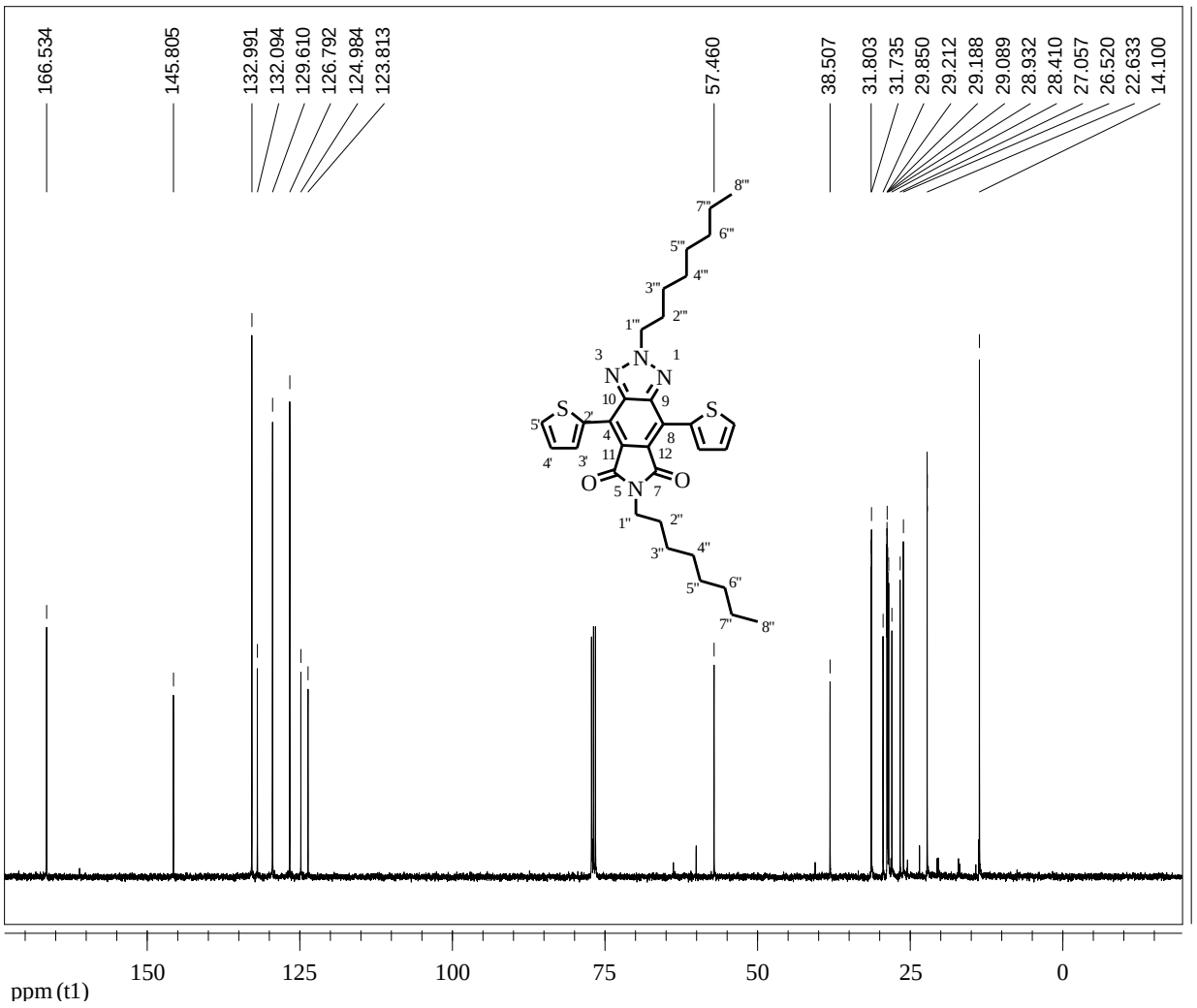

Appendix 22: ^{13}C NMR spectrum of 2-(octyl)-6-octyl-4,8-di(thiophen-2-yl)[1,2,3]triazolo[4,5-*f*]isoindole-5,7-(2*H*,6*H*)-dione (**20**).

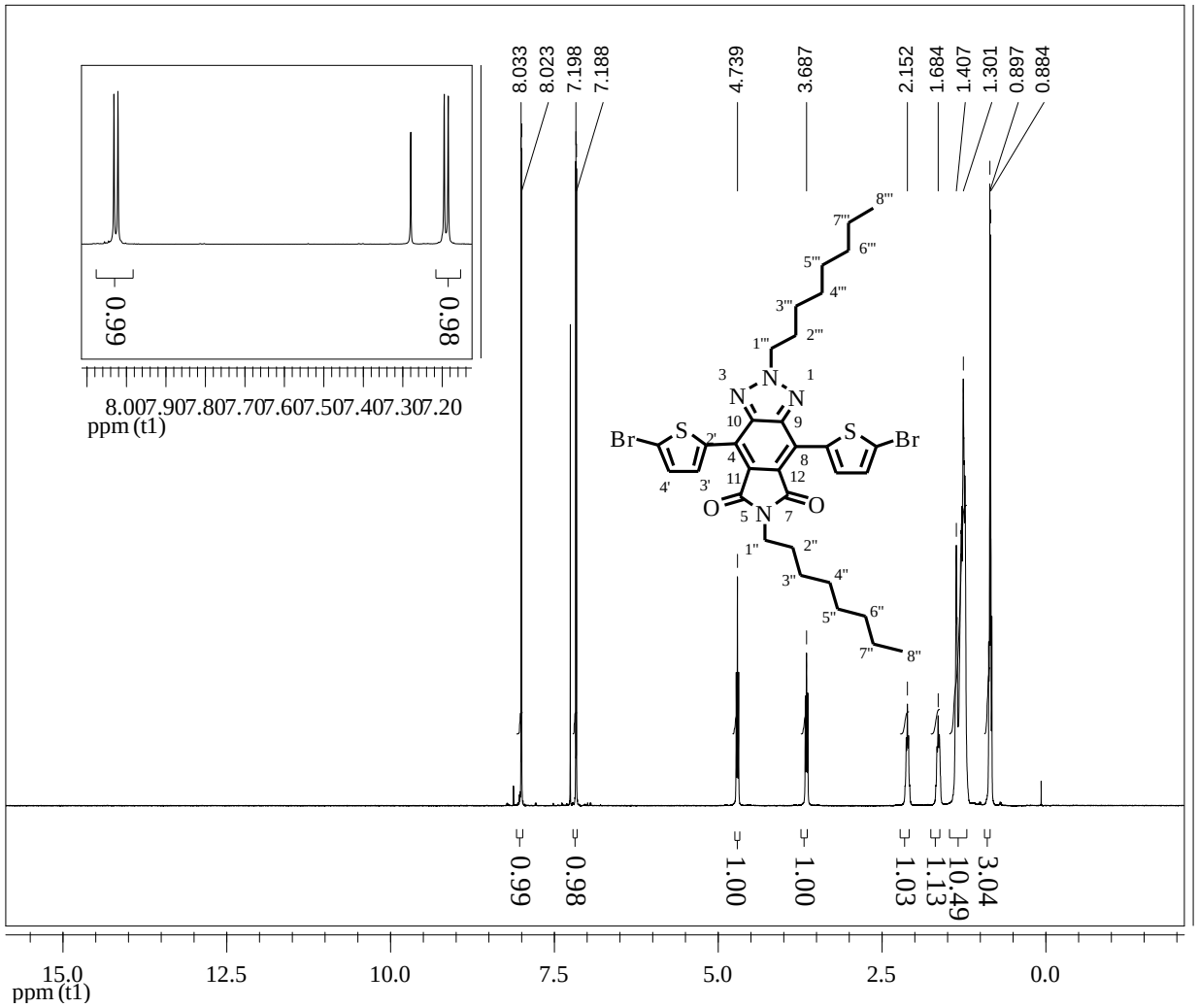

Appendix 23: ^{1}H NMR spectrum of 4,8-bis(5-bromothiophen-2-yl)-2,6-dioctyl-[1,2,3]triazolo[4,5-*f*]isoindole-5,7(2*H*,6*H*)-dione (**21**).

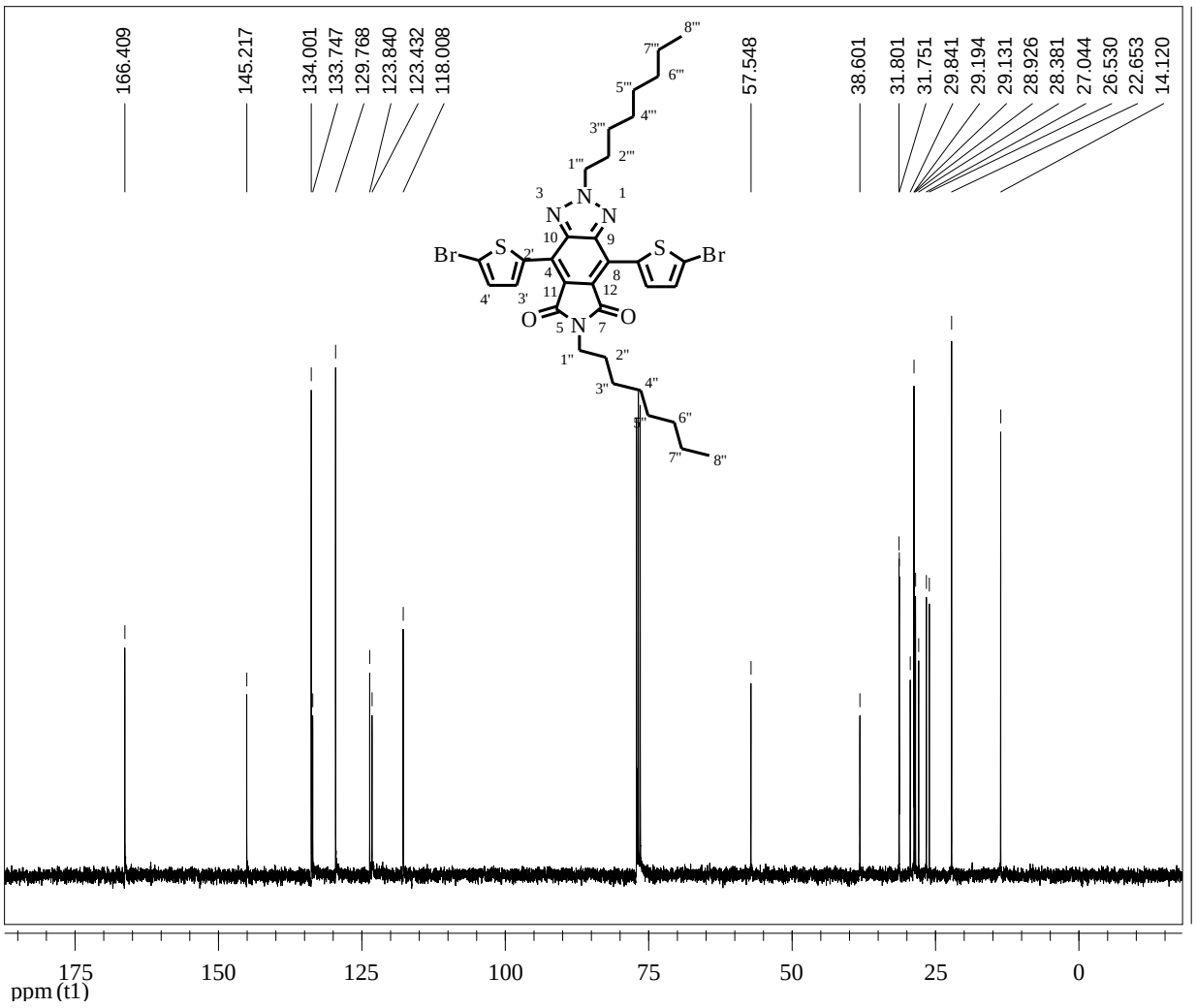

Appendix 24: ^{13}C NMR spectrum of 4,8-bis(5-bromothiophen-2-yl)-2,6-dioctyl-[1,2,3]triazolo[4,5-*f*]isoindole-5,7(2*H*,6*H*)-dione (**21**).

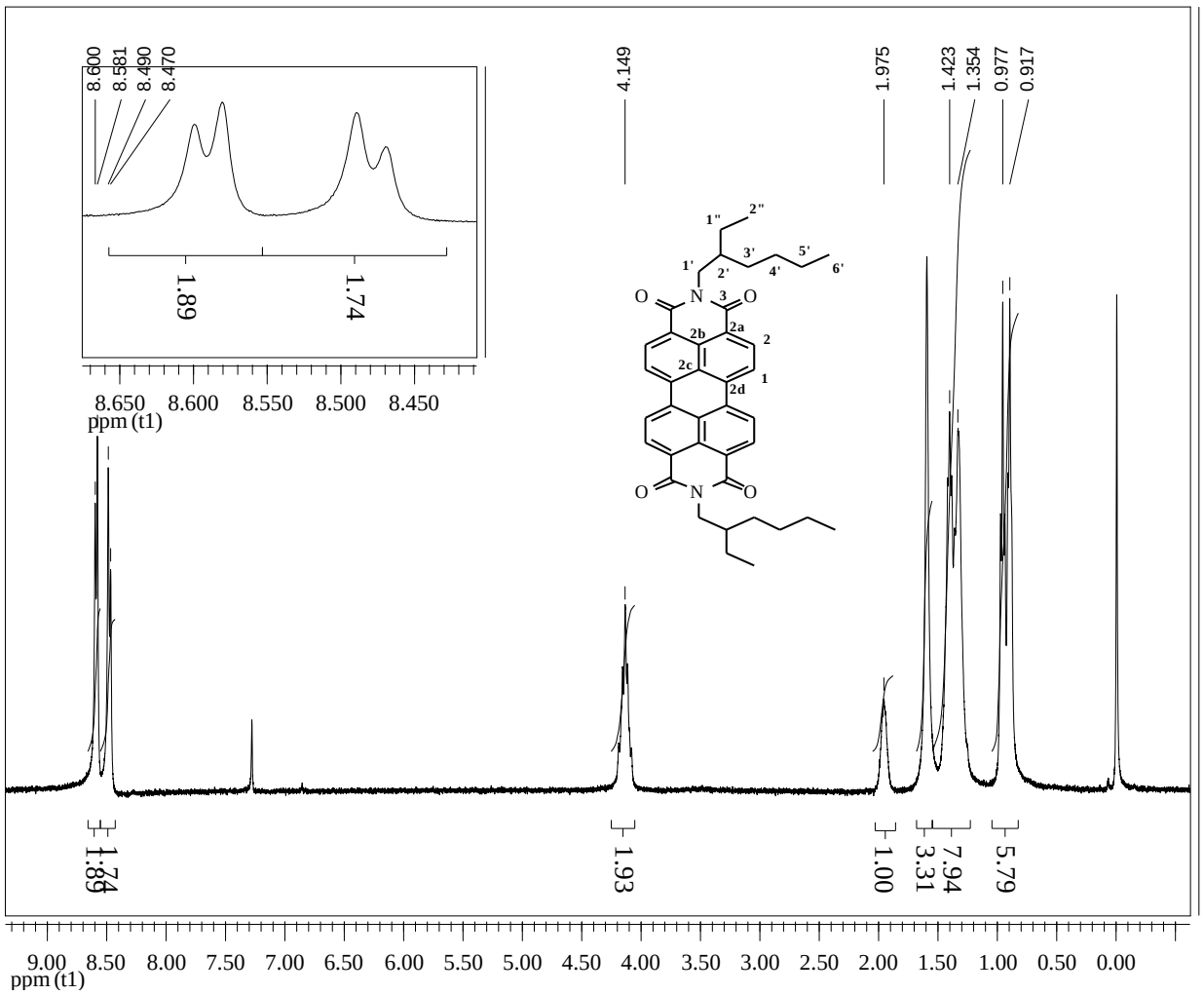

Appendix 25: ^{1}H NMR spectrum of 2,9-bis(2-ethylhexyl)anthra[2,1,9-*def*:6,5,10-*d*'e'f']diisoquinoline-1,3,8,10(2*H*,9*H*)-tetraone (**24**).

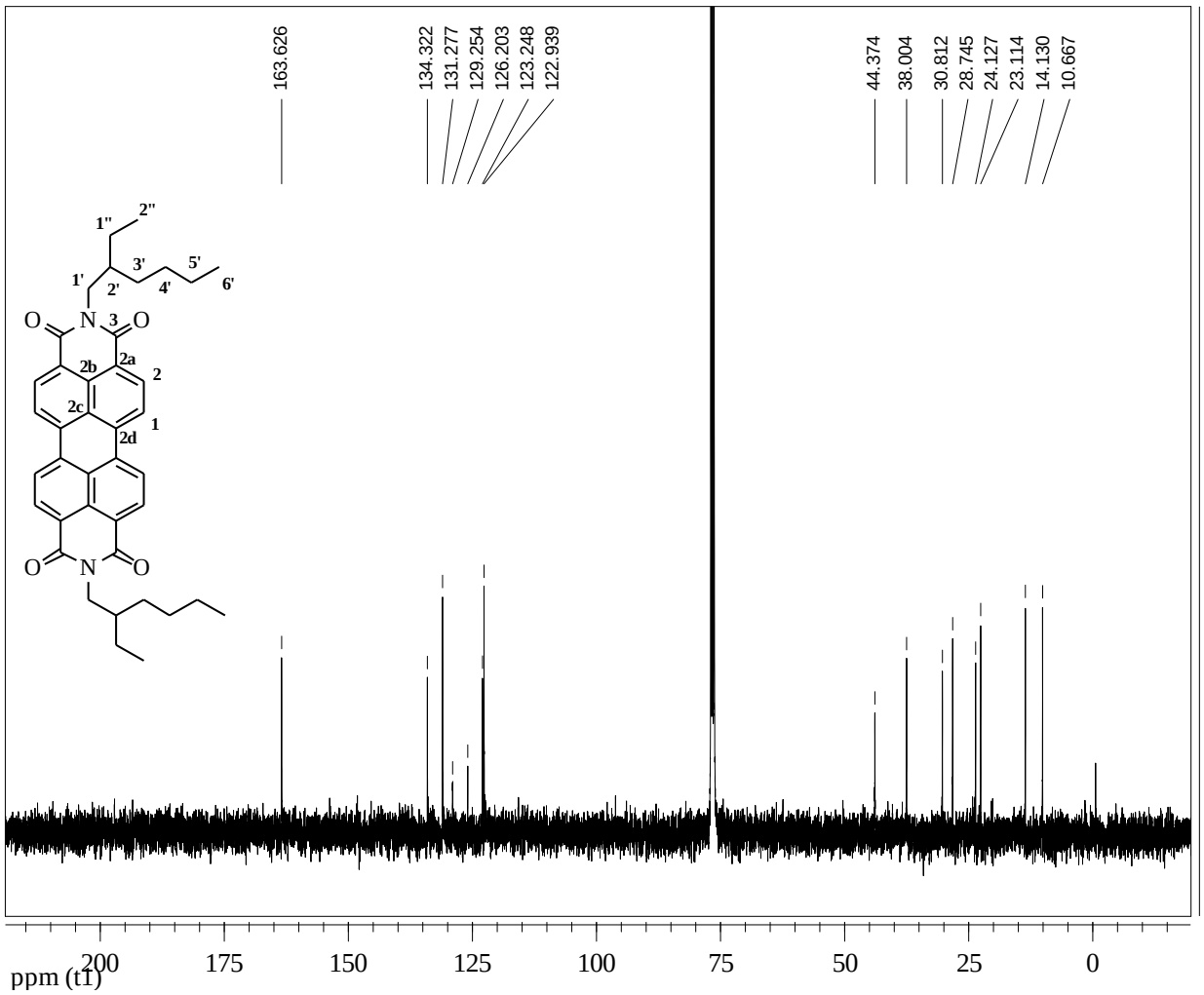

Appendix 26: ^{13}C NMR spectrum of 2,9-bis(2-ethylhexyl)anthra[2,1,9-def:6,5,10-*d*'e'f']diisoquinoline-1,3,8,10(2*H*,9*H*)-tetraone (**24**).

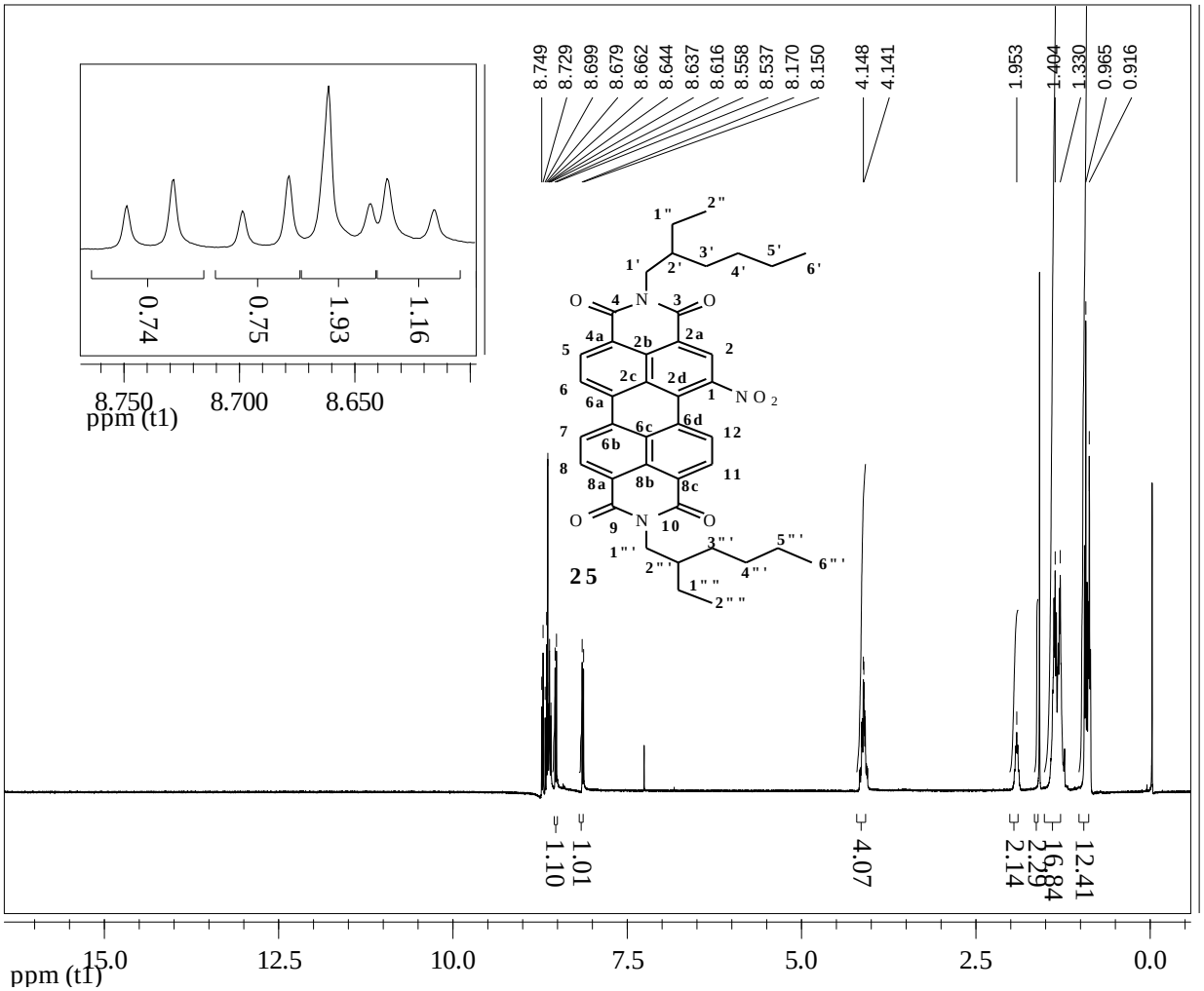

Appendix 27: ^{1}H NMR spectrum of 4,8-bis(5-bromothiophen-2-yl)-2,6-dioctyl-[1,2,3]triazolo[4,5-*f*]isoindole-5,7(2*H*,6*H*)-dione (**25**).

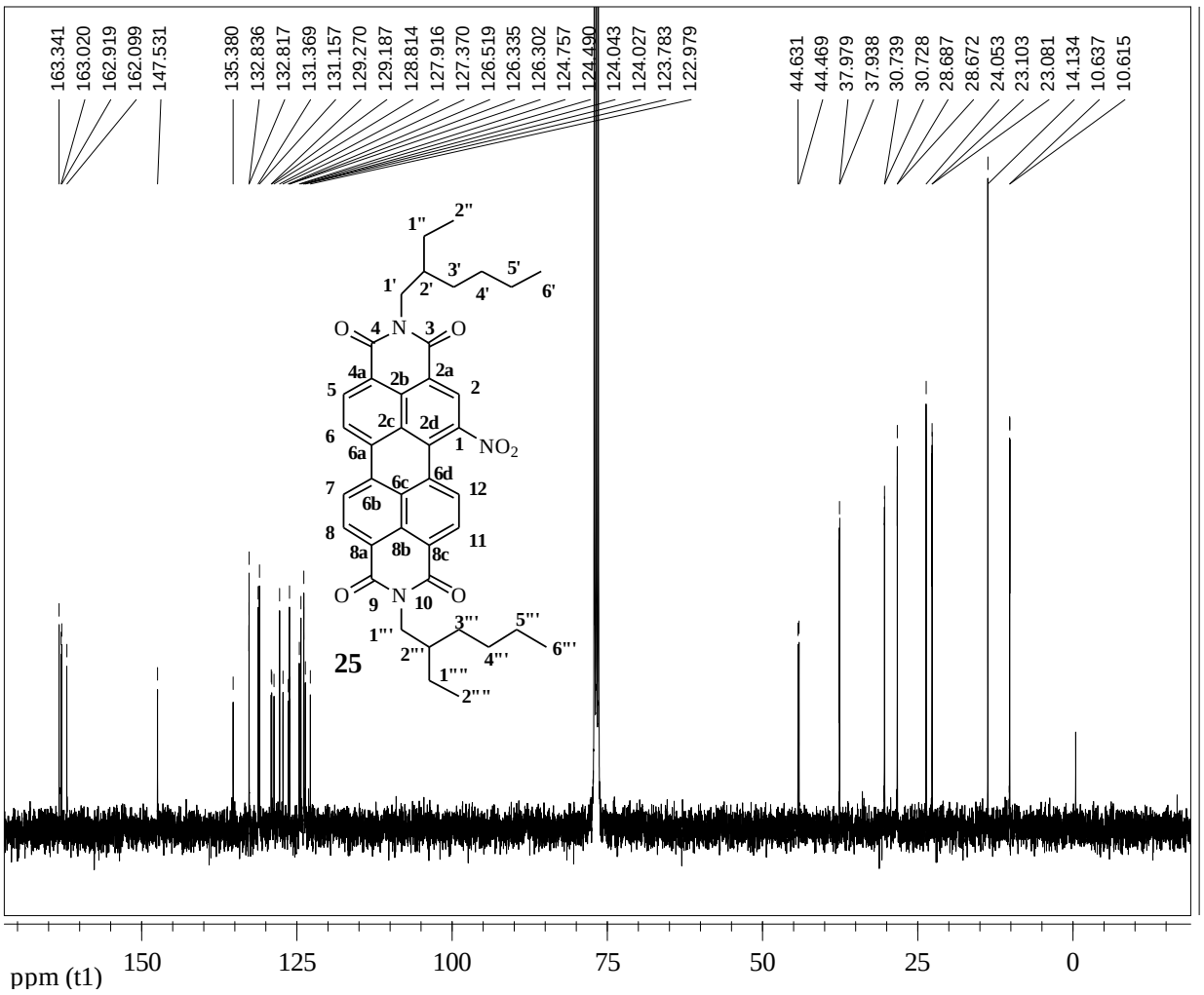

Appendix 28: ^{13}C NMR spectrum of 4,8-bis(5-bromothiophen-2-yl)-2,6-dioctyl-[1,2,3]triazolo[4,5-*f*]isoindole-5,7(2*H*,6*H*)-dione (**25**).

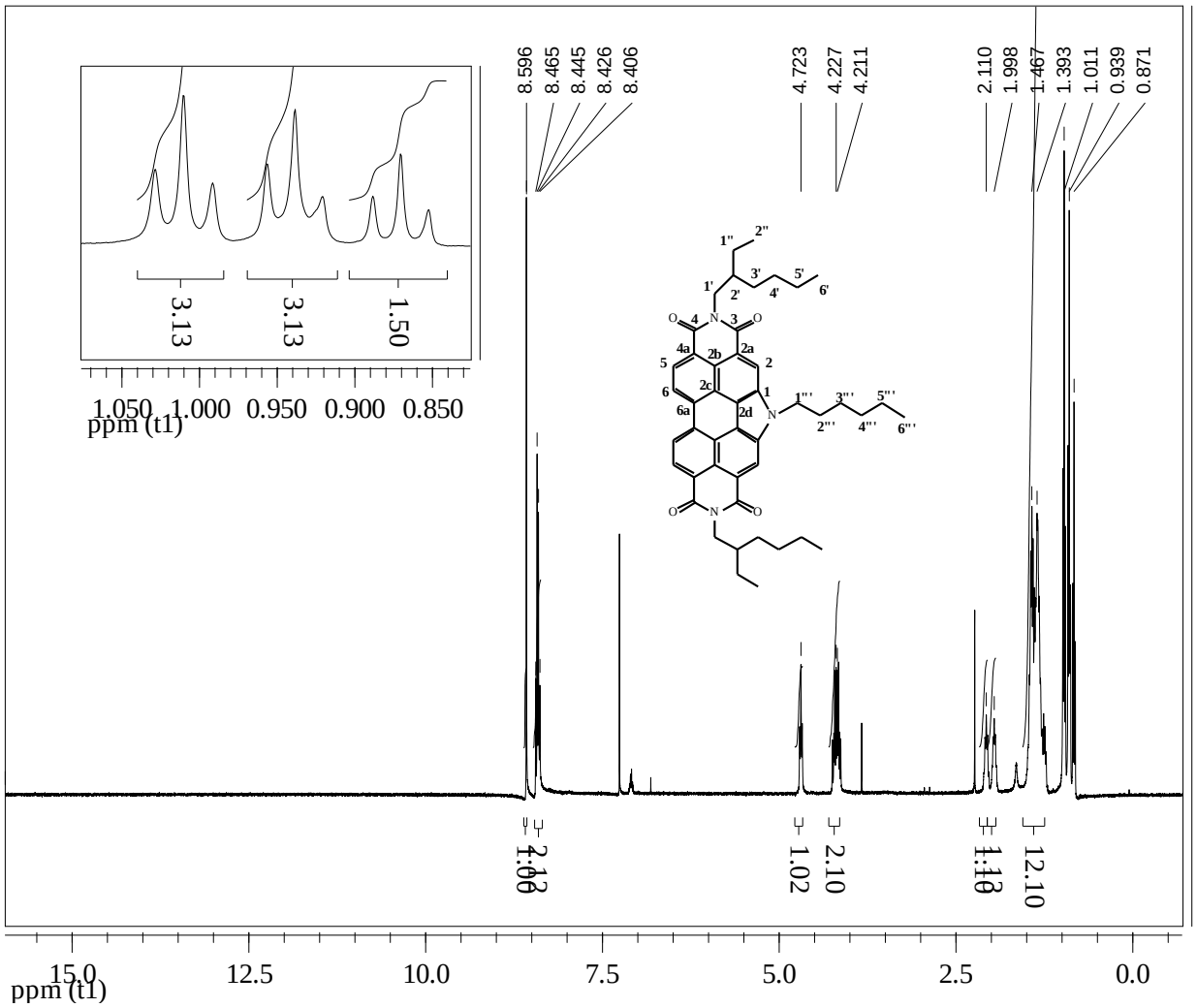

Appendix 29: ^{1}H NMR spectrum of 2,8-bis(2-ethylhexyl)-1*H*-pyrido[3',4',5':4,5]naphtho[2,1,8-*cde*]pyrido[3',4',5':4,5]naphtho[8,1,2-*ghi*]isoindole-1,3,7,9(2*H*,5*H*,8*H*)-tetraone (**27**).

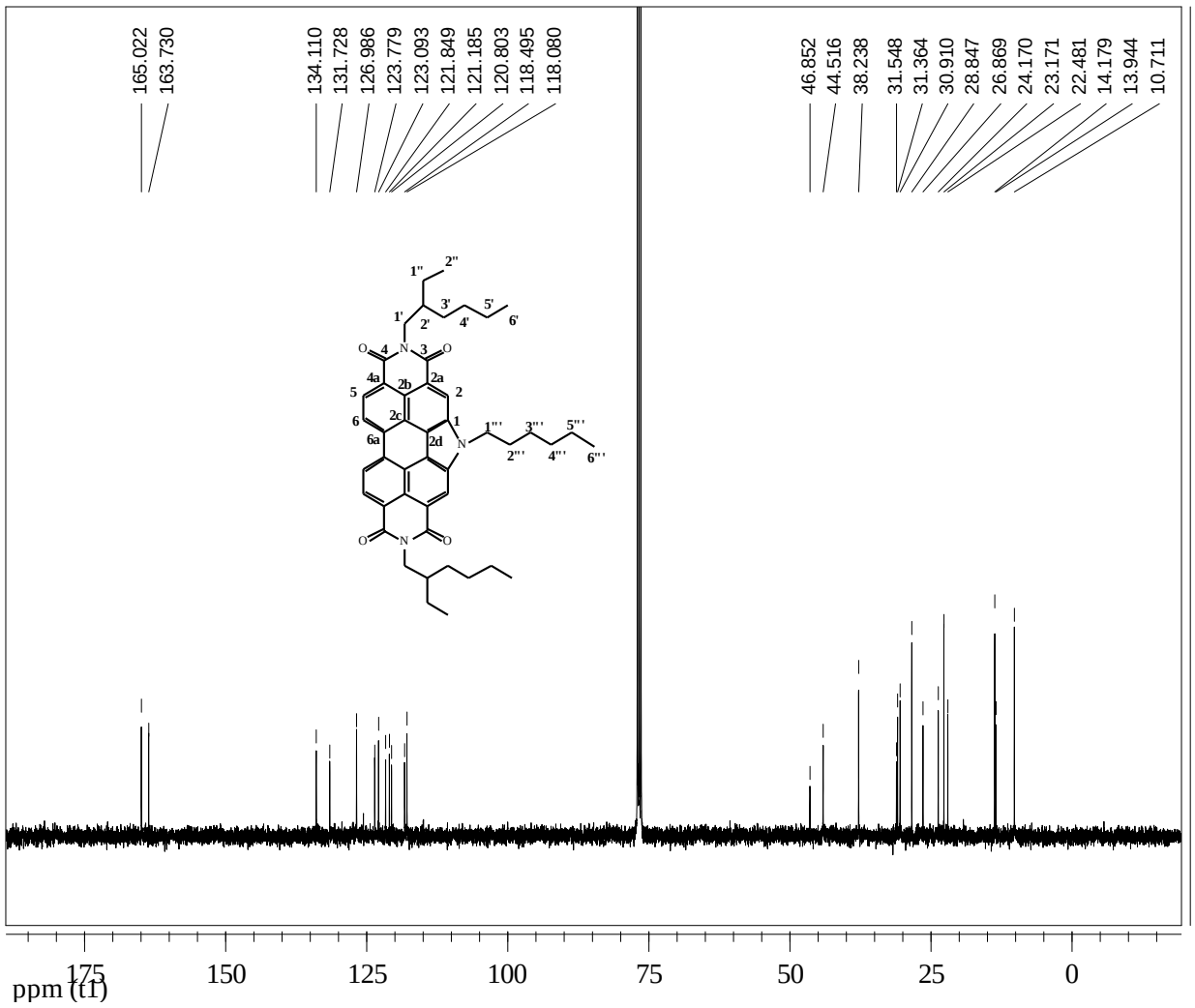

Appendix 30: ^{13}C NMR spectrum of 2,8-bis(2-ethylhexyl)-1*H*-pyrido[3',4',5':4,5]naphtho[2,1,8-*cde*]pyrido[3',4',5':4,5]naphtho[8,1,2-*ghi*]isoindole-1,3,7,9(2*H*,5*H*,8*H*)-tetraone (**27**).

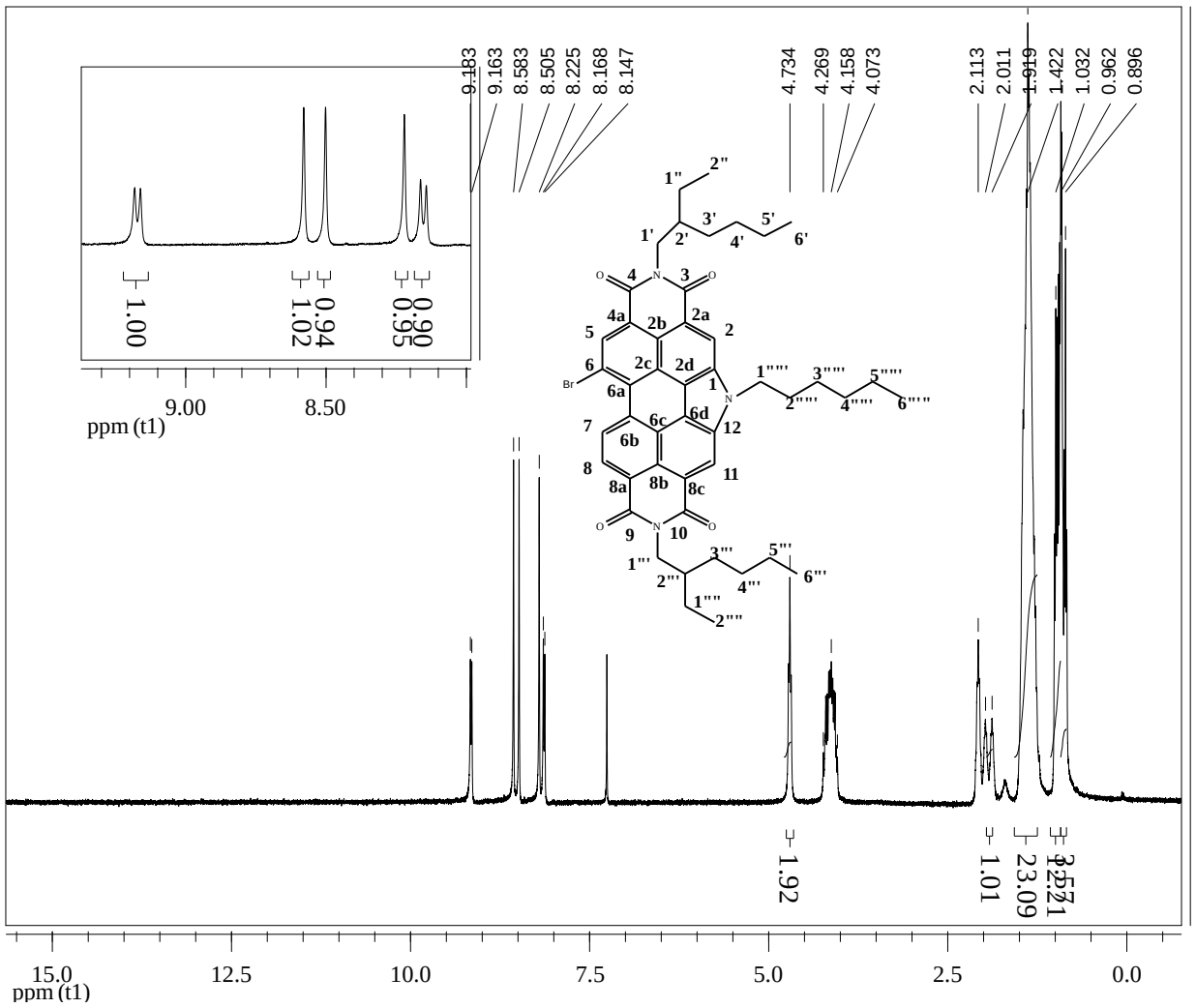

Appendix 31: ^{1}H NMR spectrum of 11-bromo-2,8-bis(2-ethylhexyl)-5-hexyl-1*H*-pyrido[3',4',5':4,5]naphtho[2,1,8-*cde*]pyrido[3',4',5':4,5]naphtho[8,1,2-*ghi*]isoindole-1,3,7,9(2*H*,5*H*,8*H*)-tetraone (**28**).

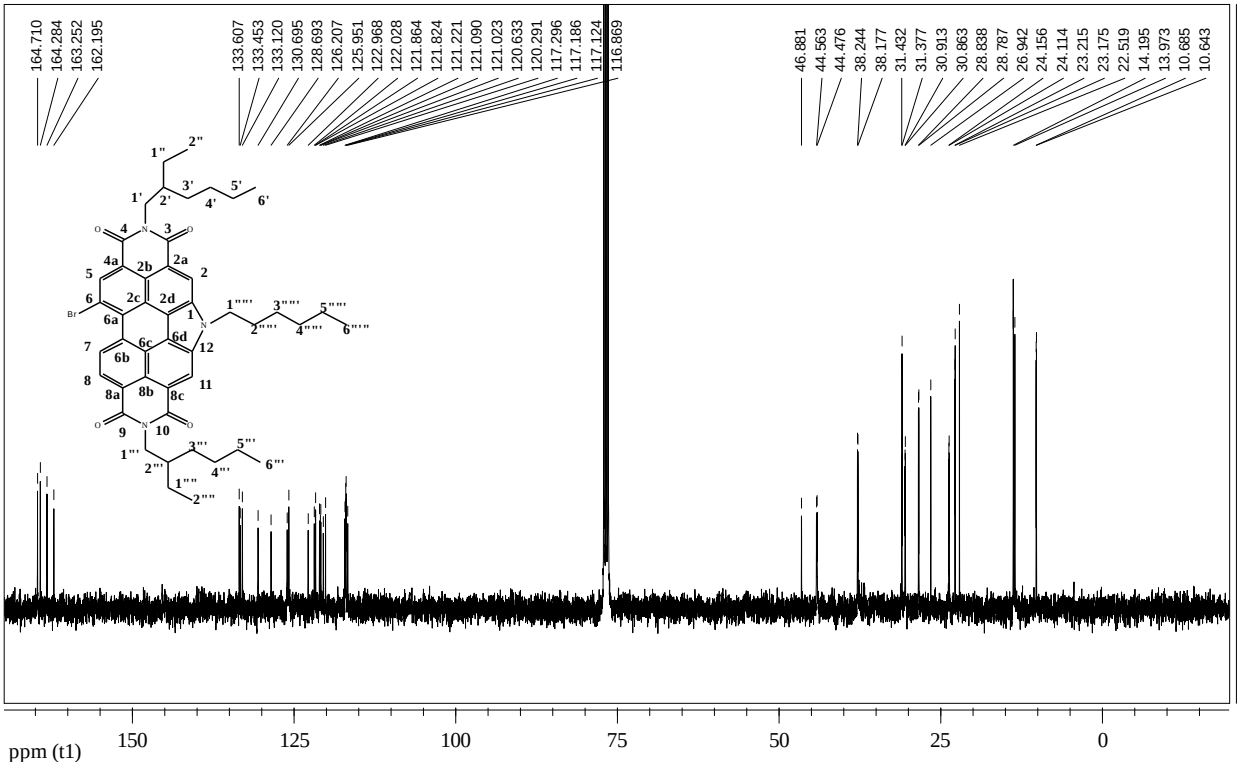

Appendix 32: ^{13}C NMR spectrum of 11-bromo-2,8-bis(2-ethylhexyl)-5-hexyl-1*H*-pyrido[3',4',5':4,5]naphtho[2,1,8-*cde*]pyrido[3',4',5':4,5]naphtho[8,1,2-*ghi*]isoindole-1,3,7,9(2*H*,5*H*,8*H*)-tetraone (**28**).

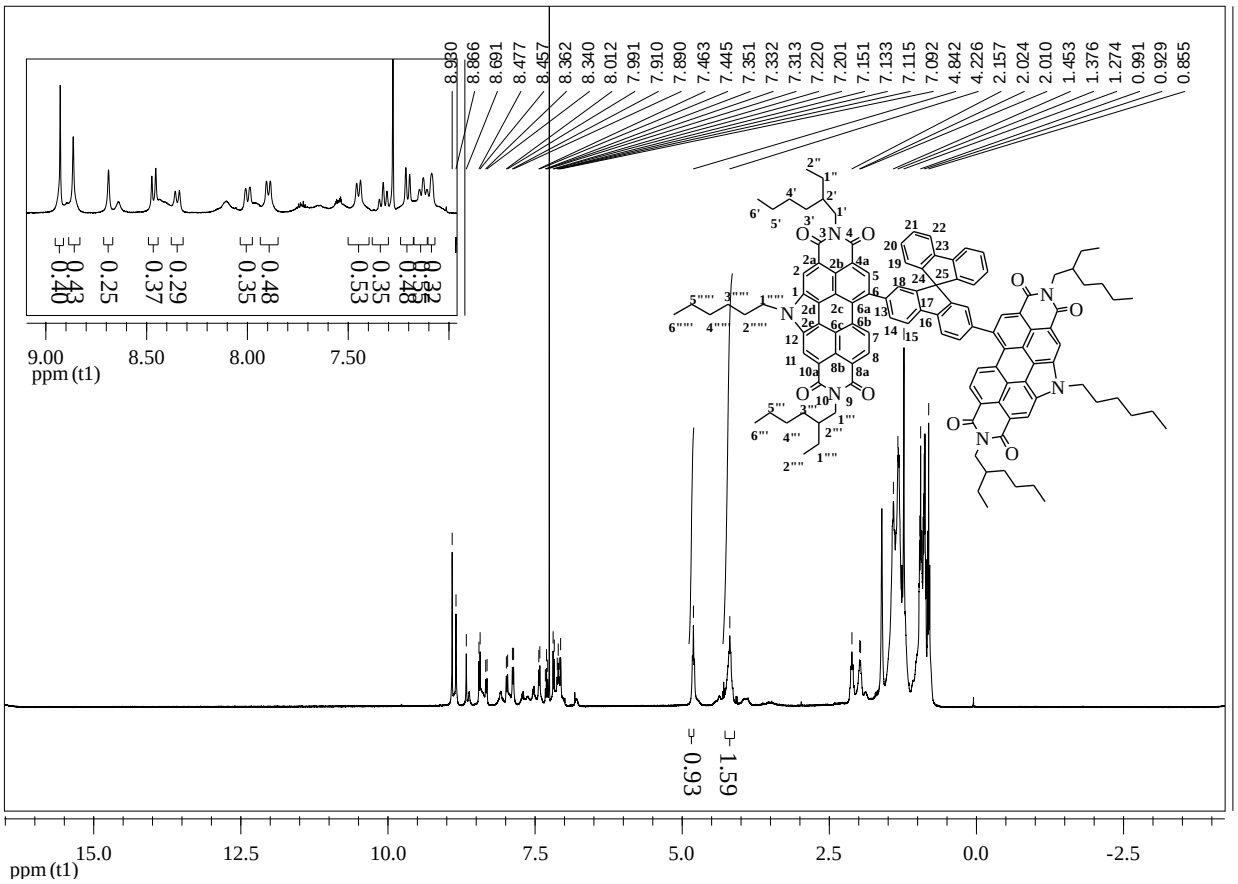

Appendix 33: ^{1}H NMR spectrum of 11,11'-(9,9'-spirobi[fluorene]-2,7-diyl)bis(2,8-bis(2-ethylhexyl)-5-hexyl-1*H*-pyrido[3',4',5':4,5]naphtho[2,1,8-*cde*]pyrido[3',4',5':4,5]naphtho[8,1,2-*ghi*]isoindole-1,3,7,9(2*H*,5*H*,8*H*)-tetraone) (**30**).

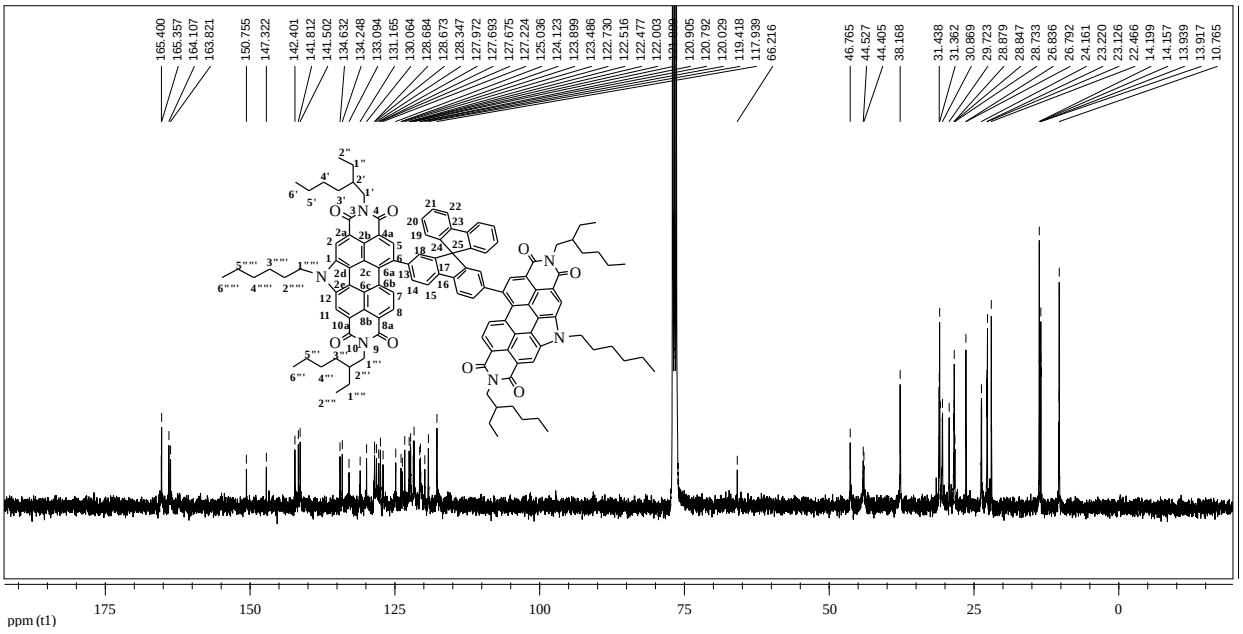

Appendix 34: ^{13}C NMR spectrum of 11,11'-(9,9'-spirobi[fluorene]-2,7-diyl)bis(2,8-bis(2-ethylhexyl)-5-hexyl-1*H*-pyrido[3',4',5':4,5]naphtho[2,1,8-*cde*]pyrido[3',4',5':4,5]naphtho[8,1,2-*ghi*]isoindole-1,3,7,9(2*H*,5*H*,8*H*)-tetraone) (**30**).